Title
Vertex-Selective Functionalization of Icosahedral Boron Clusters

Author
Dziedzic, Rafal Miroslaw

Publication Date
2019

Peer reviewed|Thesis/dissertation

UNIVERSITY OF CALIFORNIA

Los Angeles

Vertex-Selective Functionalization of Icosahedral Boron Clusters

A dissertation submitted in partial satisfaction of the
requirements for the degree Doctor of Philosophy
in Chemistry

by

Rafal Miroslaw Dziedzic

2019

ABSTRACT OF THE DISSERTATION

Vertex-Selective Functionalization of Icosahedral Boron Clusters

by

Rafal Miroslaw Dziedzic

Doctor of Philosophy in Chemistry

University of California, Los Angeles, 2019

Professor Alexander M. Spokoyny, Chair

Icosahedral boron clusters (e. g. $C_2B_{10}H_{12}$, $[CB_{11}H_{12}]^{1-}$, $[B_{12}H_{12}]^{2-}$) are aromatic molecules that can serve as 3-dimensional scaffolds in molecular materials. Vertex-selective functionalization of boron cluster B−H bonds allows tuning of the electronic properties and spatial arrangement of boron cluster-bound moieties. Vertex-selective functionalization of icosahedral boron clusters is desirable for making complex molecules based on boron cluster scaffolds. Thus new functionalization methods for boron clusters are needed which can append a variety of functional groups with atomic precision. Vertex-specific functionalization of polyhedral boranes is possible by leveraging the anisotropic electron density and inductive effects of the icosahedral boron clusters to control the site of functionalization. By adapting existing palladium-catalyzed cross-coupling chemistry to polyhedral boranes we are able to form B−O, B−N, and B−C bonds with amines, heterocycles, alkoxides, boronic acids, and small nucleophiles (e.g. −F, −OH, $-NH_2$, and −CN). Our discovery of Pd-catalyzed isomerization ("cage-walking") of bromo-*meta*-carborane

(9-Br-*m*-$C_2B_{10}H_{11}$) into four Br-*m*-$C_2B_{10}H_{11}$ regioisomers enables synthesis of several regioisomer products from a single starting material. Incorporation of the cage-walking process into Pd-catalyzed cross-coupling allows synthesis of all four boron-vertex (B(9), B(5), B(4), and B(2)) functionalized *meta*-carborane regioisomers from 9-Br-*m*-$C_2B_{10}H_{11}$. Additionally, vertex-selective functionalization enables tuning of physical properties, such as melting point and electrochemical behavior, that expand the utility of polyhedral boranes to new application. We are interested in tuning the chemical stability and weak coordination properties of polyhedral borane anions for ionic liquid electrolytes and flow-battery applications.

The dissertation of Rafal Miroslaw Dziedzic is approved.

Yves Rubin

Paula Diaconescu

Pamela Kennedy

Alexander Spokoyny, Chair

University of California, Los Angeles

2019

Table of Contents

List of Figures

Acknowledgements

Chapter 1 is a reprint of Dziedzic, R. M.; Spokoyny, A. M. Metal-Catalyzed Cross-Coupling Chemistry with Polyhedral Boranes. *Chem. Commun.* **2019**, *55* (4), 430–442. DOI: 10.1039/C8CC08693A with permission from the Royal Society of Chemistry.

R.M.D. wrote and edited the manuscript

A.M.S. edited the manuscript.

Chapter 2 is a reprint of Dziedzic, R. M.; Saleh, L. M. A.; Axtell, J. C.; Martin, J. L.; Stevens, S. L.; Royappa, A. T.; Rheingold, A. L.; Spokoyny, A. M. B-N, B-O, and B-CN Bond Formation via Palladium-Catalyzed Cross-Coupling of B-Bromo-Carboranes. *J. Am. Chem. Soc.* **2016**, *138* (29), 9081–9084. DOI: 10.1021/jacs.6b05505 with permission from the American Chemical Society.

R.M.D designed and performed experiments, and wrote and edited the manuscript

L.M.A.S. designed and performed experiments, and edited the manuscript

J.C.A. designed and performed experiments, and edited the manuscript

J.L.M. performed experiments

S.L.S. performed experiments

A.T.R. performed crystallography experiments

A.L.R. performed crystallography experiments

A.M.S. PI and edited the manuscript

Chapter 3 is a reprint of Dziedzic, R. M.; Martin, J. L.; Axtell, J. C.; Saleh, L. M. A.; Ong, T. C.; Yang, Y. F.; Messina, M. S.; Rheingold, A. L.; Houk, K. N.; Spokoyny, A. M. Cage-Walking:

Vertex Differentiation by Palladium-Catalyzed Isomerization of B(9)-Bromo-Meta-Carborane. *J. Am. Chem. Soc.* **2017**, *139* (23), 7729–7732. DOI: 10.1021/jacs.7b04080 with permission from the American Chemical Society.

R.M.D designed and performed experiments, and wrote and edited the manuscript

J.L.M. performed experiments

J.C.A. designed and performed, and edited the manuscript

L.M.A.S. designed and performed experiments, and edited the manuscript

T.C.O. performed NMR experiments

Y.Y. performed DFT experiments

M.S.M. assisted with isolation of compounds

A.L.R. performed crystallography experiments

K.N.H. PI for DFT studies

A.M.S. PI and edited the manuscript

Chapter 4 is a reprint of Dziedzic, R. M.; Axtell, J. C.; Rheingold, A. L.; Spokoyny, A. M. Off-Cycle Processes in Pd-Catalyzed Cross-Coupling of Carboranes. *Org. Process Res. Dev.* **2019**, *139* (23), 7729–7732. DOI: 10.1021/acs.oprd.9b00257 with permission from the American Chemical Society.

R.M.D designed and performed, and wrote and edited the manuscript

J.C.A. designed and performed, and edited the manuscript

L.M.A.S. designed and performed experiments, and edited the manuscript

A.L.R. performed crystallography experiments

A.M.S. PI and edited the manuscript

Chapter 5 is a reprint of Dziedzic, R. M.; Waddington, M. A.; Lee, S. E.; Kleinsasser, J.; Plumley, J. B.; Ewing, W. C.; Bosley, B. D.; Lavallo, V.; Peng, T. L.; Spokoyny, A. M. Reversible Silver Electrodeposition from Boron Cluster Ionic Liquid (BCIL) Electrolytes. *ACS Appl. Mater. Interfaces* **2018**, *10*, 6825-6830. DOI: 10.1021/acsami.7b19302 with permission from the American Chemical Society.

R.M.D designed and performed, and wrote and edited the manuscript

M.A.W. designed and performed, and wrote and edited the manuscript

S.E.L. synthesized monocarborane precusors

J.K. synthesized monocarborane precusors

J.B.P. fabricated IR transparent ITO on sapphire electrodes

W.C.E. PI

B.D.B. PI

V.L. PI

T.L.P. PI

A.M.S. PI and edited the manuscript

This research was supported by the National Defense Science and Engineering Graduate Fellowship from the Department of Defense and by the STTR Project (AF16-AT20) funding.

Biographical Sketch

Rafal Dziedzic earned a BS at the University of Wisconsin – Madison in 2014 where he studied earth-abundant nanomaterials for energy harvesting and catalysis under the supervision of Prof. Song Jin. As a graduate student in Prof. Alexander Spokoyny's research group at the University of California, Los Angeles, his primary research interests are metal-mediated functionalization of polyhedral boranes, organometallic catalysis, ionic liquid development, and design of inorganic molecular building blocks. He is currently a National Defense Science and Engineering Graduate Fellow and was an Air Force Research Laboratory Space Scholar during 2014, 2015 and 2016.

Awards and Honors

Air Force Research Laboratory Space Scholar, 2014, 2015, 2016

Excellence in Second Year Academics and Research, UCLA Dept. of Chemistry & Biochemistry, 2016

National Defense Science and Engineering Graduate Fellowship, Fellow, 2016-2019

NSF Graduate Research Fellowship Program, Honorable Mention, 2015

UW-Madison Undergraduate Research Fellowship, 2013

NSF-Research Experience for Undergraduates sponsored by 3M, 2012

Peer Reviewed Publications

1. R. M. Dziedzic, A. M. Spokoyny, "Metal-catalyzed Cross-Coupling Chemistry with Polyhedral Boranes", *Chem. Commun.*, **2019**, *55*, 430-442.

2. R. M. Dziedzic, M. A. Waddington, S. E. Lee, J. Kleinsasser, J. B. Plumley, W. C. Ewing, B. D. Bosley, V. Lavallo, T. L. Peng, A. M. Spokoyny, "Reversible Silver Electrodeposition from Boron Cluster Ionic Liquid (BCIL) Electrolytes", *ACS Appl. Mater. Interfaces*, **2018**, *10*, 6825-6830.

3. J. C. Axtell, K. O. Kirlikovali, R. M. Dziedzic, M. Gembicky, A. L. Rheingold and A. M. Spokoyny, "Magnesium Reagents Featuring a 1,1'-Bis(*o*-carborane) Ligand Platform", *Eur. J. Inorg. Chem.*, **2017**, *38-39*, 4411-4416.

4. A. C. Serino, M. E. Anderson, L. M. A. Saleh, R. M. Dziedzic, H. Mills, L. K. Heidenreich, A. M. Spokoyny and P. S. Weiss, "Work Function Control of Germanium through Carborane-Carboxylic Acid Surface Passivation", *ACS Appl. Mater. Interfaces*, **2017**, *9*, 34592-34596.

5. R. M. Dziedzic, J. L. Martin, J. C. Axtell, L. M. A. Saleh, T.-C. Ong, Y.-F. Yang, M. S. Messina, A. L. Rheingold, K. N. Houk and A. M. Spokoyny, "Cage-Walking: Vertex Differentiation by Palladium-Catalyzed Isomerization of B(9)-Bromo-*meta*-Carborane", *J. Am. Chem. Soc.*, **2017**, *139*, 7729-7732.

6. J. C. Axtell, K. O. Kirlikovali, D. Jung, R. M. Dziedzic, A. L. Rheingold and A. M. Spokoyny, "Metal-Free Peralkylation of the *closo*-Hexaborate Anion", *Organometallics*, **2017**, *36*, 1204-1210.

7. L. M. A. Saleh, R. Dziedzic and A. M. Spokoyny, "An Inorganic Twist in Nanomaterials: Making an Atomically Precise Double Helix", *ACS Cent. Sci.*, **2016**, *2*, 685-686.

8. R. M. Dziedzic, L. M. A. Saleh, J. C. Axtell, J. L. Martin, S. L. Stevens, A. T. Royappa, A. L. Rheingold and A. M. Spokoyny, "B-N, B-O and B-CN Bond Formation via Palladium Catalyzed Cross-coupling of B-Bromo-Carboranes", *J. Am. Chem. Soc.*, **2016**, *138*, 9081-9084.

9. L. M. A. Saleh, R. M. Dziedzic, S. I. Khan and A. M. Spokoyny, "Forging Unsupported Metal-Boryl Bonds with Icosahedral Carboranes", *Chem. Eur. J.*, **2016**, *22*, 8466-8470.

10. R. Ren, M. Faber, R. Dziedzic, Z. Wen, S. Jin, S. Mao and J. Chen, "Metallic CoS_2 Nanowire Electrodes for High Cycling Performance Supercapacitors", *Nanotechnology*, **2015**, *26*, 494001.

11. B. Leite, R. Dziedzic, L. Cruz, A. L. Gillian-Daniel, C. Nielsen and L. De La Fuente, "Biological Electron Microscopy Microcontact Printing of Thiols: Changing the Way Cell Attachment is Investigated", *Microscopy Today*, **2015**, *23*, 24-29.

12. R. M. Dziedzic, A. L. Gillian-Daniel, G. M. Petersen and K. J. Martínez-Hernández, "Microwave Synthesis of Zinc Hydroxy Sulfate Nanoplates and Zinc Oxide Nanorods in the Classroom", *J. Chem. Educ.*, **2014**, *91*, 1710-1714.

13. M. S. Faber, R. Dziedzic, M. A. Lukowski, N. S. Kaiser, Q. Ding and S. Jin, "High-Performance Electrocatalysis Using Metallic Cobalt Pyrite (CoS_2) Micro- and Nanostructures", *J. Am. Chem. Soc.*, **2014**, *136*, 10053-10061.

14. A. Forticaux, S. Hacialioglu, J. P. DeGrave, R. Dziedzic and S. Jin, "Three-Dimensional Mesoscale Heterostructures of ZnO Nanowire Arrays Epitaxially Grown on $CuGaO_2$ Nanoplates as Individual Diodes", *ACS Nano*, **2013**, *7*, 8224-8232.

Chapter 1. Metal-Catalyzed Cross-Coupling Chemistry with Polyhedral Boranes

This chapter provides a review of metal-catalyzed cross-coupling reactions with a variety of polyhedral boranes. In particular, it focuses on the versatility, limitations and future outlook of palladium-catalyzed cross-coupling for synthesizing new boron cluster molecules.

This article is a reprint of Dziedzic, R. M.; Spokoyny, A. M. Metal-Catalyzed Cross-Coupling Chemistry with Polyhedral Boranes. *Chem. Commun.* **2019**, *55* (4), 430–442. DOI: 10.1039/C8CC08693A with permission from the Royal Society of Chemistry.

Metal-catalyzed cross-coupling chemistry with polyhedral boranes

Rafal M. Dziedzic *[a] and Alexander M. Spokoyny *[ab]

Over the past several decades, metal-catalyzed cross-coupling has emerged as a very powerful strategy to functionalize carbon-based molecules. More recently, some of the cross-coupling methodologies have been adapted to inorganic compounds including boron-rich clusters. The development of this chemistry relies on the ability to synthesize halogenated boron-rich clusters which can serve as electrophilic cross-coupling partners with nucleophilic substrates in the presence of a metal catalyst. While the cross-coupling chemistry with boron-clusters is conceptually reminiscent of that of its hydrocarbon counterparts, several key aspects including the spheroidal bulk of clusters and the distinct nature of boron–halogen/boron–heteroatom bonds make this chemistry unique. The utility of metal-catalyzed cross-coupling can be extended to several classes of polyhedral boranes including neutral and anionic carboranes, metallaboranes, and carbon-free boranes. Importantly, cross-coupling enables a suite of boron–heteroatom (C, N, O, P, S) couplings to prepare boron cluster-based systems that can be used for ligand design, medicinal chemistry, and materials applications.

[a] *Department of Chemistry & Biochemistry, University of California, Los Angeles, 607 Charles E. Young Drive East, Los Angeles, California 90095, USA. E-mail: rdziedzic@chem.ucla.edu, spokoyny@chem.ucla.edu*
[b] *California NanoSystems Institute (CNSI), University of California, Los Angeles, 570 Westwood Plaza, Los Angeles, California 90095, USA*

Introduction

Metal-catalyzed cross-coupling is a powerful method for constructing larger molecules by covalently bonding molecular fragments.[1–7] These reactions play an important role in organic synthesis due to the adaptability of metal catalysts to specific

Rafal M. Dziedzic

Rafal Dziedzic was born in Poland and raised in Chicago. He earned a BS at the University of Wisconsin – Madison in 2014 where he studied earth-abundant nanomaterials for energy harvesting and catalysis under the supervision of Prof. Song Jin. As a graduate student in Prof. Alexander Spokoyny's research group at the University of California, Los Angeles, his primary research interests are metal-mediated functionalization of polyhedral boranes, organometallic catalysis, ionic liquid development, and design of inorganic molecular building blocks. He is currently a National Defense Science and Engineering Graduate Fellow and was an Air Force Research Laboratory Space Scholar.

Alexander M. Spokoyny

Alex Spokoyny is currently an Assistant Professor in Chemistry and Biochemistry at UCLA and a faculty member of the California NanoSystems Institute (CNSI). Prior to this he received a PhD degree in 2011 from Northwestern University in inorganic chemistry and conducted a post-doctoral stint at MIT in chemical biology until 2014. His group's research focuses on the chemistry of atomically precise clusters and encompasses an interdisciplinary approach focusing on pressing problems in chemistry, biology, medicine and materials science. Alex is a recipient of several recent awards including Cottrell Scholar from Research Corporation for Science Advancement (2018), Maximizing Investigator's Research Award (MIRA) from the NIH (2017), Alfred P. Sloan Research Fellowship (2017), Chemical and Engineering News (C&EN) Talented 12 (2016) and 3M Non-Tenured Faculty Award (2016).

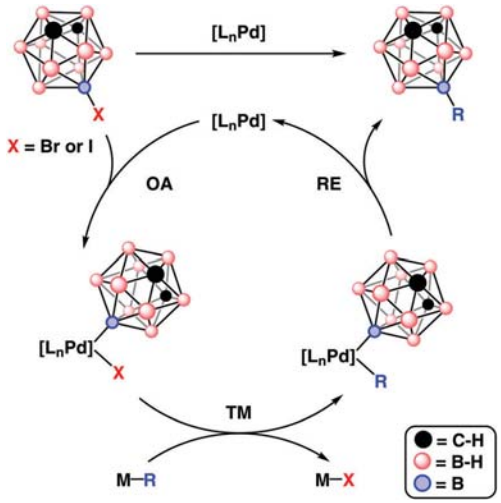

Fig. 1 Generalized Pd-catalyzed cross-coupling of a representative halocarborane (halogen is attached onto the B(9) position of a *meta*-carborane cluster). OA = oxidative addition, TM = transmetallation, RE = reductive elimination.

molecules including complex aromatic compounds and unsaturated hydrocarbons. Among such reactions, palladium-catalyzed cross-coupling between an electrophile and a nucleophile has shown broad utility in synthesis. Pd-Catalyzed cross-coupling generally features three elementary steps: oxidative addition of an electrophile, transmetallation of a nucleophile, and coupling of the electrophile and nucleophile by reductive elimination, Fig. 1.

In the 1950s researchers discovered a new class of boron-rich molecules characterized by 3-center-2-electron bonds that stabilize polyhedral borane structures into cage-like (*closo*-) structures, Fig. 2.[8] Formation of *closo*-polyhedral boranes results in a 3-dimensional (3D) σ-aromaticity that is considered a 3-dimensional analog of 2-dimensional aromatic molecules (*e.g.*, benzene). At the onset of the discovery of polyhedral boranes, a fundamental interest pertaining to the reactivity of these clusters has emerged. Several reactions observed with aromatic hydrocarbons, such as electrophilic and nucleophilic substitution,

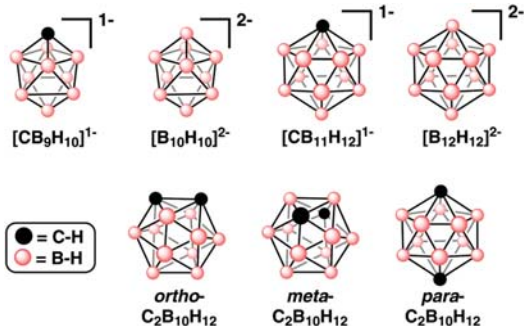

Fig. 2 Polyhedral borane clusters that can serve as precursors to electrophilic substrates that can be subsequently used in metal-catalyzed cross-coupling.

have been subsequently applied to boron clusters. This similar reactivity led to investigations into whether polyhedral boranes can undergo metal-mediated reactions like Pd-catalyzed cross-coupling reactions of aryl halides. Reactions of *ortho*/*meta*-carborane with $Hg(CF_3COO)_2$ in triflic acid yielded [$Hg(CF_3COO)$(9-B-*o*/*m*-$C_2B_{10}H_{11}$)] carboranyl compounds reminiscent of the early work by Heck with arylmercury species.[9,10] Following these results, successful Pd-catalyzed cross-coupling of B-iodo-carboranes with Grignard reagents established an early precedent for using metal-catalyzed cross-coupling to derivatize polyhedral boranes.

This article will describe how metal-catalyzed cross-coupling has been developed, and deployed, to a broad subset of polyhedral boranes. Emphasis is placed on principles that are applicable to many compositions of polyhedral boranes. First, we will present how metal-catalyzed B–C coupling with various polyhedral boranes establishes the broad utility of cross-coupling for different polyhedral borane compositions. Then, the various metal-catalyzed B–N, B–O, and B–P couplings highlight the nuances of using polyhedral boranes as cross-coupling partners.

Polyhedral boranes as substrates

Ten- and 12-vertex *closo*-boranes have garnered attention due to their stability and synthetic accessibility. Their 3D aromaticity also imparts high thermal and chemical stability that makes these polyhedral boranes interesting for molecular building blocks and for scaffolds in supramolecular materials such as metal–organic frameworks,[11] macrocycles,[12,13] dendrimers, and covalent nanoparticle cores.[14] Ten- and 12-vertex *closo*-boranes exist as neutral, anionic and dianionic molecules depending on the composition of the boron-cluster core. The commonly encountered 10-vertex *closo*-boranes are $[B_{10}H_{10}]^{2-}$ and $[CB_9H_{10}]^{1-}$; and the common 12-vertex *closo*-boranes are $[B_{12}H_{12}]^{2-}$, $[CB_{11}H_{12}]^{1-}$, and three isomers (*ortho*-, *meta*-, *para*-) of $C_2B_{10}H_{12}$, Fig. 2. These 3D aromatic molecules are frequently compared to benzene, but they are more sterically similar to adamantane.[15–17] For example, *ortho*-$C_2B_{10}H_{12}$ has a calculated van der Waals volume of 148 Å^3, whereas benzene has a volume of 79 Å^3 and the non-aromatic adamantane has a volume of 136 Å^3.[15,18] The larger volume and σ-aromaticity of polyhedral boranes require additional consideration when using them as replacements for phenyl or adamantyl moieties.[15]

Polyhedral boranes also possess exohedral σ-bonds that allow covalent bonding between a boron cluster core and other molecular fragments. The electronic coupling between exohedral moieties and the boron cluster core can be engineered by the boron-cluster composition; this tunability presents exciting opportunities for designing the electronic properties of polyhedral borane-based materials.

Controlled engineering of borane-based materials relies on precise ways of covalently attaching molecular fragments to the boron-cluster core. For polyhedral boranes that contain a cage heteroatom, such as a carbon vertex in *closo*-$C_2B_{10}H_{12}$ or [*closo*-$CB_{11}H_{12}]^{1-}$, the C–H vertex proton is much more acidic compared to the hydridic B–H vertices.[15] The higher acidity of the C–H proton allows it to be deprotonated with a strong base and the resulting C^- vertex can undergo S_N2 reactions with electrophiles to produce

carbon substituted polyhedral boranes. Such S_N2 reactions are used to selectively append functional groups to the carbon vertices of neutral and anionic carboranes. However, this functionalization approach is not useful for $[B_{10}H_{10}]^{2-}$ and $[B_{12}H_{12}]^{2-}$, which have no C–H vertices, or when seeking to attach a functional group to a boron vertex.

Inductive effects can be transmitted through polyhedral boranes to exohedral functional groups.[19] In terms of electronic effects, the more electronegative carbon vertices of carboranes (*e.g. closo*-$C_2B_{10}H_{12}$, [*closo*-CB_9H_{10}]$^{1-}$ or [*closo*-$CB_{11}H_{12}$]$^{1-}$) have an electron withdrawing effect, whereas bonding to the boron vertices produces an electron donating effect. The downside to the facile S_N2 substitution of C–H vertices is that the carboranyl fragment always acts as an electron withdrawing group and the electron donating effects of the polyhedral boranes are not conferred to the exohedral moiety. Thus, a diverse set of methods that allow functionalization of the boron vertices are critical to fully capture the utility of polyhedral boranes in hierarchal designs.

B–H functionalization

Direct B–H functionalization methods provide new synthons for studying 3D aromaticity in molecular systems. Among these methods, reactions of electrophiles (E^+) with the electron-rich B–H vertices of polyhedral boranes form a variety of B–E bonds. Halogenated polyhedral boranes can be readily synthesized by the reaction of elemental halogens with polyhedral boranes in the presence of a Lewis acid catalyst ($AlCl_3$ or $FeCl_3$), Fig. 3. These halogenation reactions also produce polyhalogenated boranes that serve as important entry-points to metal-catalyzed cross-coupling. Cage reconstruction is an additional approach to synthesizing halogenated boranes; it involves reacting an open (*nido*-)polyhedral borane with BX_3 or BH_2X (X = F, Cl, Br, or I) to install a B–X vertex and form a *closo*- structure, Fig. 3. Both electrophilic and cage reconstruction methods can be applied to produce polyhalogenated compounds.

Metal-catalyzed B-vertex functionalization

Of the known polyhedral boranes, the 12-vertex carboranes have the largest number of cross-coupling reactions demonstrated. Carboranes containing two carbon vertices, $C_2B_{10}H_{12}$, are neutral molecules with 3 isomers named by the distance (*ortho*-, *meta*-, *para*-) between the carbon atoms, Fig. 2.[20] The anisotropic σ-aromaticity of carboranes is often leveraged in different metal-catalyzed functionalization routes to install various functional groups onto different boron vertices of polyhedral boranes.[21]

Two forms of metal-catalyzed functionalization prevail in the literature: (1) metal-catalyzed B–H activation,[22–25] and (2) metal-catalyzed cross-coupling at B–X (X = Br or I) bonds. Metal-catalyzed B–H activation strategies often feature a directing group bound to the boron cluster which coordinates an electrophilic metal center near a B–H vertex and promotes B–H bond cleavage.[24–33] In contrast, metal-catalyzed cross-coupling relies on electron-rich metals to perform oxidative addition into B–X bonds, Fig. 1. These two methods are complementary because they target electronically different vertices. For example, metal-catalyzed B–H activation can be used to halogenate vertices that do not readily undergo electrophilic halogenation or to create nucleophilic cross-coupling partners for metal-catalyzed cross-coupling.

One advantage of metal-catalyzed cross-coupling is that it allows coupling wherever a halogen can be installed. This leverages the breadth of polyhedral borane halogenation reactions to create a vast library of potential substrates. Successful cross-coupling reactions with Grignard reagents were performed in the presence of Pd and Ni catalysts under conditions closely resembling those used for aryl iodides. Early on, a view emerged that carboranes are a 3-dimensional analog of benzene because of their aromaticity, susceptibility to electrophilic alkylation and halogenation, and metal-catalyzed cross-coupling. This led to the development of functionalization reactions that closely resemble those of carbon-based aromatic molecules. However, further development of polyhedral borane cross-coupling calls for methods that account for their distinct electronic and steric properties.

Boron–halogen bond activation

Most reports of polyhedral borane cross-coupling target the weakest boron–halogen bond which is a B–I bond, whereas other B–X (X = F, Cl, or Br) bonds were originally dismissed as too unreactive, Fig. 4.[34–36] The lack of reactivity in B-bromo and

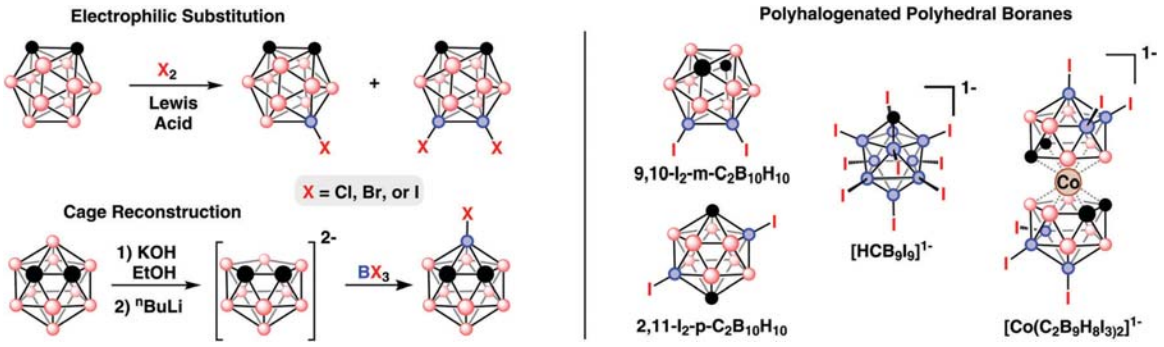

Fig. 3 (left) Electrophilic halogenation of *ortho*-carborane and cage-reconstruction of *ortho*-carborane by deboronation and subsequent "recapitation". (right) Examples of polyiodinated polyhedral boranes used in Pd-catalyzed cross-coupling.

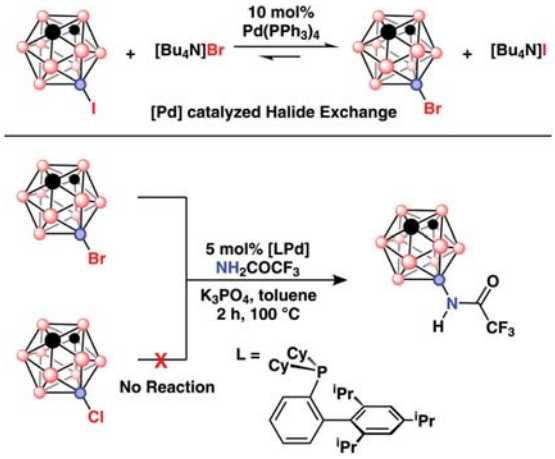

Fig. 4 (top) Pd-Catalyzed halide exchange with 9-I-*m*-$C_2B_{10}H_{11}$; the equilibrium lies heavily to the right (ref. 34). (bottom) Reactivity comparison between 9-Br-*m*-$C_2B_{10}H_{11}$ and 9-Cl-*m*-$C_2B_{10}H_{11}$ in a Pd-catalyzed amidation.

B-chloro polyhedral boranes in cross-coupling reactions was attributed to the stronger B–X bonds, compared to aryl C–X bonds, which prevented oxidative addition of B-bromo-carboranes. This difference in B–X bond strength allowed radiolabelling of carboranes with ^{76}Br and ^{19}F because the resulting B-bromo- and B-fluoro-carboranes do not undergo oxidative addition in the presence of commonly used Pd catalysts.[35,36] A survey of the catalyst systems used in cross-coupling of carboranes reveals that the majority of Pd-catalyzed reactions use a small set of phosphine ligands, mainly triphenylphosphine (PPh_3).

The reactivity of B-bromo-carboranes in Pd-catalyzed cross-coupling was finally overcome by using electron-rich dialkyl biaryl phosphines, which are known to activate C–Cl and C–OTf bonds of many carbon-based molecules, Fig. 4. Now, the difference in reactivity among B–X bonds presents heterofunctionalization pathways through catalyst-controlled sequential cross-coupling.[37]

Metal-catalyzed B–C bond formation

Despite the narrow scope of catalysts examined for polyhedral borane cross-coupling, a variety of B–C coupling reaction types have been demonstrated. The first reports of polyhedral borane cross-coupling feature reactions of B-iodo-carboranes and Grignard reagents in the presence of Pd catalysts.[38–41] Afterwards, Neigishi-type reactions were shown to produce B–C sp^3 and B–C sp^2 bonds with 5- and 6-member heterocycles.[42] Sonogishira-, Heck-, and Suzuki-type cross-coupling reactions were also demonstrated on carboranes. Many of these reactions were adapted to polyhedral boranes with different sizes, compositions, and charge. Most importantly, the body of work on polyhedral borane B–C coupling reveals general rules and trends that can inform cross-coupling methods on several classes of polyhedral boranes.

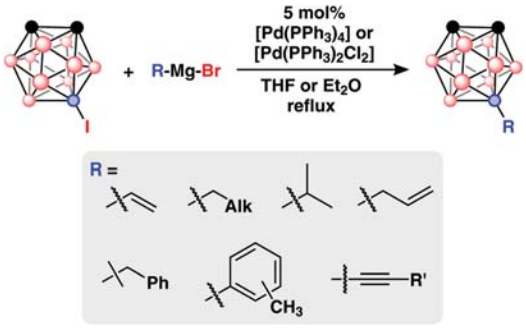

Fig. 5 Pd-Catalyzed Kumada cross-coupling with 9-I-*o*-$C_2B_{10}H_{11}$.

Kumada- and Neigishi-type coupling

Cross-coupling with Grignard reagents using Pd and Ni catalysts found $[Ni(PPh_3)_4]$ to be extremely inactive compared to $[Pd(PPh_3)_4]$.[38] This type of Pd-catalyzed cross-coupling is often used to couple alkyl, aryl, vinyl, and alkynyl groups to B-iodo-boranes. Typical reactions use ethereal solvents such as Et_2O and THF, and $[Pd(PPh_3)_2Cl_2]$ or $[Pd(PPh_3)_4]$ as the catalyst Fig. 5.[38,39,41] These reactions require several hours, or days, of refluxing depending on the Grignard reagent used. Cross-coupling of aryl, vinyl, and alkynyl substrates is more efficient than cross-coupling of alkyl groups. When using alkylmagnesium halides as the cross-coupling partner, reduction of B-iodo-carboranes ($C_2B_{10}H_{11}I$) to their parent carborane ($C_2B_{10}H_{12}$) was observed. Analogous reduction of aryl halides in the presence of Pd catalysts has been observed.[43–45] Importantly, reaction kinetics for this type of cross-coupling chemistry can be improved when precatalysts featuring biaryl ligands are used.[46]

The resulting low yields and long reaction times are attributed to palladium hydride complexes that may form by β-hydride elimination from alkylpalladium intermediates. Hawthorne and co-workers reported that addition of CuI as a co-catalyst significantly improved reaction yields by reducing the propensity toward carborane reduction.[40,47,48] Several types of metal-catalyzed cross-coupling reactions of B-iodo-carboranes with alkynes using Grignard reagents to form B–C bonds are known.[39] Later, Hawthorne and co-workers demonstrated the adventitious role of a CuI co-catalyst when using alkynyl Grignard reagents.[40,48] Importantly, these early cross-coupling methodology techniques were used to prepare rod-like carborane molecules in a step-wise iterative manner.[49]

Milder cross-coupling reactions using organozinc reagents demonstrated coupling of heterocycles to *p*- and *m*-carboranes using $[Pd(PPh_3)_2Cl_2]$, $[Pd(PPh_3)_4]$, and $[Pd(dppb)Cl_2]$, Fig. 6.[42] Notably, this allowed coupling of B-iodo-carboranes with an unprotected ethynyl steroid, 17-α-ethynylestradiol, to produce the B–C coupled product despite the presence of two alcohol groups that could have led to B–O coupled products.[50] An additional advantage of using organozinc reagents is that they do not rely on a base to generate the nucleophilic cross-coupling partner. This allows the use of 9-I-*o*-$C_2B_{10}H_{11}$ as a cross-coupling partner which is more prone to deboronation than 9-I-*m*-$C_2B_{10}H_{11}$.[51] Deboronation is a particular issue for *ortho*-carboranes because the resulting anionic

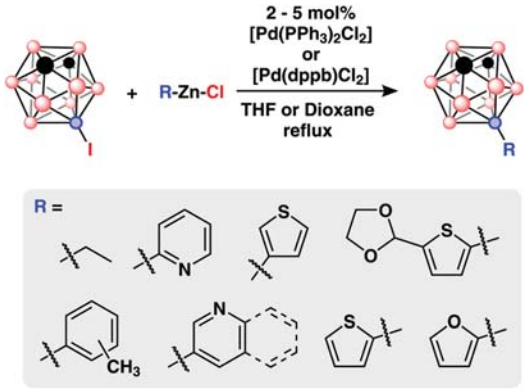

Fig. 6 Pd-Catalyzed Neigishi cross-coupling with 9-I-*m*-$C_2B_{10}H_{11}$.

nido-carboranes can act as chelating ligands that could sequester the metal catalyst from the reaction pool.

Sonogishira-, Heck-, and Suzuki-type coupling

Beletskaya *et al.* reported Sonogishira-type reactivity when coupling B-iodo-carboranes and acetylene derivatives in the presence of CuI and $[Pd(PPh_3)_2Cl_2]$ as catalysts and pyrrolidine as the solvent, Fig. 7.[42] The push to develop mild transmetallation reagents extended to B–C bond formation through Heck coupling of olefins, Fig. 7.[52] However, 2-vinylpyridine, butyl acrylate and acrylonitrile did not react, presumably due to slow coordination of the olefins to Pd. This work features the use of a Pd(II) palladacycle (Herrmann's catalyst) as a precatalyst to generate the catalytically active Pd(0) species. This was found to greatly increase the product yield by extending the lifetime of the catalyst system and points to a long standing problem with catalyst stability during carborane cross-coupling.

Interest in bench-stable transmetallation agents led to the development of cross-coupling with aryl boronic acid nucleophiles.[53a–c]

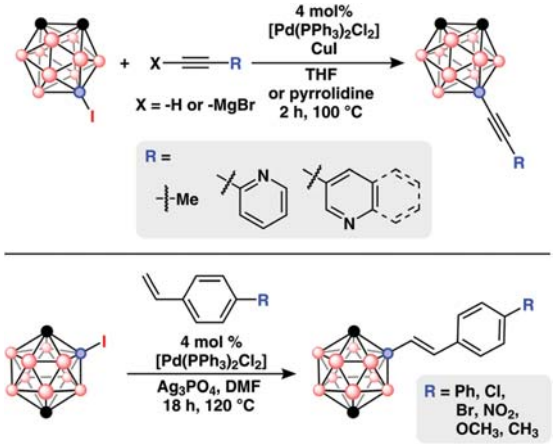

Fig. 7 (top) Pd-Catalyzed Sonogishira and Kumada cross-coupling of acetylenes with 9-I-*o*-$C_2B_{10}H_{11}$. (bottom) Pd-Catalyzed Heck cross-coupling of styrenes with 2-I-*p*-$C_2B_{10}H_{11}$.

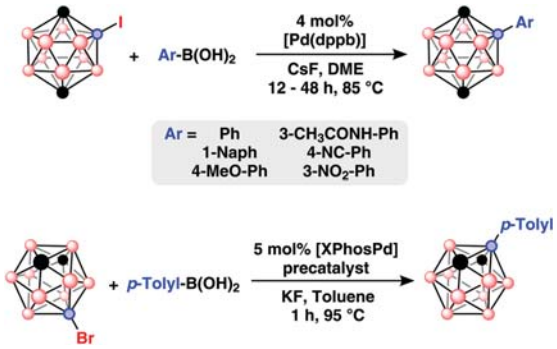

Fig. 8 (top) Pd-Catalyzed Suzuki cross-coupling of arylboronic acids with 2-I-*p*-$C_2B_{10}H_{11}$. (bottom) Pd-Catalyzed "cage-walking" and Suzuki cross-coupling of *p*-tolylboronic acid with 9-Br-*m*-$C_2B_{10}H_{11}$ to produce 2-*p*-tolyl-*m*-$C_2B_{10}H_{11}$.

Cross-coupling of aryl boronic acids was reported with 2-I-*p*-$C_2B_{10}H_{11}$ in the presence of CsF and Pd_2dba_3/dppb, Fig. 8.[53a] Suzuki cross-coupling of $PhB(OH)_2$ with 9-I-*m*-$C_2B_{10}H_{11}$ and 2-I-*o*-$C_2B_{10}H_{11}$ was also reported using $[Pd(PPh_3)_4]$ as the catalyst and K_2CO_3 as a base in toluene.[53b,c] Importantly, these cross-coupling reactions were demonstrated using arylboronic acids (4-NO_2, 3-NO_2, 3-CN, 3-CHO) that are not compatible with the previously mentioned Kumada and Neigishi reaction conditions.[53c] More recently, the Suzuki coupling of *p*-tolyl boronic acid with 9-Br-*m*-$C_2B_{10}H_{11}$ produced 2-*p*-tolyl-*m*-$C_2B_{10}H_{11}$ *via* the "cage-walking" isomerization mechanism, *vide infra*. These Suzuki cross-coupling reactions employ inorganic bases such as F^- or OH^- to facilitate the transmetallation step,[54] but these bases are strong nucleophiles that can lead to deboronation of *o*- and *m*-$C_2B_{10}H_{11}$ during cross-coupling.[51,53c]

Metal-catalyzed B–C coupling reactions with metallaboranes

In addition to carboranes, polyhedral boranes with transition metals as vertices are known to participate in halogenation reactions. Examples of metal-catalyzed cross-coupling also extend to various iodinated metallaboranes, heteroboranes, and anionic *closo*-borates. Many of these reactions feature cross-coupling of B–I bonds to form B–C bonds using methods similar to those reported for the neutral carboranes. Among the many metallacarboranes reported, metal bis(dicarbollide)s have garnered the most attention due to their simple preparation, high stability and redox activity.[55,56] Metal bis(dicarbollide)s can be prepared by deboronation of carborane and the subsequent reaction of the resulting *nido*-carborane with a metal salt precursor. Metal-catalyzed cross-coupling can be applied in two ways to metal bis(dicarbollide) synthesis. First, B-iodo-carborane can be functionalized and deboronated, then the resulting dicarbollides can be assembled from the functionalized *nido*-carboranes.[11,57,58] Second, iodinated metal bis(dicarbollides) can be subjected to Kumada and Neigishi coupling to form B–C bonds, Fig. 9.[59–62] Cross-coupling of $[8\text{-I-}3\text{-}3'\text{-Co}(1,2\text{-}C_2B_9H_{10})(1',2'\text{-}C_2B_9H_{11})]^{1-}$ with alkynes under Sonogishira conditions produced a tethered dicarbollide through an intramolecular B–H activation.[60,62]

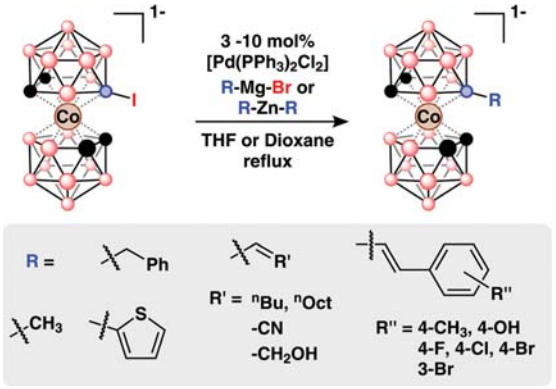

Fig. 9 Pd-Catalyzed Kumada and Neigishi cross-coupling with B-iodo-cobalt bis(dicarbollide), $[8\text{-I-}3,3'\text{-Co}(1,2\text{-}C_2B_9H_{10})(1',2'\text{-}C_2B_9H_{11})]^{1-}$.

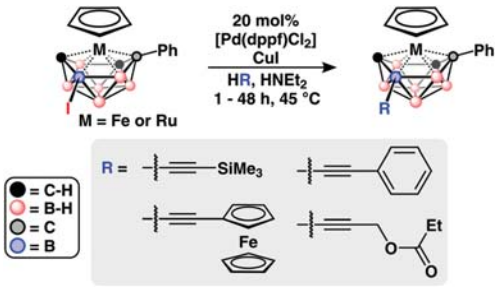

Fig. 10 Pd-Catalyzed Sonogishira cross-coupling of acetylenes with iodo-metallatricarbadecaborane.

A structurally similar metallaborane, the metallatricarbadecaboranyl, is also susceptible to Sonogishira coupling of trimethylsilyl, ester, and ferrocenyl acetylenes, Fig. 10.[63a,b]

Similar metal-catalyzed cross-coupling methods have been applied to less common metallaboranes. Neigishi coupling was demonstrated on the 6-vertex pentagonal-pyramidal *nido*-carboranes to attach ethynyl groups to the boron vertices.[64a,b] The resulting $[Cp^*Co(2,3\text{-}C_2B_4H_3)]$ compounds were assembled into dimeric and trimeric multi-metallic compounds to study the electronic coupling between the $[Cp^*Co(2,3\text{-}C_2B_4H_3)]$ metal-centers. Selective functionalization of different boron vertices of the $(2,3\text{-}C_2B_4H_3)$ ligands allowed subtle tuning of the electronic coupling between $[Cp^*Co(2,3\text{-}C_2B_4H_3)]$ metal centers.[64b] In that work, two $[Cp^*Co(2,3\text{-}C_2B_4H_3)]$ units were linked through a diethynyl bridge at two different boron vertices to form B(5)–B(5′) and B(7)–B(7′) bound dimers. Cyclic voltammetry revealed that the B(7)–B(7′) bound dimer has more Co–Co electronic communication than the B(5)–B(5′) bound dimer, further demonstrating the utility of precise B-vertex functionalization in the context of hierarchal design.

Metal-catalyzed B–C coupling reactions with polyhedral borane anions

Anionic polyhedral boranes are interesting compounds for applications in catalysis, as weakly coordinating anions, and as ionic materials such as ionic liquids, liquid crystals, or

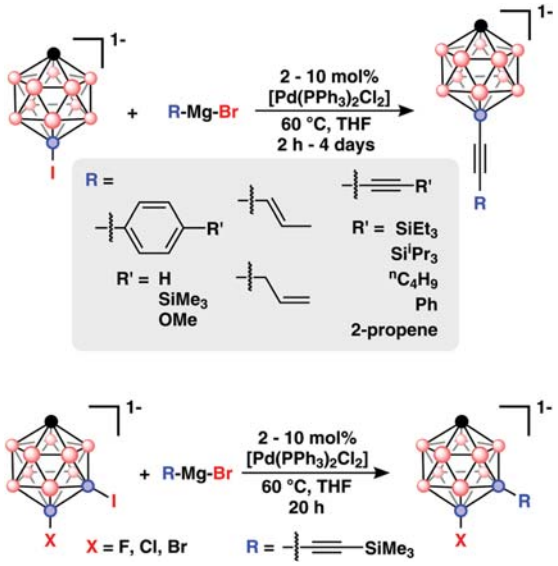

Fig. 11 (top) Pd-Catalyzed Kumada cross-coupling with $[12\text{-I-}CB_{11}H_{11}]^{1-}$. (bottom) Halide selective Pd-catalyzed Kumada cross-coupling with $[7\text{-I-}12\text{-X-}CB_{11}H_{10}]^{1-}$ (X = F, Cl, or Br).

electrolytes. The anionic $[CB_{11}H_{12}]^{1-}$ and dianionic $[B_{12}H_{12}]^{2-}$ boranes are isoelectronic with the neutral $C_2B_{10}H_{12}$ carboranes, and they exhibit higher reactivity towards electrophiles and halogens than the neutral carboranes.[65] Anionic polyhedral boranes also undergo Kumada and Neigishi coupling of alkyl, aryl and alkynyl groups in the presence of $[Pd(PPh_3)_2Cl_2]$ and $[Pd(PPh_3)_4]$ catalysts, Fig. 11.[66–74] The reaction conditions used for cross-coupling with anionic polyhedral boranes closely resemble those reported for the neutral carborane cross-coupling, although the poor solubility of the anionic polyhedral boranes in organic solvents such as Et_2O and toluene can lead to slower catalytic reactivity.

The 10- and 12-vertex monocarborane anions are also compatible with Grignard and organozinc reagents, which allows Pd-catalyzed cross-coupling of alkyl, alkenyl, alkynyl, and aryl groups. The 10-vertex $[CB_9H_{11}]^{1-}$ carborane anions bearing amino-, diazo-, sulfonium-, and carboxylate groups tolerate Pd-catalyzed cross-coupling with alkyl groups using hexylmagnesium bromide and hexylzinc chloride as nucleophiles. In addition to B–C bond formation, cross-coupling of the Pd catalyst phosphine ligand to form B–P bonds was observed when the alkylzinc or alkylmagnesium halide was not present in excess.[70,71]

Kumada reactions also function with the dianionic $[B_{10}H_9I]^{2-}$ and $[B_{12}H_{11}I]^{2-}$ as the cross-coupling electrophiles to produce B–C bound alkyl and phenyl groups, Fig. 12.[75–78] The metal-catalyzed B–C coupling reactions were adapted to the charge compensated 9-I-1,7-$(Me_2S)_2$-$B_{12}H_9$ with similar efficiency.[76] Contrary to previous reports, a CuI co-catalyst was not necessary to achieve a high yield; however, the Grignard reagents used in this study did not possess any β-hydrogens that can undergo β-hydride elimination as described previously.

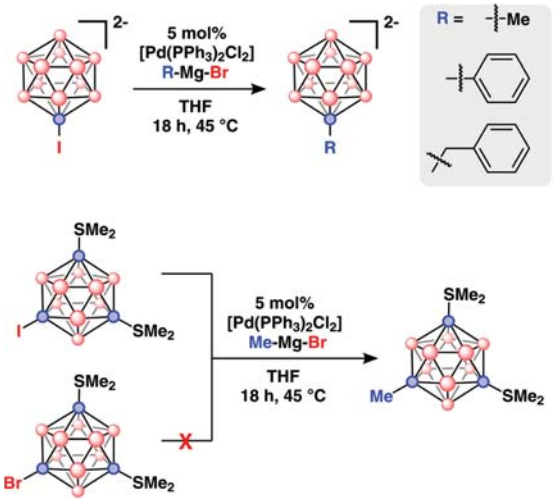

Fig. 12 (top) Pd-Catalyzed Kumada cross-coupling with $[I\text{-}B_{12}H_{11}]^{2-}$. (bottom) Halide selective Pd-catalyzed Kumada cross-coupling with the charge compensated 9-X-1,7-$(Me_2S)_2$-$B_{12}H_9$ (X = Br, or I).

Interestingly, *nido*-4-I-7-Me_3N-7-$CB_{10}H_{11}$ was successfully coupled with allylmagnesium bromide in the presence of $[Pd(PPh_3)_4]$ to yield *nido*-4-CH_2=$CHCH_2$-7-Me_3N-7-$CB_{10}H_{11}$.[66] This represents a rare example of cross-coupling using a *nido*-carborane since they are known to coordinate Pd in an η^5-fashion that can poison the metal catalyst.[79–81]

Lastly, cyanation of polyhedral boranes is of interest because the –CN group can be converted to other valuable synthons such as amides and amines. No direct electrophilic B–CN coupling methods have been reported, thus cyanation of polyhedral boranes proceeds *via* metal-catalyzed cross-coupling[37,82,83] or nucleophilic displacement of phenyliodonium reagents.[84] Notably, cyanation of $[12\text{-I-1-}CB_{11}H_{11}]^{1-}$ with CuCN can proceed at 250 °C in the absence of a Pd catalyst, albeit use of $Pd(PPh_3)_2Cl_2$ reduces the reaction time from 120 minutes to 15 min at 180 °C.[85] Likewise, in the early studies by Trofimenko at DuPont, researchers showed that perhalogenated B_{12}- and B_{10}-based clusters can undergo partial substitution with cyanide when these compounds were irradiated with high-power UV light.[86] No follow-up of this work has been reported since and the generality of photo-mediated polyhedral borate reactivity remains to be explored further.

Metal-catalyzed B–N, B–O, B–S, B–P bond formation

The reports of B–C bond formation establish that Pd-catalyzed cross-coupling can be applied to several types of polyhedral boranes and many of the strategies used in aryl halide cross-coupling can be adapted to polyhedral boranes. Progress in metal-catalyzed boron–heteroatom coupling in polyhedral boranes closely tracks with the development of new catalyst systems for aryl halide cross-coupling. In the past two decades Buchwald–Hartwig amination reactions have demonstrated a high substrate tolerance, and many effective ligand designs have been developed.[3,5] In comparison, most reports of Pd-catalyzed B–C coupling in polyhedral boranes employ triphenylphosphine or similar phosphines such as P(*o*-Tol)$_3$ and $Ph_2P(CH_2)_nPPh_2$ {n = 1–3}. The recent emergence of metal-catalyzed B–N, B–O, and B–P coupling reactions has been driven by advances in catalyst ligand design. While these catalysts were originally developed for aryl-based systems, the selection of these catalysts for boron clusters is not straightforward, further underscoring the distinct electronic and steric properties of polyhedral boranes, Fig. 13.

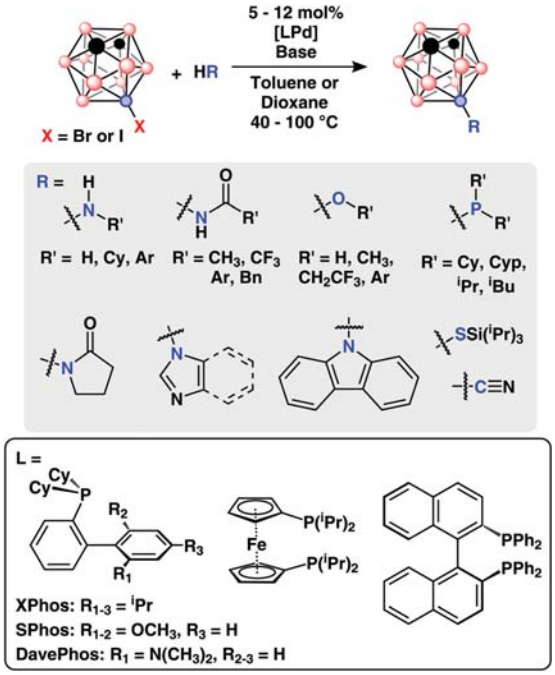

Fig. 13 (top) Pd-Catalyzed Buchwald–Hartwig reaction with 9-I-*m*-$C_2B_{10}H_{11}$; the inset shows commonly used phosphine ligands for metal-catalyzed B–N, B–O, and B–P coupling.

Metal-catalyzed B–N and B–O coupling

The first report of catalytic carborane aminations was demonstrated on 2-I-*p*-$C_2B_{10}H_{11}$ with imidazole, morpholine, and aromatic amines using Pd_2dba_3/BINAP as the catalyst and Na^{t}BuO as a base.[87] Coincidently, B–OH coupling was observed as a significant by-product of these reactions which likely formed due to residual moisture present in the reagents (base or solvent). This report also examined the efficacy of other catalyst ligands such as PR_3, IMes, and dialkyl biaryl phosphines and found that they were also capable of catalyzing B–N coupling, albeit with much lower yields. Later, the catalytic amidation of several B-iodo-$C_2B_{10}H_{11}$ isomers was reported using the dialkyl biaryl phosphine (DavePhos) and K_3PO_4 as the base.[88]

These works illuminate the critical role of the phosphine ligand in facilitating metal-catalyzed B–N coupling. When BINAP is used, a strong base (NaH) and day-long reaction times are required, whereas using DavePhos allows for a milder

base (K_3PO_4) and only 2 hour reaction times. More importantly, a screening of dialkyl biaryl phosphines revealed that di^{t}butyl biaryl phosphines were particularly ineffective and it likely explains why the dialkyl biaryl phosphines examined by Beletskaya were not as effective as BINAP in amination reactions. Using the dicyclohexyl biaryl phosphines, SPhos and XPhos, allowed B–N and B–O coupling of B-bromo-carboranes with a diverse set of coupling partners.[37,89] In order for B-bromo-carborane cross-coupling to occur it was important for the Pd precursor and phosphine ligand to be deployed as a precatalyst complex instead of using separate Pd(0) and phosphine sources.[37] A similar dependence on the catalyst precursor was observed in Heck coupling of styrenes with 2-I-*p*-$C_2B_{10}H_{11}$, *vide supra*.[52]

Pd-Catalyzed B–O coupling reactions are operationally similar to B–N amination and amidation reactions. When using the BINAP ligand a strong base was required which limited the substrate scope to carboranes that are resistant to deboronation.[90] In contrast, using SPhos allowed B–O coupling at the B(3) position (the position most susceptible to deboronation by strong nucleophiles) of 3-Br-*o*-$C_2B_{10}H_{11}$.[37] Moreover, the B–OH coupling reaction occurs in a 1 : 1 mixture of 1,4-dioxane : H_2O, and these conditions can be further adapted to B–CN coupling using $K_4[Fe(CN)_6]$ as a mild CN^- source, *vide supra*.[37]

Metal-catalyzed B–P and B–S cross-coupling

Forming boron–heteroatom bonds allowed the study of carboranes as tuneable functional groups. Although there are examples of B–P bond formation in polyhedral boranes, these routes require high temperatures or multi-step synthesis. The first Pd-catalyzed B–P coupling was observed *via* B–H activation of $[B_{10}H_{10}]^{2-}$ and $[B_{12}H_{12}]^{2-}$ by $[Pd(PMe_2Ph)Cl_2]$ which exchanged a B–H hydride for a PMe_2Ph ligand.[91] The resulting product was a mixture of mono- and disubstituted charge compensated phosphonium boranes, $[1\text{-}PMe_2\text{-}Ph\text{-}B_{12}H_{11}]^{1-}$ and 1,7-$(PMe_2Ph)_2$-$B_{12}H_{10}$. Similar reactions with $[Pd(SMe_2)Cl_2]$ produced sulfonium boranes (1,7-$(Me_2S)_2$-$B_{12}H_{10}$).[91]

The first metal-catalyzed B–P cross-coupling in polyhedral boranes was observed as a by-product in Neigishi reactions when a 10-vertex B-iodo-carborane, $[12\text{-I-}1\text{-COOH-}1\text{-}CB_9H_8]^{1-}$, was coupled with a PCy_3 ligand producing the zwitterionic 12-PCy_3-1-COOH-1-CB_9H_8.[70] Later, metal-catalyzed B–P cross-coupling with neutral carboranes was demonstrated between 9-I-*m*-$C_2B_{10}H_{11}$ and diphenylphosphine using a Pd_2dba_3/DIPPF catalyst system.[92] As with previous reports that use Pd_2dba_3 the reaction was sluggish with a 36 hour reaction time at 120 °C. Whether or not the resulting carboranyl phosphines further catalyzed the consumption of 9-I-*m*-$C_2B_{10}H_{11}$ was undetermined. The B-bound carboranyl phosphines were much better electron donors than the C-bound isomers as determined from the decreased ν[CO] in *trans*-$Rh(PR_3)_2(CO)Cl$, again showcasing the electron donating effects of bonding through the boron vertices of carboranes. These studies established the electron donating effects of the 9-*meta*-carboranyl substituent in the context of phosphine ligands and demonstrated that this substituent is more electron-donating than the majority of alkyl-based functional groups currently available.

B–S coupling *via* metal-catalyzed cross-coupling is a relatively new addition to the polyhedral borane chemists' toolbox.[93] This is because polyhedral borane B–H vertices can be converted to B–S groups through electrophilic routes.[94] However, this limits the study of thio-carboranes to the vertices susceptible to electrophilic substitution. Pd-Catalyzed cross-coupling of B-iodo-carboranes with $HSSi(^iPr)_3$ enables installation of a protected thiol group at electron-rich and electron-poor boron vertices.[93] Self-assembled monolayers of 3-SH-*o*-$C_2B_{10}H_{11}$ and 9-SH-*o*-$C_2B_{10}H_{11}$ were deposited on gold and the static water contact angle of the SAMs was measured. The 3-SH-*o*-$C_2B_{10}H_{11}$ SAM produced a contact angle of 80° *versus* the 9-SH-*o*-$C_2B_{10}H_{11}$ SAM contact angle of 62°. This difference in contact angle is attributed to the orientation of the acidic C–H protons of 9-SH-*o*-carborane SAMs forming hydrogen bonds with the water droplet which leads to a smaller contact angle. There are a number of unexplored synthetic opportunities remaining for a broader utilization of metal-catalysed cross-coupling for the synthesis of boron clusters with appended thiol and other chalcogen units that would be valuable as building blocks for materials assembly.

Mechanistic considerations of metal-catalyzed polyhedral borane cross-coupling

Choosing a catalyst system

Clearly, new catalyst systems beyond $Pd(PPh_3)_n$ $\{n = 1\text{–}3\}$ were required to facilitate boron–heteroatom metal-catalyzed cross-coupling, and an effort was made to use phosphine ligands which can enforce a *cis*-coordination at the Pd-center. Phosphine ligands such as dppb, DIPPF, BINAP, and XantPhos were found to facilitate a variety of B–N, B–O, and B–P bond forming reactions.[37,87,88,90,92,95] Notably, these works feature a broader catalyst screen which showed that electron-rich ligands such as dialkyl biaryl phosphines, PCy_3, P^tBu_3, and IMes have some activity towards B–N and B–O bond formation.[87] Furthermore, we demonstrated that, with an appropriately electron-rich ligand, B-bromo-carboranes can be excellent cross-coupling substrates.[37] This advance is also attributed to the use of Pd(II) palladacycle precatalysts, which deploy the active catalyst species without releasing inhibitory ligands such as dba.[96,97] The dba ligand is known to coordinate to palladium phosphine complexes thereby supressing the rate of oxidative addition to aryl halides. A similar effect is likely in play during cross-coupling chemistry when halo-carboranes are used as coupling partners and it would work against the presumably slow oxidative addition into B–Br bonds of B-bromo-carboranes.[37]

Oxidative addition and transmetallation

As mentioned before, most polyhedral borane cross-couplings use B-iodo-boranes, while B-bromo- and B-chloro-boranes, until recently, have been viewed as too unreactive. Attempts at isolating oxidative addition compounds of B-iodo-carborane with Pd complexes were unsuccessful, presumably due to the equilibrium strongly disfavouring oxidative addition.[34] Surrogate oxidative

addition complexes were prepared with Pt, and a pseudo-oxidative addition Pd–Hg bimetallic complex provided clues about the possible nature of catalytically relevant intermediates[98]

The calculated Connolly volume of carboranes is ~30% larger than that of benzene and they are spherical, as opposed to planar aromatic molecules.[15,18,99] This means that carboranes are a much more sterically demanding substrate at the catalyst site than their planar aromatic analogues. Several reports of Pd-catalyzed amination of carboranes feature similar dialkylbiaryl phosphine ligands albeit with dramatically different results.[37,87–89] Phosphines with –^{t}Bu groups showed poor conversion of B–I to B–N bonds,[87] whereas phosphines with cyclohexyl groups gave complete conversion in a matter of hours instead of days.[37,88,89]

Although electron-rich dialkyl biaryl phosphines have been used as ligands in B-bromo-carborane Pd-catalyzed cross-coupling, these Pd catalysts have not been able to activate the B–Cl bond of B-chloro-carboranes. Despite the inability to perform oxidative addition into B–Cl bonds, stoichiometric studies of the above mentioned Hg–Pd bimetallic complex show that B-chloro-carboranes can undergo Pd-catalyzed transmetallation to form B–N bonds.[98] This is based on a proposed oxidative addition complex that could form upon extrusion of Hg from the Hg–Pd bimetallic complex. The proposed oxidative addition complex quickly reductively eliminates B-chloro-carborane. However, in the presence of excess nucleophile, transmetallation can occur resulting in the formation of a B–N bond. This suggests that the oxidative addition complex formed with B-chloro-carborane is unstable and quickly reductively eliminates the B-chloro-carborane unless it is trapped by a nucleophile.

Catalyst systems that can perform oxidative addition into C-Br and C–Cl bonds exhibit much higher metal-catalyzed cross-coupling efficiency than aryl iodides. It is believed that weaker Pd–Br and Pd–Cl bonds enable faster transmetallation at the expense of slower oxidative addition rates. The lack of isolable carborane oxidative addition complexes has made the study of carborane transmetallation rates challenging.[34] Despite this, slow transmetallation with B-iodo-carboranes has been implicated in several cross-coupling reactions. As mentioned above, Heck coupling of styrenes bearing electron withdrawing groups with 2-I-*p*-$C_2B_{10}H_{11}$ required much longer reaction times and some did not participate in the reaction at all.[52]

Isomerization *via* cage-walking

The use of dialkyl biaryl phosphine ligands for Pd-catalyzed cross-coupling of B-bromo-carboranes led to the recent discovery of a unique isomerization mechanism, ''cage-walking'', similar to the chain-walking isomerization observed in carbon-based molecules.[89] The ''cage-walking'' isomerization enables metal-catalyzed cross-coupling to occur at vertices far from the initial location of B–Br bond activation, Fig. 15. This ''off-cycle'' mechanism is currently the only way to attach functional groups at the B(5) and B(4) positions of *meta*-carborane without relying on thermal isomerization processes. Whether the ''cage-walking'' mechanism was operative depended on the steric hindrance produced at the Pd metal center by the phosphine ligand. Using the bulkier XPhos ligand produced significantly more ''cage-walking'' regioisomers than the smaller DavePhos and SPhos ligands which showed cross-coupling mostly at the B(9) position.

Besides relying on ligand sterics, the ''cage-walking'' regioisomer distribution can be shifted from favouring B(9) to favouring B(2) substitution by changing the steric profile at the nucleophilic position of the cross-coupling partner. In a reactivity comparison between two phenols, 3,5-dimethylphenol and 2,6-dimethylphenol, the more sterically hindered 2,6-dimethylphenol yielded the B(2) isomer as the major product while the less hindered 3,5-dimethylphenol yielded an equal distribution of regioisomers.

The isomer distribution is believed to depend on the trans-metallation step, where steric bulk at the Pd center impedes transmetallation and allows the ''cage-walking'' process to generate more reactive B-bromo-carborane isomers, Fig. 14. Since the carboranyl fragment has an anisotropic electron distribution, as the carborane ''cage-walks'' to electron deficient vertices, B(2) *vs.* B(9), it produces an increasingly cationic Pd metal center that is more likely to overcome the steric repulsion between the catalyst complex and the nucleophilic cross-coupling partner.

Metal-catalyzed cross-coupling of polyhalogenated boron clusters

Aside from their unique 3D aromaticity and chemical stability, the spherical shape of polyhedral boranes presents a molecular scaffold for building three-dimensionally defined constructs. For example, functionalization of three vertices that share a common face creates a tripodal architecture that is not easily accessible with typical organic building blocks. Interest in creating polysubstituted polyhedral boranes led to the exploration of Pd-catalyzed cross-coupling methods for attaching several functional groups onto polyhalogenated boranes.

Pd-Catalyzed cross-coupling of disubstituted carboranes was first reported for the Kumada cross-coupling of B-diiodo-carboranes, I_2-$C_2B_{10}H_{10}$,[41,48] then extended to anionic[69,72,73] and dianionic boranes.[76,85] Later Hawthorne and co-workers reported the Pd-catalyzed methylation of hexaiodo cobalt bis(dicarbollide) with MeMgBr to produce hexamethyl cobalt bis(dicarbollide), Fig. 16.[59] The most metal-catalyzed cross-coupling reactions performed on a single polyhedral borane substrate was reported for the $[1\text{-H-}CB_9I_9]^{1-}$ anion where all nine B–I bonds were cross-coupled with methyl-magnesium bromide in the presence of $[Pd(PPh_3)_2Cl_2]$ over the course of 10 days.[100] These examples demonstrate the feasibility of functionalizing an entire face of a polyhedral borane using cross-coupling reactions. Such Pd-catalyzed polysubstitution was applied to B-tetraiodo-*ortho*-carborane (8,9,10,12-I_4-*o*-$C_2B_{10}H_8$) to synthesize 8,10-Ph_2-9,12-I_2-*o*-$C_2B_{10}H_8$ and 8,9,10,12-$(allyl)_4$-*o*-$C_2B_{10}H_8$. Noteworthy was the selective arylation of the B(8) and B(10) vertices when using phenylmagnesium bromide as a cross-coupling partner.[101] This selectivity was attributed to the steric bulk of the phenyl substituents which may have prevented functionalization of the more sterically hindered B(9) and B(12) vertices. Similar steric restrictions were observed for the Pd-catalyzed cross-coupling of the hexaiodo monocarborane anion, $[1\text{-Ph-}7,8,9,10,11,12\text{-}I_5\text{-}CB_{11}H_5]^-$, where cross-coupling occurred at the less sterically congested B(7–11) positions, but not at the B(12) position, to yield $[1\text{-Ph-}7,8,9,10,11\text{-}(tolyl)_5\text{-}12\text{-I-}CB_{11}H_5]^-$.[102]

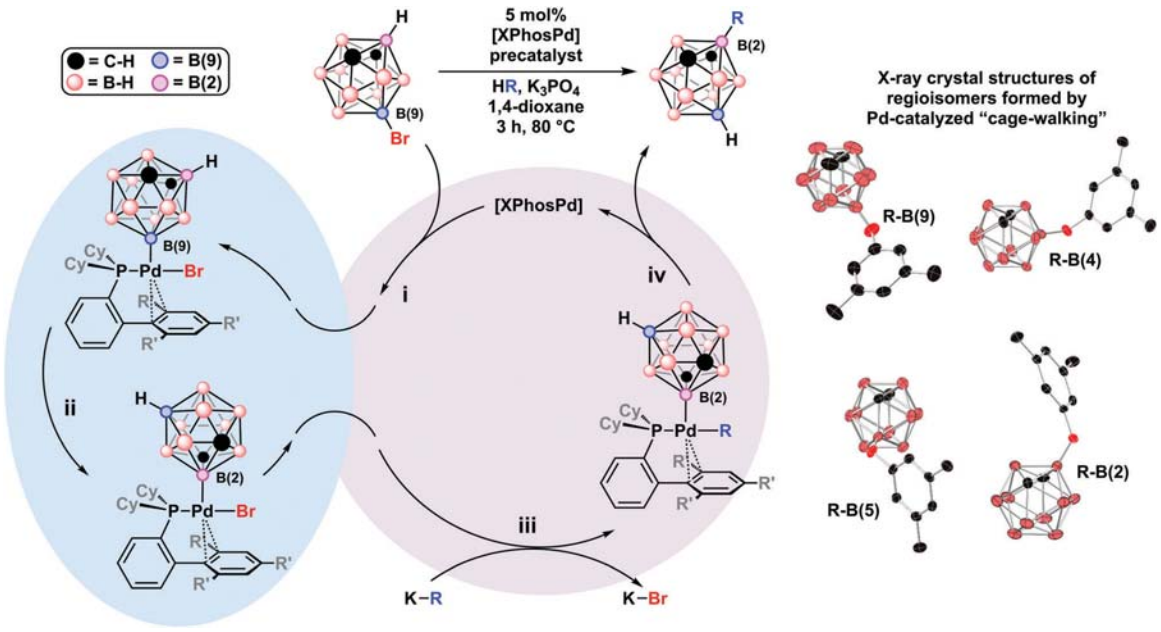

Fig. 14 Proposed cross-coupling cycle for the formation of ''cage-walking'' products, Step (i) oxidative addition, Step (ii) ''cage-walking'' isomerization, Step (iii) transmetallation, Step (iv) reductive elimination. X-ray crystal structures of ''cage-walking'' regioisomers of B-3,5-dimethylphenoxy-*m*-$C_2B_{10}H_{11}$.

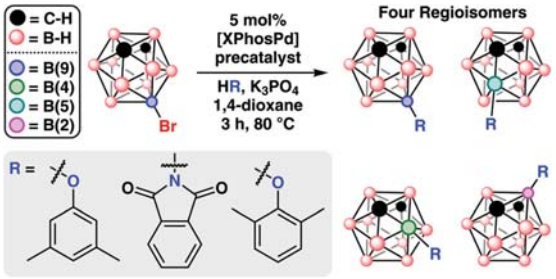

Fig. 15 Four regioisomers of R-*meta*-carborane produced by Pd-catalyzed ''cage-walking''.

Recently we demonstrated the first example of a sequential metal-catalyzed B–C coupling at a B–I vertex followed by B–O coupling at a B–Br vertex by using different phosphine ligands for Pd-catalyzed B–I and B–Br bond activation, Fig. 16.[37] In this work [$Pd(PPh_3)_2Cl_2$] was used to selectively perform Kumada B–C coupling at the B–I vertex of 9-I-10-*B*-*m*-$C_2B_{10}H_{10}$ to produce 9-Et-10-Br-*m*-$C_2B_{10}H_{10}$ which was then subjected to Buchwald–Hartwig B–O coupling at the B–Br vertex using [SPhosPd] to produce 9-Et-10-(O-3,5-dimethylphenoxy)-*m*-$C_2B_{10}H_{10}$.

An alternative approach to heterodifunctionalization may be realized by relying on a chelate effect to limit the number of functional groups that get installed. Such a chelate effect is believed to limit Pd-catalyzed B–O coupling of OH^- to a single B–Br vertex of 9,10-Br_2-*m*-$C_2B_{10}H_{10}$ to produce the monohydroxylated compound 9-Br-10-OH-*m*-$C_2B_{10}H_{10}$ whereas coupling of 3,5-dimethylphenolate afforded the disubstituted product,

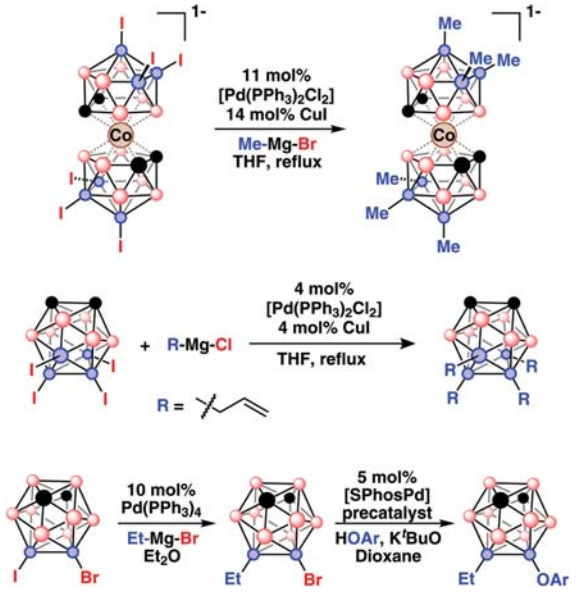

Fig. 16 (top) Pd-Catalyzed methylation of [3,3′-*commo*-(8,9,12-I_3-$CoC_2B_9H_8)_2$]. (middle) Pd-Catalyzed alkylation of 8,9,10,12-I_4-*o*-$C_2B_{10}H_8$ to produce 8,9,10,12-(allyl)$_4$-*o*-$C_2B_{10}H_8$. (bottom) Sequential Pd-catalyzed B–I then B–Br bond cross-coupling of 9-I-10-Br-*m*-$C_2B_{10}H_{10}$.

9,10-(O-3,5-dimethylphenoxy)$_2$-*m*-$C_2BM_{10}H_{10}$.[37] This difference in reactivity may also be due to the steric bulk of the phenolate, which may reduce the propensity towards chelating the Pd center, and the possible deprotonation of the hydroxyl group of

9-Br-10-OH-*m*-$C_2B_{10}H_{10}$ may lead to a stronger chelate effect. Alternatively, chelation of a metal catalyst to a polyhedral borane can allow functionalization of B–H vertices adjacent to the chelating moiety. This approach was used to install five aryl groups onto $[1\text{-COOH-}CB_{11}H_{11}]^{1-}$ at B–H vertices adjacent to the carboxylic acid directing group *via* metal-catalyzed B–H activation.[29] Similar metal-catalyzed B–H polyfunctionalization strategies were reported for 10- and 12-vertex polyhedral boranes.[24,31,33]

Conclusions and outlook

Metal-catalyzed cross-coupling is emerging as a powerful method for installing functional groups at the boron vertices of polyhedral boranes. A large body of work has demonstrated that cross-coupling strategies are applicable to several classes of polyhedral boranes.[103] Subsequently, metal-catalyzed cross-coupling of polyhedral boranes enabled their use in materials science, organometallic chemistry, surface science, and medicinal chemistry, Fig. 17. For example, the vertex specificity of metal-catalyzed cross-coupling allowed the synthesis of a linear cobalt bis(dicarbollide) used to construct metal–organic frameworks with high methane uptake capacity.[11] Additionally, the vertex specific cross-coupling was used to control the dipole moment orientation of surface adsorbed carborane thiols and carboxylic acids on Au and Ge surfaces, respectively.[93,104] Using polyhedral boranes as surface ligands allowed nearly defect free self-assembly and tuning of surface properties such as work function and wettability. Similarly, the vertex specific cross-coupling of B-iodo-carboranes enabled synthesis of a panel of carborane-based anesthetics (''boronicaines'') analogous to lidocaine to study their molecular docking characteristics relative to lidocaine and an adamantyl-based analog. Noteworthy was the ability to control the duration and efficacy of the boronicaine isomers which surpassed those of their phenyl- and adamantyl-based analogues.[105]

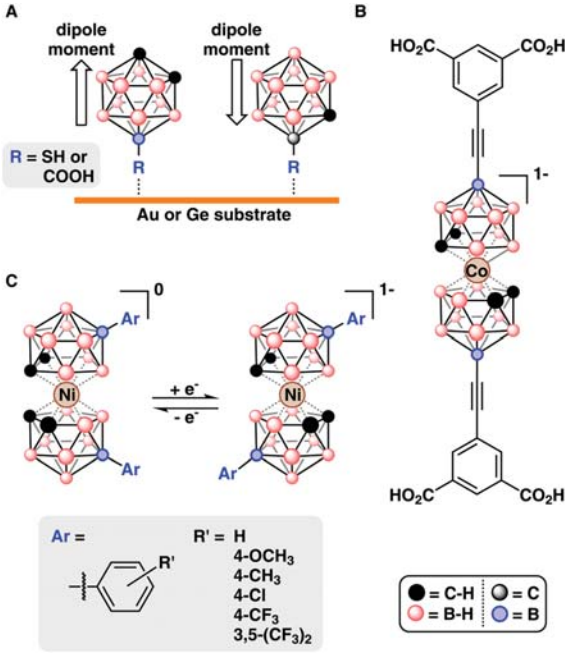

Fig. 17 (A) Functionalized *o*-carborane thiols and carboxylic acids used for self-assembled monolayers on gold and germanium surfaces, respectively. (B) A linear cobalt bis(dicarbollide) used for constructing metal–organic frameworks. (C) Arylated nickel bis(dicarbollide)s used as redox shuttles in dye-sensitized solar cells.

Furthermore, the broad functional group tolerance of metal-catalyzed cross-coupling allowed the study of structure–activity relationships in arylated nickel bis(dicarbollide) redox shuttles in dye-sensitized solar cells. Researchers showed that tuning the inductive effects of the aryl groups attached to the cobalt bis(dicarbollide) cage can tune the electrochemical $Ni^{III/IV}$ redox couple and the resulting open circuit voltage of dye-sensitized solar cells.[57] Recently, our group demonstrated control of the linkage isomerism of a bis(*o*-carborane) ligand to preferentially bind in a κ^2-B,C-binding mode in phosphorescent Pt(II) coordination complexes by addition of ethyl groups to bis(*o*-carborane) to form B-tetraethyl-bis(*o*-carborane), 9,9′,12,12′-Et_4-1,1′-bis-(*o*-$C_2B_{10}H_9$).[106] Such differences in the κ^2 binding mode of bis(*o*-carborane) (κ^2-B,C- *vs.* κ^2-C,C-bound) manifest as subtle differences in the electrochemical redox potential and luminescent properties of Pt(II) coordination complexes.[107]

Many of the new cross-coupling methods for polyhedral boranes leverage the growing number of aryl halide cross-coupling catalysts to generate B–C, B–N, B–O, B–S, and B–P bonds. These examples of metal-catalyzed boron–heteroatom coupling may provide clues in the future to generate B–B and B–Si bonds comparable to the C–B and C–Si bonds reported for aryl halides. Notably, while carborane species with exopolyhedral B–B bonds were recently synthesized *via* a B–H activation route,[108] B–Si analogues have remained elusive. Progress in these topics opens opportunities for preparing polyhedral borane nucleophilic cross-coupling partners[108] and the possibility of cross-coupling polyhedral boranes with each other providing access to a new class of linked polyboranes. Another outstanding challenge in polyhedral borane cross-coupling chemistry is the inactivity of B–Cl bonds and B–OTf bonds toward oxidative addition. And a new question arises: what type of catalyst system has the right electronic and steric features to activate B–Cl and B–OTf bonds? We note that Ni-based catalyst systems have been recently developed to activate strong bonds in organic substrates (*e.g.* C–N, C–O) and these and/or similar methods could be applied to solve this issue.[109–114] Furthermore, metal-mediated photoredox catalysis on boron cluster electrophiles has not been reported, albeit such reaction manifolds are well documented in the 2D aromatic molecule literature.[115]

It is important to recognize that B-halo-carboranes are similar, but different, from their 2D aromatic aryl halides. In the context of metal-catalyzed cross-coupling the spheroidal steric bulk and stronger B–X (X = Cl, Br, I) bonds differentiate polyhedral borane cross-coupling from hydrocarbon cross-coupling. Although this difference in reactivity stymied polyhedral borane cross-coupling, it also gives rise to functionalization strategies that are not readily accessible in hydrocarbon chemistry. Namely, the

orthogonal reactivity toward B–X bonds with different catalysts and ''cage-walking'' isomerization open avenues to new boron cluster molecules and advance our ability to use polyhedral boranes as scaffolds for unique three-dimensionally defined building blocks.

Conflicts of interest

There are no conflicts to declare.

Acknowledgements

A. M. S. thanks the UCLA Department of Chemistry and Biochemistry for start-up funds, 3M for a Non-Tenured Faculty Award, the Alfred P. Sloan Foundation for a Fellowship in Chemistry, Research Corporation for Science Advancement (RCSA) for a Cottrell Scholar Award, and the National Institutes of Health (NIH) for a Maximizing Investigators Research Award (MIRA, R35GM124746). R. M. D. is grateful for support from the Department of Defense through the National Defense Science and Engineering Graduate Fellowship. We thank all past and present co-workers at UCLA for contributing to the work highlighted in this article.

Notes and references

1 *Metal-Catalyzed Cross-Coupling Reactions*, ed. A. de Meijere and F. Diederich, Wiley-VCH Verlag GmbH, Weinheim, Germany, 2004.
2 C. C. C. Johansson Seechurn, M. O. Kitching, T. J. Colacot and V. Snieckus, *Angew. Chem., Int. Ed.*, 2012, **51**, 5062–5085.
3 P. Ruiz-Castillo and S. L. Buchwald, *Chem. Rev.*, 2016, **116**, 12564–12649.
4 A. Biffis, P. Centomo, A. Del Zotto and M. Zecca, *Chem. Rev.*, 2018, **118**, 2249–2295.
5 J. F. Hartwig, *Acc. Chem. Res.*, 2008, **41**, 1534–1544.
6 J. Twilton, C. C. Le, P. Zhang, M. H. Shaw, R. W. Evans and D. W. C. MacMillan, *Nat. Rev. Chem.*, 2017, **1**, 0052.
7 I. P. Beletskaya and V. P. Ananikov, *Chem. Rev.*, 2011, **111**, 1596–1636.
8 R. B. King, *Chem. Rev.*, 2001, **101**, 1119–1152.
9 L. I. Zakharkin and I. V. Pisareva, *Izv. Akad. Nauk SSSR, Ser. Khim.*, 1978, 252.
10 R. F. Heck, *J. Am. Chem. Soc.*, 1968, **90**, 5546–5548.
11 R. D. Kennedy, D. J. Clingerman, W. Morris, C. E. Wilmer, A. A. Sarjeant, C. L. Stern, M. O'Keeffe, R. Q. Snurr, J. T. Hupp, O. K. Farha and C. A. Mirkin, *Cryst. Growth Des.*, 2014, **14**, 1324–1330.
12 R. N. Grimes, *Angew. Chem., Int. Ed.*, 1993, **32**, 1289–1290.
13 I. H. A. Badr, M. Diaz, M. F. Hawthorne and L. G. Bachas, *Anal. Chem.*, 1999, **71**, 1371–1377.
14 J. C. Axtell, L. M. A. Saleh, E. A. Qian, A. I. Wixtrom and A. M. Spokoyny, *Inorg. Chem.*, 2018, **57**, 2333–2350.
15 M. Scholz and E. Hey-Hawkins, *Chem. Rev.*, 2011, **111**, 7035–7062.
16 F. Issa, M. Kassiou and L. M. Rendina, *Chem. Rev.*, 2011, **111**, 5701–5722.
17 Z. J. Leśnikowski, *J. Med. Chem.*, 2016, **59**, 7738–7758.
18 S. Ristori, J. Oberdisse, I. Grillo, A. Donati and O. Spalla, *Biophys. J.*, 2005, **88**, 535–547.
19 M. Otsuka, R. Takita, J. Kanazawa, K. Miyamoto, A. Muranaka and M. Uchiyama, *J. Am. Chem. Soc.*, 2015, **137**, 15082–15085.
20 V. I. Bregadze, *Chem. Rev.*, 1992, **92**, 209–223.
21 Z. Qiu, *Tetrahedron Lett.*, 2015, **56**, 963–971.
22 E. L. Hoel and M. F. Hawthorne, *J. Am. Chem. Soc.*, 1974, **96**, 6770–6771.
23 M. G. L. Mirabelli and L. G. Sneddon, *J. Am. Chem. Soc.*, 1988, **110**, 449–453.
24 Y. Quan, Z. Qiu and Z. Xie, *Chem. – Eur. J.*, 2018, **24**, 2795–2805.
25 S. Duttwyler, *Pure Appl. Chem.*, 2018, **90**, 733–744.
26 Y. Zhang, Y. Sun, F. Lin, J. Liu and S. Duttwyler, *Angew. Chem., Int. Ed.*, 2016, **55**, 15609–15614.
27 H. Lyu, Y. Quan and Z. Xie, *Chem. – Eur. J.*, 2017, **23**, 14866–14871.
28 R. Cheng, B. Li, J. Wu, J. Zhang, Z. Qiu, W. Tang, S. L. You, Y. Tang and Z. Xie, *J. Am. Chem. Soc.*, 2018, **140**, 4508–4511.
29 F. Lin, J.-L. Yu, Y. Shen, S.-Q. Zhang, B. Spingler, J. Liu, X. Hong and S. Duttwyler, *J. Am. Chem. Soc.*, 2018, **140**, 13798–13807.
30 Y. Zhang, T. Wang, L. Wang, Y. Sun, F. Lin, J. Liu and S. Duttwyler, *Chem. – Eur. J.*, 2018, **24**, 15812–15817.
31 X. Liang, Y. Shen, K. Zhang, J. Liu and S. Duttwyler, *Chem. Commun.*, 2018, **54**, 9–12.
32 B. J. Eleazer, M. D. Smith and D. V. Peryshkov, *Organometallics*, 2016, **35**, 106–112.
33 B. J. Eleazer, M. D. Smith and D. V. Peryshkov, *J. Organomet. Chem.*, 2017, **829**, 42–47.
34 W. J. Marshall, R. J. Young and V. V. Grushin, *Organometallics*, 2001, **20**, 523–533.
35 K. J. Winberg, E. Mume, V. Tolmachev and S. Sjöberg, *J. Labelled Compd. Radiopharm.*, 2005, **48**, 195–202.
36 K. Ishita, A. Khalil, R. Tiwari, J. Gallucci and W. Tjarks, *Eur. J. Inorg. Chem.*, 2018, 2821–2825.
37 R. M. Dziedzic, L. M. A. Saleh, J. C. Axtell, J. L. Martin, S. L. Stevens, A. T. Royappa, A. L. Rheingold and A. M. Spokoyny, *J. Am. Chem. Soc.*, 2016, **138**, 9081–9084.
38 L. I. I. Zakharkin, A. I. I. Kovredov, V. A. A. Ol'shevskaya and Z. S. S. Shaugumbekova, *J. Organomet. Chem.*, 1982, **226**, 217–222.
39 L. I. Zakharkin, A. I. Kovredov, V. A. Ol'shevskaya, V. A. Ol and P. Constants, *Bull. Acad. Sci. USSR, Div. Chem. Sci.*, 1985, **34**, 809–812.
40 Z. Zheng, W. Jiang, A. A. Zinn, C. B. Knobler and M. F. Hawthorne, *Inorg. Chem.*, 1995, **34**, 2095–2100.
41 J. Li, C. F. Logan and M. Jones, *Inorg. Chem.*, 1991, **30**, 4866–4868.
42 I. P. Beletskaya, V. I. Bregadze, V. A. Ivushkin, P. V. Petrovskii, I. B. Sivaev, S. Sjöberg and G. G. Zhigareva, *J. Organomet. Chem.*, 2004, **689**, 2920–2929.
43 K. Tamao, K. Sumitani, Y. Kiso, M. Zembayashi, A. Fujioka, S. Kodama, I. Nakajima, A. Minato and M. Kumada, *Bull. Chem. Soc. Jpn.*, 1976, **49**, 1958–1969.
44 A. Zask and P. Helquist, *J. Org. Chem.*, 1978, **43**, 1619–1620.
45 M. S. Viciu, G. A. Grasa and S. P. Nolan, *Organometallics*, 2001, **20**, 3607–3612.
46 K. P. Anderson, H. A. Mills, C. Mao, K. O. Kirlikovali, J. C. Axtell, A. L. Rheingold and A. M. Spokoyny, *Tetrahedron*, 2018, DOI: 10.1016/j.tet.2018.11.040.
47 X. Yang, C. B. Knobler, Z. Zheng and M. F. Hawthorne, *J. Am. Chem. Soc.*, 1994, **116**, 7142–7159.
48 W. Jiang, C. B. Knobler, C. E. Curtis, M. D. Mortimer and M. Frederick Hawthorne, *Inorg. Chem.*, 1995, **34**, 3491–3498.
49 A. Herzog, S. S. Jalisatgi, C. B. Knobler, T. J. Wedge and M. F. Hawthorne, *Chem. – Eur. J.*, 2005, **11**, 7155–7174.
50 I. P. Beletskaya, V. I. Bregadze, V. A. Ivushkin, G. G. Zhigareva, P. V. Petrovskii and I. B. Sivaev, *Russ. J. Org. Chem.*, 2005, **41**, 1359–1366.
51 M. A. Fox and K. Wade, *J. Organomet. Chem.*, 1999, **573**, 279–291.
52 L. Eriksson, K. J. Winberg, R. T. Claro and S. Sjöberg, *J. Org. Chem.*, 2003, **68**, 3569–3573.
53 (*a*) L. Eriksson, I. P. Beletskaya, V. I. Bregadze, I. B. Sivaev and S. Sjoberg, *J. Organomet. Chem.*, 2002, **657**, 267–272; (*b*) L. I. Zakharkin, E. V. Balagurova and V. N. Lebedev, *Russ. J. Gen. Chem.*, 1998, **68**, 922–924; (*c*) Y. Endo, K. Aizawa and K. Ohta, *Heterocycles*, 2010, **80**, 369.
54 A. J. J. Lennox and G. C. Lloyd-Jones, *Angew. Chem., Int. Ed.*, 2013, **52**, 7362–7370.
55 I. B. Sivaev and V. I. Bregadze, *Collect. Czech. Chem. Commun.*, 1999, **64**, 783–805.
56 B. P. Dash, R. Satapathy, B. R. Swain, C. S. Mahanta, B. B. Jena and N. S. Hosmane, *J. Organomet. Chem.*, 2017, **849–850**, 170–194.
57 A. M. Spokoyny, T. C. Li, O. K. Farha, C. W. Machan, C. She, C. L. Stern, T. J. Marks, J. T. Hupp and C. A. Mirkin, *Angew. Chem., Int. Ed.*, 2010, **49**, 5339–5343.
58 A. V. Safronov, Y. V. Sevryugina, K. R. Pichaandi, S. S. Jalisatgi and M. F. Hawthorne, *Dalton Trans.*, 2014, **43**, 4969.
59 M. D. Mortimer, C. B. Knobler and M. F. Hawthorne, *Inorg. Chem.*, 1996, **35**, 5750–5751.
60 I. Rojo, F. Teixidor, R. Kivekäs, R. Sillanpää and C. Viñas, *J. Am. Chem. Soc.*, 2003, **125**, 14720–14721.
61 I. Rojo, F. Teixidor, C. Viñas, R. Kivekäs and R. Sillanpää, *Chem. – Eur. J.*, 2003, **9**, 4311–4323.

62 P. Farràs, D. Olid-Britos, C. Viñas and F. Teixidor, *Eur. J. Inorg. Chem.*, 2011, 2525–2532.
63 (*a*) R. Butterick III, P. J. Carroll and L. G. Sneddon, *Organometallics*, 2008, **27**, 4419–4427; (*b*) A. Perez-Gavilan, P. J. Carroll and L. G. Sneddon, *J. Organomet. Chem.*, 2012, **721–722**, 62–69.
64 (*a*) J. M. Russell, M. Sabat and R. N. Grimes, *Organometallics*, 2002, **21**, 4113–4128; (*b*) H. Yao, M. Sabat, R. N. Grimes, P. Zanello and F. Fabrizi de Biani, *Organometallics*, 2003, **22**, 2581–2593.
65 T. Jelínek, P. Baldwin, W. R. Scheidt and C. A. Reed, *Inorg. Chem.*, 1993, **32**, 1982–1990.
66 J. H. Morris, W. Henderson and V. A. Ol'shevskaya, *J. Chem. Soc., Dalton Trans.*, 1998, 1951–1959.
67 B. Grüner, Z. Janoušek, B. T. King, J. N. Woodford, C. H. Wang, V. Všetečka and J. Michl, *J. Am. Chem. Soc.*, 1999, **121**, 3122–3126.
68 A. Franken, C. A. Kilner, M. Thornton-Pett and J. D. Kennedy, *J. Organomet. Chem.*, 2002, **657**, 176–179.
69 M. Finze, *Inorg. Chem.*, 2008, **47**, 11857–11867.
70 B. Ringstrand, H. Monobe and P. Kaszynski, *J. Mater. Chem.*, 2009, **19**, 4805.
71 B. Ringstrand, P. Kaszynski, A. Januszko and V. G. Young, *J. Mater. Chem.*, 2009, **19**, 9204–9212.
72 A. Himmelspach and M. Finze, *J. Organomet. Chem.*, 2010, **695**, 1337–1345.
73 A. Himmelspach, G. J. Reiss and M. Finze, *Inorg. Chem.*, 2012, **51**, 2679–2688.
74 M. Hailmann, S. Z. Konieczka, A. Himmelspach, J. Löblein, G. J. Reiss and M. Finze, *Inorg. Chem.*, 2014, **53**, 9385–9399.
75 T. Peymann, C. B. Knobler and M. F. Hawthorne, *Inorg. Chem.*, 1998, **37**, 1544–1548.
76 R. G. Kultyshev, S. Liu, H. T. Leung, J. Liu and S. G. Shore, *Inorg. Chem.*, 2003, **42**, 3199–3207.
77 R. Bernard, D. Cornu, D. Luneau, D. Naoufal, J. P. Scharff and P. Miele, *J. Organomet. Chem.*, 2005, **690**, 2745–2749.
78 E. Rzeszotarska, I. Novozhilova and P. Kaszyński, *Inorg. Chem.*, 2017, **56**, 14351–14356.
79 L. Warren Jr and M. Hawthorne, *J. Am. Chem. Soc.*, 1968, **90**, 4823–4828.
80 S. A. Jasper, J. C. Huffman and L. J. Todd, *Inorg. Chem.*, 1995, **34**, 6430–6439.
81 S. A. Jasper, J. C. Huffman and L. J. Todd, *Inorg. Chem.*, 1998, **37**, 6060–6064.
82 A. J. Rosenbaum, D. H. Juers and M. A. Juhasz, *Inorg. Chem.*, 2013, **52**, 10717–10719.
83 L. M. Wingen and M. S. Scholz, *Inorg. Chem.*, 2016, **55**, 8274–8276.
84 P. Kaszyński and B. Ringstrand, *Angew. Chem., Int. Ed.*, 2015, **54**, 6576–6581.
85 G. E. Dwulet and M. A. Juhasz, *Inorg. Chem. Commun.*, 2015, **51**, 26–28.
86 S. Trofimenko, *U.S. Pat.*, 3373098, 1968.
87 I. P. Beletskaya, V. I. Bregadze, K. Z. Kabytaev, G. G. Zhigareva, P. V. Petrovskii, I. V. Glukhov and Z. A. Starikova, *Organometallics*, 2007, **26**, 2340–2347.
88 Y. Sevryugina, R. L. Julius and M. F. Hawthorne, *Inorg. Chem.*, 2010, **49**, 10627–10634.
89 R. M. Dziedzic, J. L. Martin, J. C. Axtell, L. M. A. Saleh, T. C. Ong, Y. F. Yang, M. S. Messina, A. L. Rheingold, K. N. Houk and A. M. Spokoyny, *J. Am. Chem. Soc.*, 2017, **139**, 7729–7732.
90 K. Z. Kabytaev, S. N. Mukhin, I. V. Glukhov, Z. A. Starikova, V. I. Bregadze and I. P. Beletskaya, *Organometallics*, 2009, **28**, 4758–4763.
91 S. A. Jasper, R. B. Jones, J. Mattern, J. C. Huffman and L. J. Todd, *Inorg. Chem.*, 1994, **33**, 5620–5624.
92 A. M. Spokoyny, C. D. Lewis, G. Teverovskiy and S. L. Buchwald, *Organometallics*, 2012, **31**, 8478–8481.
93 K. Z. Kabytaev, T. A. Everett, A. V. Safronov, Y. V. Sevryugina, S. S. Jalisatgi and M. F. Hawthorne, *Eur. J. Inorg. Chem.*, 2013, 2488–2491.
94 L. Jain, V. K. Jain, N. Kushwah, M. K. Pal, A. P. Wadawale, V. I. Bregadze and S. A. Glazun, *Coord. Chem. Rev.*, 2014, **258–259**, 72–118.
95 S. N. Mukhin, K. Z. Kabytaev, G. G. Zhigareva, I. V. Glukhov, Z. A. Starikova, V. I. Bregadze and I. P. Beletskaya, *Organometallics*, 2008, **27**, 5937–5942.
96 C. Amatore and A. Jutand, *Coord. Chem. Rev.*, 1998, **178–180**, 511–528.
97 I. J. S. Fairlamb, *Org. Biomol. Chem.*, 2008, **6**, 3645.
98 L. M. A. Saleh, R. M. Dziedzic, S. I. Khan and A. M. Spokoyny, *Chem. – Eur. J.*, 2016, **22**, 8466–8470.
99 M. L. Connolly, *J. Am. Chem. Soc.*, 1985, **107**, 1118–1124.
100 C. W. Tsang, Q. Yang, E. T. P. Sze, T. C. W. Mak, D. T. W. Chan and Z. Xie, *Inorg. Chem.*, 2000, **39**, 3582–3589.
101 D. Olid, C. Viñas and F. Teixidor, *Chem. – Eur. J.*, 2012, **18**, 12936–12940.
102 T. Jelínek, J. Plešek, S. Heřmánek and B. Štíbr, *Collect. Czech. Chem. Commun.*, 1986, **51**, 819–829.
103 D. Olid, R. Núñez, C. Viñas and F. Teixidor, *Chem. Soc. Rev.*, 2013, **42**, 3318.
104 A. C. Serino, M. E. Anderson, L. M. A. Saleh, R. M. Dziedzic, H. Mills, L. K. Heidenreich, A. M. Spokoyny and P. S. Weiss, *ACS Appl. Mater. Interfaces*, 2017, **9**, 34592–34596.
105 G. R. Kracke, M. R. VanGordon, Y. V. Sevryugina, P. J. Kueffer, K. Kabytaev, S. S. Jalisatgi and M. F. Hawthorne, *ChemMedChem*, 2015, **10**, 62–67.
106 K. O. Kirlikovali, J. C. Axtell, A. Gonzalez, A. C. Phung, S. I. Khan and A. M. Spokoyny, *Chem. Sci.*, 2016, **7**, 5132–5138.
107 K. O. Kirlikovali, J. C. Axtell, K. Anderson, P. I. Djurovich, A. L. Rheingold and A. M. Spokoyny, *Organometallics*, 2018, **37**, 3122–3131.
108 R. Cheng, Z. Qiu and Z. Xie, *Nat. Commun.*, 2017, **8**, 1–7.
109 J. E. Dander, E. L. Baker and N. K. Garg, *Chem. Sci.*, 2017, **8**, 6433–6438.
110 A. D. Ibrahim, K. Tokmic, M. R. Brennan, D. Kim, E. M. Matson, M. J. Nilges, J. A. Bertke and A. R. Fout, *Dalton Trans.*, 2016, **45**, 9805–9811.
111 N. Ichiishi, C. A. Malapit, A. Woźniak and M. S. Sanford, *Org. Lett.*, 2018, **20**, 44–47.
112 M. L. Scheuermann, E. J. Johnson and P. J. Chirik, *Org. Lett.*, 2015, **17**, 2716–2719.
113 J. Wei, K. M. Liu and X. F. Duan, *J. Org. Chem.*, 2017, **82**, 1291–1300.
114 J. J. Mousseau and A. B. Charette, *Acc. Chem. Res.*, 2013, **46**, 412–424.
115 M. H. Shaw, J. Twilton and D. W. C. MacMillan, *J. Org. Chem.*, 2016, **81**, 6898–6926.

Chapter 2. B-N, B-O, and B-CN Bond Formation via Palladium-Catalyzed Cross-Coupling of B-Bromo-carboranes

This chapter describes the conditions necessary to activate boron-bromine bonds of B-Bromo-carboranes, such as 9-Br-1,7-dicarba-*closo*-dodecaborane, by using palladium(0) ligated by dialkyl biaryl phosphine ligands. It is the first report of B-bromo-carboranes participating in palladium-catalyzed cross-coupling, whereas all previous reported methods of palladium catalyzed cross-coupling were only successful with B-iodo-carboranes.

Chapter 2 is a reprint of Dziedzic, R. M.; Saleh, L. M. A.; Axtell, J. C.; Martin, J. L.; Stevens, S. L.; Royappa, A. T.; Rheingold, A. L.; Spokoyny, A. M. B-N, B-O, and B-CN Bond Formation via Palladium-Catalyzed Cross-Coupling of B-Bromo-Carboranes. *J. Am. Chem. Soc.* **2016**, *138* (29), 9081–9084. DOI: 10.1021/jacs.6b05505 with permission from the American Chemical Society.

Additional supporting information is available free of charge from https://pubs.acs.org/doi/10.1021/jacs.6b05505.

B–N, B–O, and B–CN Bond Formation via Palladium-Catalyzed Cross-Coupling of B-Bromo-Carboranes

Rafal M. Dziedzic,[†] Liban M. A. Saleh,[†] Jonathan C. Axtell,[†] Joshua L. Martin,[†] Simone L. Stevens,[†] A. Timothy Royappa,[‡,§] Arnold L. Rheingold,[‡] and Alexander M. Spokoyny*[,†]

[†]Department of Chemistry and Biochemistry, University of California, Los Angeles, 607 Charles E. Young Drive East, Los Angeles, California 90095, United States

[‡]Department of Chemistry and Biochemistry, University of California, San Diego, 9500 Gilman Drive, La Jolla, California 92093, United States

[§]Department of Chemistry, University of West Florida, 11000 University Parkway, Pensacola, Florida 32514, United States

Supporting Information

ABSTRACT: Carboranes are boron-rich molecules that can be functionalized through metal-catalyzed cross-coupling. Here, for the first time, we report the use of bromo-carboranes in palladium-catalyzed cross-coupling for efficient B–N, B–O, and unprecedented B–CN bond formation. In many cases bromo-carboranes outperform the traditionally utilized iodo-carborane species. This marked difference in reactivity is leveraged to circumvent multistep functionalization by directly coupling small nucleophiles (-OH, -NH_2, and -CN) and multiple functional groups onto the boron-rich clusters.

Icosahedral carboranes are boron-rich molecular clusters that are often described as three-dimensional (3D) analogs to benzene.[1] Their unique delocalized 3D aromatic bonding, high stability, and potential for site-selective functionalization make them attractive building blocks for tunable pharmacophores, unique ligand scaffolds, and building blocks for materials applications.[2] Further development of these and other applications with carboranes requires efficient methods for cluster synthesis and functionalization, where ultimately each individual vertex can be specifically addressed.[1]

Over the past 50 years, palladium-catalyzed cross-coupling has emerged as a powerful synthetic method for creating new molecules.[3] In particular, the emergence of designer ligands (beyond PPh_3) for Pd-catalyzed cross-coupling dramatically expanded the scope of electrophile substrates beyond aryl iodides.[4a] These new catalyst systems demonstrated a clear ability to cross-couple aryl-bromides and aryl-chlorides, thereby facilitating transformations of synthetically challenging substrates. Among existing ligand platforms, biaryl phosphine ligands significantly increased the efficacy of Pd-catalyzed C–C, C–N, and C–O bond formation.[4]

Despite these advances in catalyst design for aromatic substrates, effective methodologies for metal-catalyzed B–N, B–O and B–C cross-coupling in carboranes are lacking. In fact, only B-iodo-carboranes have been used in Pd-catalyzed cross-coupling thus far.[5] Yet, analogy between carboranes and arenes provides a clear hypothesis that other B-functionalized electrophiles, beyond B-iodo-carboranes, may be competent cross-coupling partners. Here we report our discovery validating this hypothesis by demonstrating for the first time that B-bromo-carboranes can be efficient electrophiles for B–N, B–O, and B–CN bond formation in Pd-catalyzed cross-coupling. Furthermore, we show conditions where these B-bromo-carboranes are superior to the iodinated congeners enabling the synthesis of previously inaccessible B-substituted carboranes. This chemistry is furthermore attractive given the greater synthetic accessibility of B-bromo-carboranes compared to their iodo-based congeners (see SI).[1]

Hawthorne and co-workers recently reported Pd-catalyzed amidation of 9-I-*m*-carborane (**I-mCB**) utilizing the biaryl phosphine ligand DavePhos (**L1**, Figure 1).[5h] To test our hypothesis, we replaced **I-mCB** with the bromo-carborane congener, 9-Br-*m*-carborane (**Br-mCB**), as a substrate under the reported cross-coupling conditions. However, our initial attempts at cross-coupling trifluoroacetamide with **Br-mCB** proved unsuccessful. Rapid formation of Pd metal was observed without any consumption of **Br-mCB**. We postulated that the Pd(0) precursor (Pd_2dba_3, dba = dibenzylideneacetone) was not efficiently forming the catalytically active species [**L1**Pd^0]. To resolve this issue, we employed a commercially available Pd(II) precatalyst (Figure 1B inset), which has been previously shown to dramatically improve catalytic activity across a large pool of aryl-based substrates and catalytic conditions.[6] Importantly, this change tremendously improved the catalytic conversion of **Br-mCB** producing **1a** in nearly quantitative conversion within 2 h (Figure 1A). This discovery demonstrates for the first time that one can efficiently activate a relatively inert B–Br bond in a carborane with electron-rich Pd-based species supported by a biaryl phosphine ligand (Figure 1B).

This example demonstrates the potential competence of **Br-mCB** toward cross-coupling (Figure 1B), which does not have any literature precedent. This advance was also appealing given that **Br-mCB** can be synthesized in a fraction of the time (1 h) that is required for the synthesis of **I-mCB** (1 day). We therefore investigated the scope of Pd-catalyzed cross-coupling

Received: May 28, 2016
Published: July 6, 2016

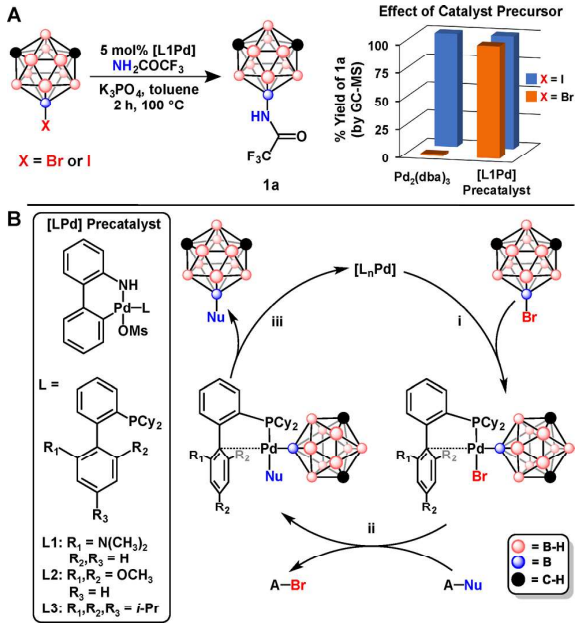

Figure 1. (A) General amidation conditions (inset, GC-MS yield of **1a** from **Br-mCB** and **I-mCB** using different palladium precursors). (B) Proposed catalytic cycle employing biaryl phosphine ligands (step i, oxidative addition; step ii, transmetalation; step iii, reductive elimination).

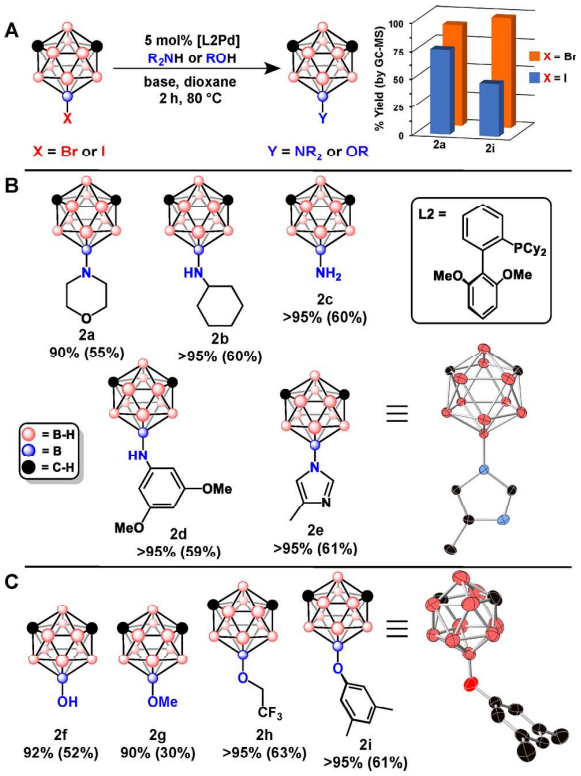

Figure 2. (A) General amination and alkoxylation conditions (inset, GC-MS yield of **2a** obtained from **Br-mCB** and **I-mCB**). (B) Amination scope using **Br-mCB** and X-ray crystal structure confirming B–N bond formation. (C) Alkoxylation scope using **Br-mCB** and X-ray crystal structure confirming B–O bond formation (ellipsoids at 50% probability and H atoms omitted for clarity). GC-MS yields, and isolated yields in parentheses. *K^{t}BuO used as a base except for: **2e**, anhydrous K_3PO_4; **2f**, 1 M aqueous K_3PO_4; **2g**, $NaOCH_3$.

of **Br-mCB** with other nucleophiles utilizing biaryl-ligand containing precatalysts.

To further probe the scope of B–N bond formation using **Br-mCB**, we evaluated several conditions and substrates for Pd-catalyzed amination. Using morpholine as a substrate (**2a**, Figure 2), we evaluated the cross-coupling efficiency of three precatalysts featuring **L1**, SPhos (**L2**), and XPhos (**L3**) ligands (see SI). For this transformation, **L2** afforded complete consumption of **Br-mCB** and a high amount of B–N coupling product **2a** as determined by GC-MS analysis. Evaluation of various bases indicated the superior performance of K^{t}BuO for forming **2a**. Importantly, **Br-mCB** showed superior cross-coupling efficiency compared to **I-mCB** for the formation of **2a** (Figure 2A). Using these optimized conditions, cross-coupling of **Br-mCB** proceeds with primary, secondary, aromatic, and heterocyclic amines in nearly quantitative conversion affording the corresponding B–N compounds (**2b–2e**, Figure 2B and SI).

In general, cross-coupling using unprotected nitrogen-rich heterocyclic substrates is known to be challenging.[6c] Amination of halocarboranes has only been shown on the 2-I-*p*-carborane, which is a significantly more reactive substrate than **Br-mCB**.[7] The cross-coupling methodology we developed addresses this issue for the first time in the context of *m*-carborane chemistry since, to the best of our knowledge, **2e** represents the first product resulting from the direct cross-coupling of an unprotected five-membered heterocycle with a B-halo-*m*-carborane.

The versatility of **Br-mCB** as a cross-coupling partner can be further seen from its efficient reaction with challenging nucleophiles. For example, **Br-mCB** cross-couples with ammonia producing **2c** (Figure 2B), whereas previously **2c** could only be prepared by lengthy hydrolysis of **1a**.[5h]

Importantly, our method represents the first example of a direct cross-coupling leading to **2c** and is enabled by the previously unrecognized reactivity of **Br-mCB** when using biaryl phosphine supported Pd-based catalysts.

During the course of our amination studies, we observed B–OH coupling with **Br-mCB** (**2f**, see SI) when nonanhydrous bases were used. This is remarkable, given that the only example of a Pd-catalyzed carborane B–O bond formation was reported on 2-I-*p*-carborane. Importantly, the **I-mCB** congener was previously deemed too unreactive.[8a]

Based on these observations, we developed a new cross-coupling protocol enabling the direct coupling of water, methanol, trifluoroethanol, and 3,5-dimethylphenol with **Br-mCB** (**2f–2i**, Figure 2C).

This constitutes the first reported Pd-catalyzed cross-coupling leading to a B–O bond formation with *m*-carborane substrates. Significantly, a control reaction where **I-mCB** was used as a substrate led to a significantly lower conversion to **2i** (Figure 2A). This Pd-catalyzed route is also superior to the exisiting method for forming related B–O compounds utilizing carborane B-halonium salts.[8b] Additionally, **2f** can be readily converted to **2g** by deprotonation with NaH and followed by treatment with MeI, demonstrating the added synthetic utility of **2f**.

The versatility of **Br-mCB** cross-coupling with small nucleophiles led us to investigate B—CN bond formation. Cyanide is known to be a difficult cross-coupling partner in metal catalysis due to its propensity toward binding to catalytically active species, resulting in their deactivation.[9] Recently several groups reported efficient protocols for cyanation of aromatic substrates using $K_4[Fe(CN)_6]$ as a mild cyanide source.[9b,d] Pd-catalyzed cyanation of **Br-mCB** using $K_4[Fe(CN)_6]$ with an **L3**-based precatalyst led to the formation of 9-CN-*m*-carborane in a nearly quantitive conversion (**3a**, Figure 3A). This example represents the first

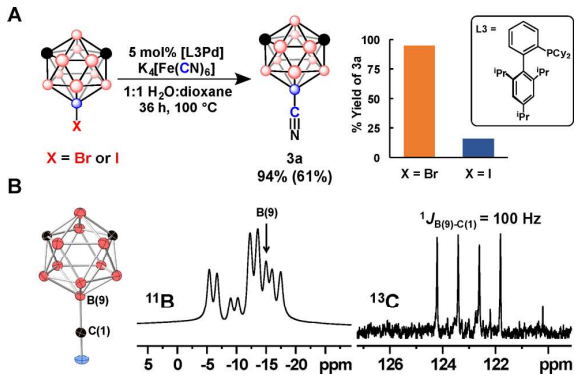

Figure 3. (A) Cyanation protocol; GC-MS yield of **3a** obtained from **Br-mCB** and **I-mCB** (isolated yield in parentheses). (B) X-ray crystal structure, ^{11}B and $^{13}C\{^1H\}$ NMR spectra of **3a** (ellipsoids at 50% probability and H atoms omitted for clarity).

direct cyanation of a halogenated derivative of dicarba-*closo*-dodecaborane. Importantly, cross-coupling activity of the **I-mCB** species under these conditions is dramatically diminished compared to **Br-mCB** (Figure 3A).

The ability to append multiple functional groups is crucial to developing carboranes for new and existing materials.[2,10,11] While polyfunctionalization of arene-based electrophiles via cross-coupling is well-established, similar methods for carboranes are rare.[5,10] Our methodology can be applied toward disubstitution cross-coupling chemistry. Specifically, 9,10-Br_2-*m*-carborane (**4a**) can be functionalized with two bulky 3,5-dimethylphenolate substituents (**4c**, Figure 4). Interestingly, under B—OH cross-coupling conditions (*vide supra*), **4a** undergoes exclusive monosubstitution to produce **4d**.

In addition, given the pronounced orthogonal reactivity of B—Br versus B—I bonds in cross-coupling, our methodology can be used to heterofunctionalize mixed halo-carborane substrates. We leveraged the selectivity of $PdCl_2(PPh_3)_2$ for B—I bond functionalization to produce 9-Br-10-Et-*m*-carborane (**4e**) from 9-Br-10-I-*m*-carborane (**4b**, Figure 4 and SI).

Selective Pd-catalyzed cross-coupling of the B—Br moiety in **4e** with **L2**-containing precatalyst yields the heterofunctionalized 9-O-(3,5-$Me_2C_6H_3$)-10-Et-*m*-carborane (**4f**). This transformation represents the first metal-catalyzed B-heterofunctionalization of dicarba-*closo*-dodecaborane via cross-coupling demonstrating that B-Br-carboranes offer an additional pathway for multifunctionalization. These experiments also suggest that our methodology is amenable to sterically encumbered carborane-based electrophiles.

Ortho-carboranes are the most challenging substrates in cross-coupling methodologies, since these species undergo

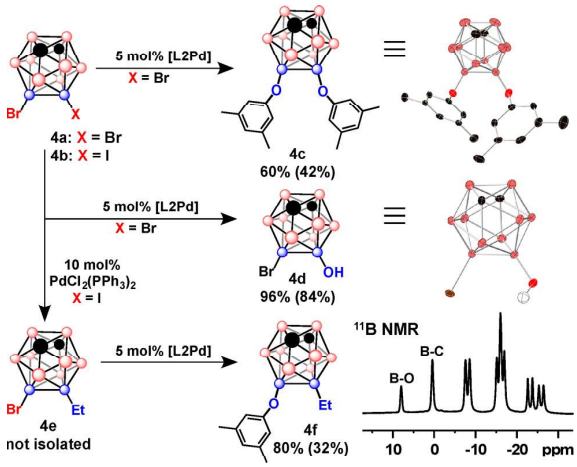

Figure 4. Difunctionalization conditions and X-ray crystal structure confirming B—O bond formation. X-ray crystal structure (ellipsoids at 50% probability and H atoms omitted for clarity); see SI for detailed conditions. GC-MS yields, and isolated yields in parentheses.

facile deboronation in the presence of nucleophiles.[12] Our conditions are sufficiently mild and enable the cross-coupling of 3-Br-*o*-carborane (**Br-oCB**, see SI for details) with amine and alcohol substrates that are not strongly nucleophilic (**5a—5b**, Figure 5). Using 3-Br-*o*-carborane in this case is preferred, given its higher conversion efficiency and ease of preparation compared to the 3-I-*o*-carborane analogue.

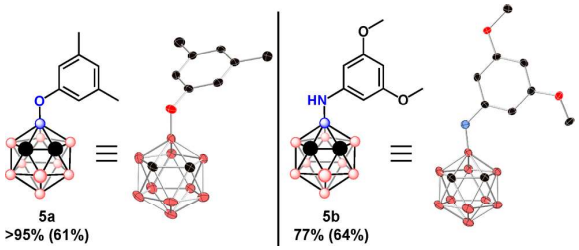

Figure 5. Alkoxylation and amination of *ortho*-carboranes using **Br-oCB** (ellipsoids at 50% probability and H atoms omitted for clarity). GC-MS yields, and isolated yields in parentheses.

In summary, we discovered that B-bromo-*m*-carboranes undergo efficient Pd-catalyzed B—N, B—O, and B—CN cross-coupling enabled by precatalysts featuring electron-rich biaryl phosphine ligands. The higher reactivity of **Br-mCB** likely stems from faster transmetalation (Figure 1B, step II) due to a weaker Pd—Br bond compared to Pd—I congener. This is consistent with previously observed trends in palladium-catalyzed transformations using aryl halide electrophiles and Pd-based catalysts supported by bulky electron-rich phosphine ligands.[13,14] The use of B-bromo-carboranes allows direct access to previously unknown B-functionalizations of these clusters. In addition, judicious use of Pd-catalyst systems with either iodo- or bromo-functionalized carborane was used to access unprecedented heterofunctionalized species. This approach is also amenable to *o*-carborane, which is the most challenging carborane substrate. Notably, this cross-coupling chemistry is complementary to the recently developed efforts in directed B—H functionalization strategies[15] and, if successfully

combined, may provide unprecedented densely functionalized carborane species.[16] Further expansion of this methodology to other cross-coupling chemistry[17] along with a full mechanistic investigation[18] is currently underway in our laboratory.

■ ASSOCIATED CONTENT

Supporting Information

The Supporting Information is available free of charge on the ACS Publications website at DOI: 10.1021/jacs.6b05505.

Full procedures and other characterization data (PDF)
Crystallographic data (CIF)

■ AUTHOR INFORMATION

Corresponding Author

*spokoyny@chem.ucla.edu

Notes

The authors declare no competing financial interest.

■ ACKNOWLEDGMENTS

The authors acknowledge the Department of Chemistry and Biochemistry at UCLA for start-up funds and the NSF for partial support (CHE-1048804). We thank Dr. Gregory Khitrov and Elamar Hakim Moully for help with mass spectrometry. A.M.S. thanks 3M for a Non-Tenured Faculty Award.

■ REFERENCES

(1) (a) Grimes, R. N. *Carboranes*, 2nd ed.; Elsevier: Oxford, 2011. (b) Spokoyny, A. M. *Pure Appl. Chem.* **2013**, *85*, 903.

(2) Selected examples: (a) Issa, F.; Kassiou, M.; Rendina, L. M. *Chem. Rev.* **2011**, *111*, 5701. (b) McArthur, S. G.; Geng, L.; Guo, J.; Lavallo, V. *Inorg. Chem. Front.* **2015**, *2*, 1101. (c) Böhling, L.; Brockhinke, A.; Kahlert, J.; Weber, L.; Harder, R. A.; Yufit, D. S.; Howard, J. A. K.; MacBride, J. A. H.; Fox, M. A. *Eur. J. Inorg. Chem.* **2016**, *2016*, 403. (d) Jude, H.; Disteldorf, H.; Fischer, S.; Wedge, T.; Hawkridge, A. M.; Arif, A. M.; Hawthorne, M. F.; Muddiman, D. C.; Stang, P. J. *J. Am. Chem. Soc.* **2005**, *127*, 12131. (e) Farha, O. K.; Spokoyny, A. S.; Mulfort, K. L.; Hawthorne, M. F.; Mirkin, C. A.; Hupp, J. T. *J. Am. Chem. Soc.* **2007**, *129*, 12680. (f) Thomas, J. C.; Boldog, I.; Auluck, H. S.; Bereciartua, P. J.; Dušek, M.; Macháček, J.; Bastl, Z.; Weiss, P. S.; Baše, T. *Chem. Mater.* **2015**, *27*, 5425. (g) Yao, Z.-J.; Zhang, Y.-Y.; Jin, G.-X. *J. Organomet. Chem.* **2015**, *798*, 274. (h) Douvris, C.; Ozerov, O. V. *Science* **2008**, *321*, 1188. (i) Julius, R. L.; Farha, O. K.; Chiang, J.; Perry, L. J.; Hawthorne, M. F. *Proc. Natl. Acad. Sci. U. S. A.* **2007**, *104*, 4808. (j) Endo, Y.; Iijima, T.; Yamakoshi, Y.; Fukasawa, H.; Miyaura, C.; Inada, M.; Kubo, A.; Itai, A. *Chem. Biol.* **2001**, *8*, 341. (k) Kirlikovali, K. O.; Axtell, J. C.; Gonzalez, A.; Phung, A. C.; Khan, S. I.; Spokoyny, A. M. *Chem. Sci.* **2016**. (l) Lugo, C. A.; Moore, C.; Rheingold, A.; Lavallo, V. *Inorg. Chem.* **2015**, *54*, 2094. (m) Shi, C.; Sun, H.; Tang, X.; Lv, W.; Yan, H.; Zhao, Q.; Wang, J.; Huang, W. *Angew. Chem.* **2013**, *125*, 13676. (n) Lee, Y.-H.; Park, J.; Lee, J.; Lee, S. U.; Lee, M. H. *J. Am. Chem. Soc.* **2015**, *137*, 8018. (o) Zhang, X.; Dai, H.; Yan, H.; Zou, W.; Cremer, D. *J. Am. Chem. Soc.* **2016**, *138*, 4334. (p) Joost, M.; Zeineddine, A.; Estévez, L.; Mallet-Ladeira; Mique, K.; Amgoune, A.; Bourissou, D. *J. Am. Chem. Soc.* **2014**, *136*, 14654. (q) Eleazer, B. J.; Smith, M. D.; Peryshkov, D. V. *Organometallics* **2016**, *35*, 106.

(3) de Meijere, A.; Diederich, F. *Metal-catalyzed Cross-coupling Reactions*, 2nd ed.; Wiley-VCH: Weinheim, 2008.

(4) (a) Jacobsen, E. N. *Adv. Synth. Catal.* **2015**, *357*, 2173. (b) Surry, D. S.; Buchwald, S. L. *Angew. Chem., Int. Ed.* **2008**, *47*, 6338.

(5) (a) Zakharkin, L. I.; Kovredov, A. I.; Ol'Shevskaya, V. A.; Shaugumbekova, Zh. S. *Izv. Akad. Nauk SSSR, Ser. Khim.* **1980**, 1691. (b) Zakharkin, L. I.; Kovredov, A. I.; Ol'Shevskaya, V. A.; Shaugumbekova, Zh. S. *J. Organomet. Chem.* **1982**, *226*, 217. (c) Li, J.; Logan, C. F.; Jones, M., Jr. *Inorg. Chem.* **1991**, *30*, 4866. (d) Zheng, Z.; Jiang, W.; Zinn, A. A.; Knobler, C. B.; Hawthorne, M. F. *Inorg. Chem.* **1995**, *34*, 2095. (e) Jiang, W.; Knobler, C. B.; Curtis, C. E.; Mortimer, M. D.; Hawthorne, M. F. *Inorg. Chem.* **1995**, *34*, 3491. (f) Viñas, C.; Barberà, G.; Oliva, J. M.; Teixidor, F.; Welch, A. J.; Rosair, G. M. *Inorg. Chem.* **2001**, *40*, 6555. (g) Mukhin, S. N.; Kabytaev, K. Z.; Zhigareva, G. G.; Glukhov, I. V.; Starikova, Z. A.; Bregadze, V. I.; Beletskaya, I. P. *Organometallics* **2008**, *27*, 5937. (h) Sevryugina, Y.; Julius, R. L.; Hawthrone, M. F. *Inorg. Chem.* **2010**, *49*, 10627. (i) Olid, D.; Núñez, R.; Viñas, C.; Teixidor, F. *Chem. Soc. Rev.* **2013**, *42*, 3318. (j) Qui, Z. *Tetrahedron Lett.* **2015**, *56*, 963. (k) Kracke, G. N.; VanGordon, M. R.; Sevryugina, Y. V.; Kueffer, P. J.; Kabytaev, K.; Jalisatgi, S. S.; Hawthorne, M. F. *ChemMedChem* **2015**, *10*, 62.

(6) (a) Biscoe, M. R.; Fors, B. P.; Buchwald, S. L. *J. Am. Chem. Soc.* **2008**, *130*, 6686. (b) Bruno, N. C.; Tudge, M. T.; Buchwald, S. L. *Chem. Sci.* **2013**, *4*, 916. (c) Düfert, M. A.; Billingsley, K. L.; Buchwald, S. L. *J. Am. Chem. Soc.* **2013**, *135*, 12877.

(7) Beletskaya, I. P.; Bregadze, V. I.; Kabytaev, K. Z.; Zhigareva, G. G.; Petrovskii, P. V.; Glukhov, I. V.; Starikova, Z. A. *Organometallics* **2007**, *26*, 2340.

(8) (a) Kabytaev, K. Z.; Mukhin, S. N.; Glukhov, I. V.; Starikova, Z. A.; Bregadze, V. I.; Beletskaya, I. P. *Organometallics* **2009**, *28*, 4758. (b) Grushin, V. V. *Acc. Chem. Res.* **1992**, *25*, 529.

(9) (a) Sundermeier, M.; Zapf, A.; Mutyala, S.; Baumann, W.; Sans, J.; Weiss, S.; Beller, M. *Chem. - Eur. J.* **2003**, *9*, 1828. (b) Schareina, T.; Zapf, A.; Beller, M. *J. Organomet. Chem.* **2004**, *689*, 4576. (c) Erhardt, S.; Grushin, V. V.; Kilpatrick, A. H.; Macgregor, S. A.; Marshall, W. J.; Roe, D. C. *J. Am. Chem. Soc.* **2008**, *130*, 4828. (d) Senecal, T. D.; Shu, W.; Buchwald, S. L. *Angew. Chem., Int. Ed.* **2013**, *52*, 10035.

(10) (a) Puga, A. V.; Teixidor, F.; Sillanpää, R.; Kivekäs, R.; Viñas, C. *Chem. Commun.* **2011**, *47*, 2252. (b) Kabytaev, K. Z.; Everett, T. A.; Safronov, A. V.; Sevryugina, Y. V.; Jalisatgi, S. S.; Hawthorne, M. F. *Eur. J. Inorg. Chem.* **2013**, *2013*, 2488.

(11) (a) Konieczka, S. Z.; Himmelspach, A.; Hailmann, M.; Finze, M. *Eur. J. Inorg. Chem.* **2013**, *2013*, 134. (b) Wright, J. H., ll; Kefalidis, C. E.; Tham, F. S.; Maron, L.; Lavallo, V. *Inorg. Chem.* **2013**, *52*, 6223. (c) Zhao, D.; Zhang, J.; Xie, Z. *Angew. Chem., Int. Ed.* **2014**, *53*, 8488.

(12) Fox, M. A.; Wade, K. *J. Organomet. Chem.* **1999**, *573*, 279.

(13) (a) Salvi, L.; Davis, N. R.; Ali, S. Z.; Buchwald, S. L. *Org. Lett.* **2012**, *14*, 170. (b) Friis, S. D.; Skrydstrup, T.; Buchwald, S. L. *Org. Lett.* **2014**, *16*, 4296.

(14) (a) Roy, A. H.; Hartwig, J. F. *Organometallics* **2004**, *23*, 1533. (b) Sheppard, T. D. *Org. Biomol. Chem.* **2009**, *7*, 1043.

(15) (a) Quan, Y.; Xie, Z. *J. Am. Chem. Soc.* **2014**, *136*, 15513. (b) Quan, Y.; Xie, Z. *J. Am. Chem. Soc.* **2015**, *137*, 3502−3505. (c) Lyu, H.; Quan, Y.; Xie, Z. *Angew. Chem.* **2015**, *127*, 10769. (d) Quan, Y.; Xie, Z. *Angew. Chem.* **2016**, *128*, 1317. (e) Wang, Z.; Ye, H.; Li, Y.; Yan, H. *J. Am. Chem. Soc.* **2013**, *135*, 11289.

(16) Molinos, E.; Brayshaw, S. K.; Kociok-Köhn, G.; Weller, A. S. *Organometallics* **2007**, *26*, 2370.

(17) (a) Kabytaev, K. Z.; Safronov, A. V.; Sevryugina, Y. V.; Barnes, C. L.; Jalisatgi, S. S.; Hawthorne, M. F. *Inorg. Chem.* **2015**, *54*, 4143. (b) Kabytaev, K. Z.; Everett, T. A.; Safronov, A. V.; Sevryugina, Y. V.; Jalisatgi, S. S.; Hawthorne, M. F. *Eur. J. Inorg. Chem.* **2013**, *2013*, 2488. (c) Spokoyny, A. M.; Lewis, C. D.; Teverovskiy, G.; Buchwald, S. L. *Organometallics* **2012**, *31*, 8478.

(18) Saleh, L. M. A.; Dziedzic, R. M.; Khan, S. I.; Spokoyny, A. M. *Chem. - Eur. J.* **2016**, *22*, 8466.

Chapter 3. Cage-Walking: Vertex Differentiation by Palladium-Catalyzed Isomerization of B(9)-Bromo-*meta*-carborane

This chapter describes the discovery of a Pd-catalyzed isomerization mechanism (cage-walking) that allows synthesis of all possible boron-functionalized regioisomers of B-bromo-carborane from 9-Br-1,7-dicarba-*closo*-dodecaborane. When the cage-walking mechanism is operative in parallel with a cross-coupling mechanism the B-bromo-carborane regioisomers react preferentially at the B(2) position to make B(2) substituted cross-coupling products. The tandem cage-walking/cross-coupling process allows synthesis of B(2)-, B(4)-, B(5)- and B(9)-functionalized regioisomers of 1,7-dicarba-*closo*-dodecaborane.

Chapter 3 is a reprint of Dziedzic, R. M.; Martin, J. L.; Axtell, J. C.; Saleh, L. M. A.; Ong, T. C.; Yang, Y. F.; Messina, M. S.; Rheingold, A. L.; Houk, K. N.; Spokoyny, A. M. Cage-Walking: Vertex Differentiation by Palladium-Catalyzed Isomerization of B(9)-Bromo-Meta-Carborane. *J. Am. Chem. Soc.* **2017**, *139* (23), 7729–7732. DOI: 10.1021/jacs.7b04080 with permission from the American Chemical Society.

Additional supporting information is available free of charge from https://pubs.acs.org/doi/10.1021/jacs.7b04080.

Cage-Walking: Vertex Differentiation by Palladium-Catalyzed Isomerization of B(9)-Bromo-*meta*-Carborane

Rafal M. Dziedzic,[†] Joshua L. Martin,[†] Jonathan C. Axtell,[†] Liban M. A. Saleh,[†] Ta-Chung Ong,[†] Yun-Fang Yang,[†] Marco S. Messina,[†] Arnold L. Rheingold,[‡] K. N. Houk,[†] and Alexander M. Spokoyny*[,†,§]

[†]Department of Chemistry and Biochemistry, University of California, Los Angeles, 607 Charles E. Young Drive East, Los Angeles, California 90095, United States

[‡]Department of Chemistry and Biochemistry, University of California, San Diego, 9500 Gilman Drive, La Jolla, California 92093, United States

[§]California NanoSystems Institute (CNSI), University of California, Los Angeles, 570 Westwood Plaza, Los Angeles, California 90095, United States

Supporting Information

ABSTRACT: We report the first observed Pd-catalyzed isomerization ("cage-walking") of B(9)-bromo-*meta*-carborane during Pd-catalyzed cross-coupling, which enables the formation of B–O and B–N bonds at all boron vertices (B(2), B(4), B(5), and B(9)) of *meta*-carborane. Experimental and theoretical studies suggest this isomerization mechanism is strongly influenced by the steric crowding at the Pd catalyst by either a biaryl phosphine ligand and/or substrate. Ultimately, this "cage-walking" process provides a unique pathway to preferentially introduce functional groups at the B(2) vertex using B(9)-bromo-*meta*-carborane as the sole starting material through substrate control.

Isomerization mechanisms such as chain-walking via β-hydride elimination/reinsertion and aryne-based rearrangements (Figure 1A) are ubiquitous in metal-catalyzed transformations of organic molecules.[1,2] Through judicious choice of catalyst design, these mechanistic pathways can be biased to form specific regioisomers. Thus, metal-catalyzed isomerization control can provide a means of incorporating functional groups in molecules at positions remote from where initial bond activation occurs.[1−3]

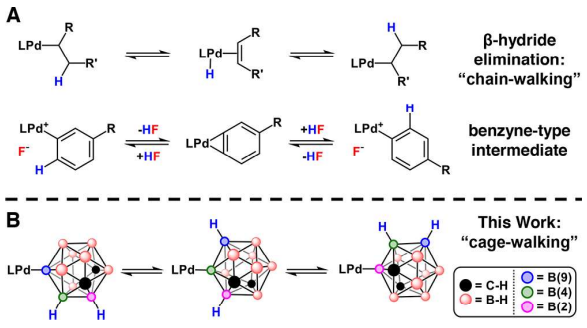

Figure 1. (A) Pd-catalyzed olefin isomerization through β-hydride elimination and arene regioisomer formation through a proposed benzyne intermediate. (B) Pd-catalyzed isomerization of *meta*-carboranyl through "cage-walking".

Boron clusters are unique molecular scaffolds that feature three-dimensional (3D) electronic delocalization.[4] Specifically, in the case of icosahedral carboranes ($C_2B_{10}H_{12}$) this delocalization is nonuniform.[5] This charge distribution makes carboranes an interesting alternative to classical carbon-based structural building blocks such as aryl and alkyl groups.[6] Because of their inherent robustness, carboranes can be promising molecular building blocks for applications ranging from pharmacophores to photoactive materials.[7] Ultimately, vertex-specific functionalization routes (vertex differentiation) are critical for constructing carborane-containing molecules and materials.[7,8]

Recent developments in carborane functionalization have relied on several metal-catalyzed routes, including B–H activation (either directed or undirected) and cross-coupling of halogenated carborane electrophiles at both C and B vertices.[8,9] Even so, these approaches provide limited access to rational, vertex-specific B–H functionalization. Surprisingly, metal-catalyzed isomerization reactivity commonly observed with classical organic substrates (vide supra) has never been reported for any boron cluster systems, including carboranes. Herein we disclose our discovery of a Pd-catalyzed activation of B(9)-bromo-*meta*-carborane (**Br–B(9)**), which can undergo subsequent "cage-walking", leading to the formation of B(2)-, B(4)-, B(5)-, and B(9)-functionalized clusters in the presence of a suitable nucleophile (Figure 1B).

Recently we reported the Pd-catalyzed cross-coupling of **Br–B(9)** to generate B(9)–O and B(9)–N bonds with a wide range of substrates.[9] This cross-coupling relied on biaryl phosphine ligands to generate monoligated palladium(0) species ([**LPd**]) capable of undergoing oxidative addition into the B–Br bond of **Br–B(9)**. To our surprise, during the course of subsequent investigations, when the DavePhos (**L1**) or SPhos (**L2**) ligand was replaced with the bulkier XPhos

Received: April 25, 2017
Published: May 25, 2017

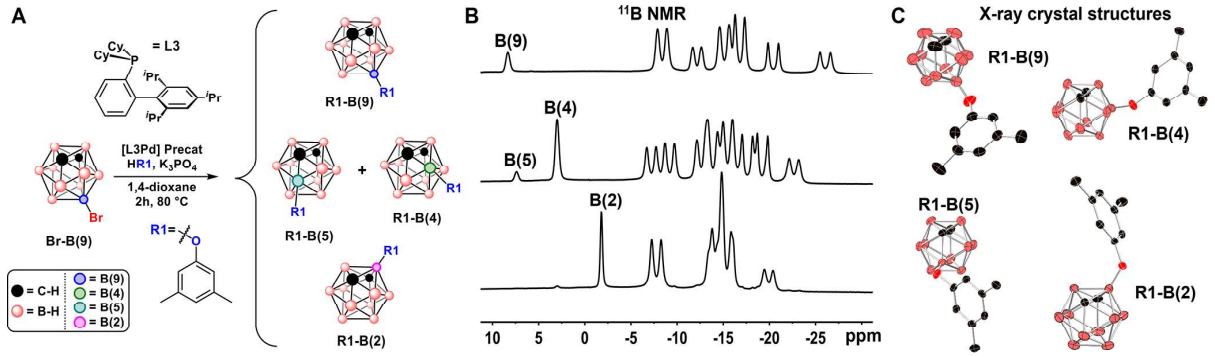

Figure 2. (A) Reaction conditions that result in the formation of **R1**-*meta*-carborane regioisomers. (B) ^{11}B NMR spectra of the isolated regioisomers. Singlet resonances (no ^{11}B–^{1}H coupling) corresponding to the B–O-bonded vertex are labeled; all other resonances correspond to doublet resonances arising from ^{11}B–^{1}H couplings. (C) Single-crystal X-ray structures of **R1-B(*n*)**, *n* = 2, 4, 5, 9 (ellipsoids drawn at 50% probability and H atoms omitted for clarity).

congener (**L3**) in the presence of alcohol or amine substrates, we consistently observed not one but rather three distinct peaks with identical *m*/*z* by gas chromatography–mass spectrometry (GC–MS). For example, using 3,5-dimethylphenol (**R1**) as a cross-coupling partner with **Br–B(9)**, we observed several products with identical *m*/*z* (see the Supporting Information (SI)). Upon chromatographic separation of the reaction mixture on silica gel, we identified four distinct **R1**-carborane compounds by ^{11}B, ^{1}H, and ^{13}C NMR spectroscopy (Figure 2).

The isolated carborane-containing molecules show a distinct downfield singlet in the ^{11}B NMR spectrum corresponding to **R1** bound at a B(2), B(4), B(5), or B(9) vertex of *meta*-carborane (**R1–B(2)**, **R1–B(4)**, **R1–B(5)**, and **R1–B(9)**, respectively). Although we were unable to chromatographically separate **R1–B(5)** and **R1–B(4)**, we identified the isomer ratio as 15:85 by ^{11}B and ^{1}H NMR spectroscopy: **R1–B(4)** is C_1-symmetric, resulting in 10 ^{11}B NMR resonances (one singlet and nine doublets), whereas **R1–B(5)** contains a mirror plane, resulting in six ^{11}B NMR resonances (one singlet and five doublets). Thus, the more intense singlet at ~3 ppm (Figure 2B) is assigned to the dominant pattern of **R1–B(4)**. Similarly, two sets of ^{1}H and ^{13}C NMR resonances corresponding to **R1–B(5)** and **R1–B(4)** were observed in a 15:85 signal ratio for the CH aromatic and aliphatic regions, respectively (see the SI). These structural assignments are further supported by single-crystal X-ray diffraction studies of the four regioisomers (Figure 2C). Interestingly, **R1–B(4)** is the only monofunctionalized *meta*-carborane regioisomer that exhibits chirality. **R1–B(4)** crystallized as two distinct polymorphs, with both polymorphs containing equal amounts of the two enantiomers in the unit cell. Chiral HPLC analysis further supports the presence of two **R1–B(4)** enantiomers in the isolated mixture (Figure S12).

To further assess the generality of this isomerization process, we examined three biaryl phosphine ligands and several substrates to generate B–O- and B–N-bound carborane regioisomers (Figure 3). Consistent with our previous report, [**L1Pd**] and [**L2Pd**] generate B(9) isomers almost exclusively with O- and N-based nucleophiles.[9] However, [**L3Pd**] generates appreciable amounts of regioisomers under the same conditions. Noteworthy was the presence of bromo-*meta*-carborane regioisomers when the cross-coupling reactions were stopped early, indicating that isomerization of **Br–B(9)** occurs in addition to the cross-coupling reaction. Furthermore, **Br–B(9)** forms bromo-*meta*-carborane isomers in the presence

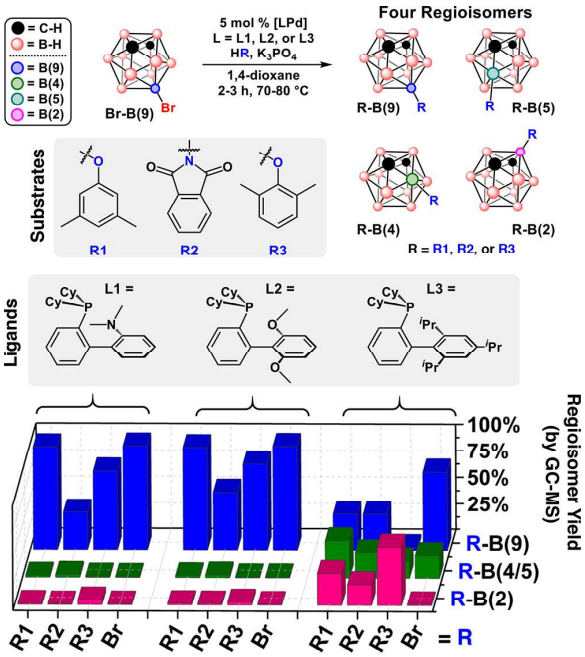

Figure 3. Reaction conditions for forming B-functionalized *meta*-carborane isomers using different substrates (**R1–R3**) and biaryl phosphine ligands (**L1–L3**). Yields were obtained by GC–MS. See the SI for full experimental conditions.

of [**L3Pd**] precatalyst and triethylamine, implying that isomerization can occur prior to transmetalation of a cross-coupling partner and subsequent reductive elimination of the B-functionalized *meta*-carborane. Hence, this metal-catalyzed isomerization may provide a convenient pathway to B(2)-, B(4)-, and B(5)-functionalized *meta*-carborane species that circumvents laborious and often low-yielding protocols such as deboronation/capitation or thermal isomerization strategies.[10,11]

Since bromo-*meta*-carboranyl isomerization can occur before all of the carborane regioisomers are depleted by cross-coupling (vide supra), we hypothesized that the isomerization process might operate separately from the main cross-coupling cycle. To further explore the isomerization mechanics, we attempted

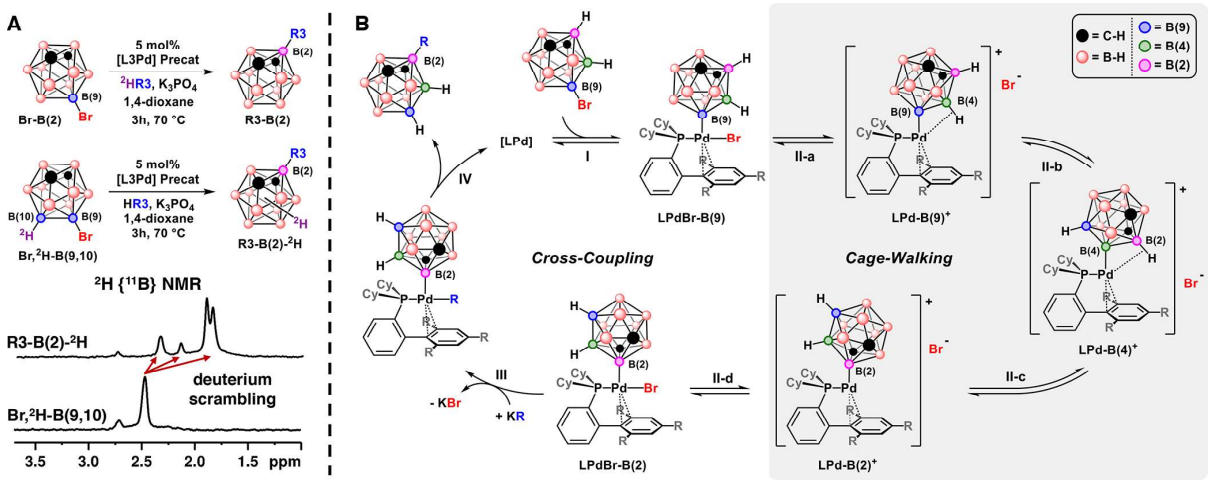

Figure 4. (A) Deuterium labeling experiments. The resonance at 2.7 ppm is present from polydeuterated **Br–B(9)**. See the SI for full experimental details. (B) Proposed metal-catalyzed isomerization of bromo-*meta*-carborane through a "cage-walking" mechanism: (I) oxidative addition; (II-a) bromide dissociation; (II-b, II-c) "cage-walking"; (II-d) bromide association; (III) transmetalation; (IV) reductive elimination.

to inhibit transmetalation by increasing the steric bulk of the cross-coupling partner, thereby allowing the active catalyst species to operate in the isomerization pathway for a longer time (Figure 4, step II). Indeed, cross-coupling reactions using bulky **L3** and sterically congested 2,6-dimethylphenol (**R3**) yielded **R3–B(2)** as the major product (Figure 3). As a control experiment, equimolar amounts of 3,5-dimethylphenol (**R1**) and 2,4,6-trimethylphenol (**R3′**, a variant of **R3** to permit separation of the products by GC–MS) were reacted with **Br–B(9)** in the presence of [**L3Pd**] and K_3PO_4 in 1,4-dioxane at 80 °C (Figures S5 and S6). GC–MS analysis of the reaction mixture showed complete consumption of **Br–B(9)** with **R1**-*meta*-carborane isomers as the major products, suggesting that the size of the nucleophile is linked to the rate of product formation. Since oxidative addition is likely rapid in this process,[12] it appears that by decreasing the rate of transmetalation and/or reductive elimination one can increase the yield of the B(2) regioisomer (Figure 4B). This type of Pd-catalyzed remote vertex functionalization is unprecedented and demonstrates the utility of a metal-catalyzed route to *meta*-carborane vertex differentiation. Importantly, it contrasts with known thermal rearrangements that are limited to thermally resistant functional groups (above 300 °C) and produce isomer mixtures with B(2) substituted *meta*-carboranes as the minor product.[11]

We attribute this difference in reactivity between "cage-walking" (when using **L3**) and cross-coupling exclusively at the B(9) vertex (when using **L1**/**L2**) to steric crowding at the Pd center. The combination of a sterically demanding ligand and nucleophile appears to inhibit transmetalation,[13] allowing the catalyst to operate through several "cage-walking" steps before re-entering the traditional cross-coupling cycle (vide supra). On the basis of these observations, we propose a Pd-catalyzed "cage-walking" mechanism for isomerization of **Br–B(9)** (Figure 4B). Beginning with the oxidative addition complex [**LPdBr–B(9)**], an open Pd(II) coordination site is generated by bromide dissociation[2d] (Figure 4, step II-a) to form [**LPd–B(9)**]$^+$. Consistent with this hypothesis, cross-coupling experiments between **Br–B(9)** and **R3** in the presence of tetrabutylammonium bromide show decreased **Br–B(9)** consumption and decreased formation of **R3**-*meta*-carborane (Figure S7). These experiments suggest that bromide dissociation is an important step in the overall cross-coupling process.[14] After bromide dissociation, two possible "cage-walking" pathways were envisioned for the formally cationic [**LPd–B(9)**]$^+$: (1) deprotonation of an adjacent B–H vertex to form a B(4),B(9)-bound carborane species that isomerizes upon reprotonation to form [**LPd–B(4)**]$^+$ (Figure S9) and (2) a Pd-mediated B–H activation that leads to an intramolecular β-hydride shift (Figure S10). Deuterium labeling experiments in which 2,6-$Me_2C_6H_4OD$ was used as the nucleophile did not result in deuterium incorporation at any B–H vertex, as judged by GC–MS and ^{2}H and ^{11}B NMR spectroscopy, likely ruling out isomerization pathway 1. However, with the deuterated congener of **Br–B(9)**, 9-Br-10-D-*meta*-$C_2B_{10}H_{10}$, and 2,6-$Me_2C_6H_4OH$ as the nucleophile, we observed five B–^{2}H resonances in the ^{2}H{^{11}B} NMR spectrum of **R3–B(2)**, indicating deuterium scrambling across the carborane B–H framework (Figure 4A). We postulate that this β-hydride shift exchanges the B(10) deuterium with an adjacent B(5) proton and enables "cage-walking" to form [**LPd–B(4)**]$^+$ (Figure 4B, step II-b). The "cage-walking" process can occur again to generate [**LPd–B(2)**]$^+$ (Figure 4B, step II-c). Similar reports of metal-catalyzed carborane B–H activation processes have been reported;[8,15,16] however, they are limited to B–H vertices adjacent to carborane-bound directing groups, whereas the presently reported "cage-walking" accesses all of the *meta*-carborane B–H vertices from one starting point in a diversity-oriented fashion.

Through the "cage-walking" process, the carboranyl fragment eventually binds the Pd center through the most electron-deficient boron vertex, B(2), resulting in a more electrophilic Pd center that can overcome the steric repulsion between the cationic [**LPd–B(2)**]$^+$ and the anionic cross-coupling partner. Density functional theory (DFT) calculations (B3LYP/LANL2DZ 6-31G* and M06/SDD/6-311++G**, SMD(1,4-dioxane)) on [**LPd–B(9)**]$^+$, [**LPd–B(4)**]$^+$, and [**LPd–B(2)**]$^+$ indicate that [**LPd–B(2)**]$^+$ has the most cationic Pd center, which likely results in a lower transmetalation barrier due to a stronger electrostatic attraction between the Pd center and the

phenoxide nucleophile (Figures S13–S16). Furthermore, the ΔG of B–O and B–N bond formation decreases accordingly, B(9) > B(5) ~ B(4) > B(2), for the cross-coupling between **Br–B(9)** and **R1–R3**. Similar electronic effects of substrate and ligand were observed in Pd-catalyzed aryl halide cross-coupling.[17]

In summary, we have discovered the first example of metal-catalyzed isomerization ("cage-walking") of *meta*-carboranyl fragment. The isomerization process appears to operate in conjunction with a classical cross-coupling mechanism, leading to a distribution of carborane regioisomers. The rate of cross-coupling relative to "cage-walking" can be adjusted to achieve selective B-vertex functionalization. We have demonstrated this selectivity by controlling the steric crowding at the Pd center by appropriate choice of catalyst ligand and cross-coupling substrate. Preliminary studies have shown that this "cage-walking" strategy can be applied to carborane B(2)–C_{aryl} bond formation using an arylboronic acid (Figure S17). Overall, this approach provides a unique pathway to vertex differentiation of boron clusters.

■ ASSOCIATED CONTENT

Supporting Information

The Supporting Information is available free of charge on the ACS Publications website at DOI: 10.1021/jacs.7b04080.

Full procedures and additional data (PDF)
Crystallographic data (CIF)

■ AUTHOR INFORMATION

Corresponding Author

*spokoyny@chem.ucla.edu

ORCID

Yun-Fang Yang: 0000-0002-6287-1640
K. N. Houk: 0000-0002-8387-5261
Alexander M. Spokoyny: 0000-0002-5683-6240

Notes

The authors declare no competing financial interest.

■ ACKNOWLEDGMENTS

We thank the donors of the American Chemical Society Petroleum Research Fund (56562-DNI3 to A.M.S.), UCLA (startup funds to A.M.S.), NSF (CHE-1048804 and CHE1361104), 3M (Non-Tenured Faculty Award to A.M.S.), and the National Defense Science and Engineering Graduate Fellowship Program (to R.M.D.) for support.

■ REFERENCES

(1) (a) Guan, Z.; Cotts, P. M.; McCord, E. F.; McLain, S. J. *Science* **1999**, *283*, 2059–2062. (b) Shultz, L. H.; Brookhart, M. *Organometallics* **2001**, *20*, 3975–3982. (c) Tempel, D. J.; Johnson, L. K.; Huff, R. L.; White, P. S.; Brookhart, M. *J. Am. Chem. Soc.* **2000**, *122*, 6686–6700. (d) Curran, K.; Risse, W.; Hamill, M.; Saunders, P.; Muldoon, J.; Asensio de la Rosa, R.; Tritto, I. *Organometallics* **2012**, *31*, 882–889. (e) Engle, K. M.; Mei, T.-S.; Wasa, M.; Yu, J.-Q. *Acc. Chem. Res.* **2012**, *45*, 788–802.

(2) (a) Buchwald, S. L.; Nielsen, R. B. *Chem. Rev.* **1988**, *88*, 1047–1058. (b) Hartwig, J. F.; Bergman, R. G.; Andersen, R. A. *J. Am. Chem. Soc.* **1991**, *113*, 3404–3418. (c) Jones, W. M.; Klosin, J. *Adv. Organomet. Chem.* **1998**, *42*, 147–221. (d) Milner, P. J.; Kinzel, T.; Zhang, Y.; Buchwald, S. L. *J. Am. Chem. Soc.* **2014**, *136*, 15757–15766.

(3) (a) Grotjahn, D. B.; Larsen, C. R.; Gustafson, J. L.; Nair, R.; Sharma, A. *J. Am. Chem. Soc.* **2007**, *129*, 9592–9593. (b) Mei, T.-S.; Patel, H. H.; Sigman, M. S. *Nature* **2014**, *508*, 340–344.

(4) Grimes, R. N. *Carboranes*, 2nd ed.; Elsevier: Oxford, U.K., 2011.

(5) King, R. B. *Chem. Rev.* **2001**, *101*, 1119–1152.

(6) (a) Lugo, C. A.; Moore, C.; Rheingold, A.; Lavallo, V. *Inorg. Chem.* **2015**, *54*, 2094–2096. (b) Joost, M.; Zeineddine, A.; Estévez, L.; Mallet-Ladeira; Miqueu, K.; Amgoune, A.; Bourissou, D. *J. Am. Chem. Soc.* **2014**, *136*, 14654–14657. (c) Douvris, C.; Ozerov, O. V. *Science* **2008**, *321*, 1188–1190. (d) Böhling, L.; Brockhinke, A.; Kahlert, J.; Weber, L.; Harder, R. A.; Yufit, D. S.; Howard, J. A. K.; MacBride, J. A. H.; Fox, M. A. *Eur. J. Inorg. Chem.* **2016**, *2016*, 403–412. (e) Puga, A. V.; Teixidor, F.; Sillanpää, R.; Kivekäs, R.; Viñas, C. *Chem. Commun.* **2011**, *47*, 2252–2254.

(7) (a) Dash, B. P.; Satapathy, R.; Gaillard, E. R.; Norton, K. M.; Maguire, J. A.; Chug, N.; Hosmane, N. S. *Inorg. Chem.* **2011**, *50*, 5485–5493. (b) Nishino, K.; Yamamoto, H.; Tanaka, K.; Chujo, Y. *Org. Lett.* **2016**, *18*, 4064–4067. (c) Kim, T.; Kim, H.; Lee, K. M.; Lee, Y. S.; Lee, M. H. *Inorg. Chem.* **2013**, *52*, 160–168. (d) Valliant, J. F.; Guenther, K. J.; King, A. S.; Morel, P.; Schaffer, P.; Sogbein, O. O.; Stephenson, K. A. *Coord. Chem. Rev.* **2002**, *232*, 173–230. (e) Issa, F.; Kassiou, M.; Rendina, L. M. *Chem. Rev.* **2011**, *111*, 5701–5722. (f) Kennedy, R. D.; Krungleviciute, V.; Clingerman, D. J.; Mondloch, J. E.; Peng, Y.; Wilmer, C. E.; Sarjeant, A. A.; Snurr, R. Q.; Hupp, J. T.; Yildirim, T.; Farha, O. K.; Mirkin, C. A. *Chem. Mater.* **2013**, *25*, 3539–3543. (g) Axtell, J. C.; Kirlikovali, K. O.; Djurovich, P. I.; Jung, D.; Nguyen, V. T.; Munekiyo, B.; Royappa, A. T.; Rheingold, A. L.; Spokoyny, A. M. *J. Am. Chem. Soc.* **2016**, *138*, 15758–15765.

(8) (a) Quan, Y.; Xie, Z. *Angew. Chem., Int. Ed.* **2016**, *55*, 1295–1298. (b) Lyu, H.; Quan, Y.; Xie, Z. *J. Am. Chem. Soc.* **2016**, *138*, 12727–12730.

(9) Dziedzic, R. M.; Saleh, L. M. A.; Axtell, J. C.; Martin, J. L.; Stevens, S. L.; Royappa, A. T.; Rheingold, A. L.; Spokoyny, A. M. *J. Am. Chem. Soc.* **2016**, *138*, 9081–9084 (and references within).

(10) (a) Safronov, A. V.; Kabytaev, K. Z.; Jalisatgi, S. S.; Hawthorne, M. F. *Dalton Trans.* **2014**, *43*, 12467–12469. (b) Bondarev, O.; Sevryugina, Y. V.; Jalisatgi, S. S.; Hawthorne, M. F. *Inorg. Chem.* **2012**, *51*, 9935–9942. (c) Ramachandran, B. M.; Knobler, C. B.; Hawthorne, M. F. *Inorg. Chem.* **2006**, *45*, 336–340.

(11) (a) Kaesz, H. D.; Bau, R.; Beall, H. A.; Lipscomb, W. N. *J. Am. Chem. Soc.* **1967**, *89*, 4218–4220. (b) Roscoe, J. S.; Kongpricha, S.; Papetti, S. *Inorg. Chem.* **1970**, *9*, 1561–1563. (c) Kalinin, V. N.; Kobel'kova, N. I.; Zakharkin, L. I. *J. Organomet. Chem.* **1979**, *172*, 391–395.

(12) (a) Marshall, W. J.; Young, R. J., Jr.; Grushin, V. V. *Organometallics* **2001**, *20*, 523–533. (b) Saleh, L. M. A.; Dziedzic, R. M.; Khan, S. I.; Spokoyny, A. M. *Chem. - Eur. J.* **2016**, *22*, 8466–8470.

(13) (a) Sergeev, A. G.; Artamkina, G. A.; Beletskaya, I. P. *Tetrahedron Lett.* **2003**, *44*, 4719–4723. (b) Shen, Q.; Ogata, T.; Hartwig, J. F. *J. Am. Chem. Soc.* **2008**, *130*, 6586–6596. (c) Hicks, J. D.; Hyde, A. M.; Cuezva, A. M.; Buchwald, S. L. *J. Am. Chem. Soc.* **2009**, *131*, 16720–16734. (d) Park, N. H.; Vinogradova, E. V.; Surry, D. S.; Buchwald, S. L. *Angew. Chem., Int. Ed.* **2015**, *54*, 8259–8262.

(14) Fors, B. P.; Davis, N. R.; Buchwald, S. L. *J. Am. Chem. Soc.* **2009**, *131*, 5766–5768.

(15) (a) Qiu, Z.; Ren, S.; Xie, Z. *Acc. Chem. Res.* **2011**, *44*, 299–309 (and references within). (b) Cheng, R.; Qiu, Z.; Xie, Z. *Nat. Commun.* **2017**, *8*, 14827.

(16) (a) Behnken, P. E.; Marder, T. B.; Baker, R. T.; Knobler, C. B.; Thompson, M. R.; Hawthorne, M. F. *J. Am. Chem. Soc.* **1985**, *107*, 932–940. (b) Eleazer, B. J.; Smith, M. D.; Popov, A. A.; Peryshkov, D. V. *J. Am. Chem. Soc.* **2016**, *138*, 10531–10538. (c) Eleazer, B. J.; Smith, M. D.; Peryshkov, D. V. *J. Organomet. Chem.* **2017**, *829*, 42–47.

(17) (a) Hartwig, J. F. *Acc. Chem. Res.* **1998**, *31*, 852–860. (b) Widenhoefer, R. A.; Buchwald, S. L. *J. Am. Chem. Soc.* **1998**, *120*, 6504–6511.

Chapter 4. Off-Cycle Processes in Pd-Catalyzed Cross-Coupling of Carboranes

This chapter details how off-cycle processes in Pd-catalyzed cross-coupling, such as cage-walking or deboronation, affect the overall reaction efficiency, regioisomer distribution and by-product formation. It also outlines a general approach to controlling the tandem cage-walking/cross-coupling process so that it can be adapted to a broad set of cross-coupling partners.

Chapter 4 is a reprint of Dziedzic, R. M.; Axtell, J. C.; Rheingold, A. L.; Spokoyny, A. M. Off-Cycle Processes in Pd-Catalyzed Cross-Coupling of Carboranes. *Org. Process Res. Dev.* **2019**, *139* (23), 7729–7732. DOI: 10.1021/acs.oprd.9b00257 with permission from the American Chemical Society.

Additional supporting information is available free of charge from https://pubs.acs.org/doi/abs/10.1021/acs.oprd.9b00257

Off-Cycle Processes in Pd-Catalyzed Cross-Coupling of Carboranes

Rafal M. Dziedzic,[†] Jonathan C. Axtell,[†] Arnold L. Rheingold,[‡] and Alexander M. Spokoyny*[,†,§]

[†]Department of Chemistry and Biochemistry, University of California, Los Angeles, 607 Charles E. Young Drive East, Los Angeles, California 90095, United States

[‡]Department of Chemistry and Biochemistry, University of California, San Diego, 9500 Gilman Drive, La Jolla, California 92093, United States

[§]California NanoSystems Institute (CNSI), University of California, Los Angeles, 570 Westwood Plaza, Los Angeles, California 90095, United States

Supporting Information

ABSTRACT: Off-cycle processes in a catalytic reaction can dramatically influence the outcome of the chemical transformation and affect its yield, selectivity, rate, and product distribution. While the generation of off-cycle intermediates can complicate reaction coordinate analyses or hamper catalytic efficiency, the generation of such species may also open new routes to unique chemical products. We recently reported the Pd-mediated functionalization of carboranes with a range of O-, N-, and C-based nucleophiles. By utilizing a Pd-based catalytic system supported by a biarylphosphine ligand developed by Buchwald and co-workers, we discovered an off-cycle isomerization process ("cage-walking") that generates four regioisomeric products from a single halogenated boron cluster isomer. Here we describe how several off-cycle processes affect the regioisomer yield and distribution during Pd-catalyzed tandem cage-walking/cross-coupling. In particular, tuning the transmetalation step in the catalytic cycle allowed us to incorporate the cage-walking process into Pd-catalyzed cross-coupling of sterically unencumbered substrates, including cyanide. This work demonstrates the feasibility of using tandem cage-walking/cross-coupling as a unique low-temperature method for producing regioisomers of monosubstituted carboranes.

KEYWORDS: *off-cycle, catalysis, carboranes, cage-walking, deboronation*

INTRODUCTION

Since the discovery of metal-catalyzed cross-coupling, researchers have observed off-cycle processes in the manipulation of hydrocarbon-based molecules (e.g., metal-mediated β-hydride elimination and chain-walking).[1−3] While off-cycle processes may lead to catalytically inactive byproducts that hamper the efficiency of catalytic cycles,[4,5] understanding these off-cycle processes is critical for improving the reaction selectivity and suppressing detrimental reaction pathways. Off-cycle processes in metal-catalyzed reactions can have utility as alternate reaction pathways that enable new or nonintuitive reactivity in synthesis.[6−12]

An appealing aspect of off-cycle processes is the isomerization of a substrate molecule into regioisomers that cannot be easily synthesized.[13] Such isomerization reactions are particularly useful when studying structure−activity relationships among isomers because these reactions can help identify lead compounds from a single reactant.[14]

We and others have recently been expanding the application of Pd-based cross-coupling methodology to three-dimensional (3D) icosahedral carborane substrates.[15−27] These compounds possess several unique spectroscopic features such as NMR-active ^{11}B and ^{10}B nuclei, IR- and Raman-active B−H bond stretching modes, and distinct ^{11}B/^{10}B isotopic patterns in mass spectrometry, enabling detection of icosahedral boranes by a variety of analytical methods.[28−31] In particular, the three isomers (ortho, meta, and para) of dicarba-*closo*-dodecaboranes ($o/m/p$-$C_2B_{10}H_{12}$) are of interest because of their commercial availability and their utility as 3D scaffolds in molecular design. The o- and m-$C_2B_{10}H_{12}$ isomers both have pronounced dipole moments, four sets of chemically inequivalent B−H vertices, and one set of chemically equivalent C−H vertices. The variety of substituted regioisomers available to carboranes allows them to act as electronically distinct, isosteric functional groups (Figure 1). The electronic diversity among carborane regioisomers has enabled tuning of their hydrophobicity, pharmacological properties, photoluminescence, and surface chemistry.[32]

Among the presently available boron vertex functionalization methods, metal-catalyzed transformations enable the installation of the broadest class of chemical groups. These metal-catalyzed methods can be loosely grouped into (1) directed B−H activation and (2) cross-coupling at B−X bonds (X = Br, I).[33−35] While B−H activation methods often target the electron-deficient B−H vertices (those closest to the carbon vertices),[36,37] cross-coupling at B−X bonds can occur at electron-rich and electron-poor boron vertices.[38] Thus, direct and selective synthesis of halocarborane regioisomers is the main challenge for synthesizing the corresponding regioisomeric carborane products via metal-catalyzed cross-coupling. The two strategies are reminiscent of methods used for the functionalization of aromatic and heteroaromatic hydrocarbon

Special Issue: Honoring 25 Years of the Buchwald-Hartwig Amination

Received: June 6, 2019
Published: August 5, 2019

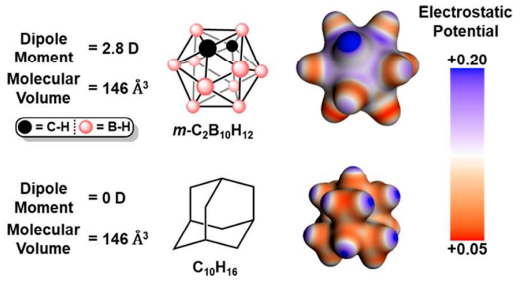

Figure 1. Electrostatic potential maps of *m*-carborane and adamantane and molecular volumes based on the Connolly solvent-excluded volume using a 1.4 Å probe sphere (see the Supporting Information for computational details).

congeners and are complementary in their nature. However, despite the prevalence of metal-catalyzed isomerization chemistry for hydrocarbon molecules, the methodology for accessing all four boron-substituted regioisomers for icosahedral carboranes is still fundamentally underexplored.

In the case of *m*-carborane (**mCB**), facile electrophilic halogenation occurs at the electron-rich B(9)−H vertex to produce 9-Br-*m*-carborane (**Br-B(9)**). However, synthesis of the other regioisomers (5-Br-*m*-carborane, **Br-B(5)**; 4-Br-*m*-carborane, **Br-B(4)**; and 2-Br-*m*-carborane, **Br-B(2)**) is more challenging. For example, deboronation and halogenation followed by boron vertex reinsertion enable the synthesis of some non-B(9)-vertex halogenated regioisomers.[39,40] Alternatively, thermal isomerization of **Br-B(9)** occurs at temperatures >300 °C and produces a statistical distribution of 9/5/4/2-bromo-*m*-carborane (**Br-mCB**) isomers.[41−44] The thermal isomerization process is one of the few methods to synthesize **Br-B(5)** and **Br-B(4)**. The difficulty associated with synthesizing these **mCB** regioisomers is perceived as a significant obstacle to the study of carborane-based molecules and their regioisomers.

We recently reported the discovery of an off-cycle **Br-mCB** isomerization process ("cage-walking") that bypasses the need to synthesize the B(9/5/4/2) **Br-mCB** regioisomers for subsequent cross-coupling to form B(9/5/4/2)-functionalized **mCB** regioisomers.[45] The cage-walking process isomerizes the **Br-B(9)** substrate into all four **Br-mCB** regioisomers (Figure 2). This tandem cage-walking/cross-coupling process allows **Br-B(9)** to serve as a precursor to B(9/5/4/2)-substituted **mCB**. The selectivity for cross-coupling at the B(5), B(4), and B(2) vertices appears to be driven by the increased electrophilicity of the Pd(II) center when the carborane is bound through the more electron-poor (B(2) > B(4) > B(5)) boron vertices.[45] However, to date the utility of the tandem cage-walking/cross-coupling process has been limited to sterically hindered nucleophiles. Thus, we set out to (1) understand the reaction conditions necessary to access the cage-walking process and (2) identify methods for controlling the cross-coupling of sterically unencumbered nucleophiles.

RESULTS AND DISCUSSION

Cage-Walking Isomerization by [LPd]. In order to integrate the cage-walking process into various Pd-catalyzed cross-coupling reactions, we set out to identify the reaction components that facilitate Pd-catalyzed **Br-B(9)** isomerization. In our previous studies we used an [XPhos-Pd-G3] precatalyst to generate the active [XPhosPd] catalytic species.[45] This method required the use of an exogenous base to deprotonate the precatalyst, which produced [XPhosPd] by reductive elimination of a carbazole molecule.[46] To evaluate whether cage-walking occurs in the absence of precatalyst byproducts, we prepared the [XPhosPd] catalyst by using [Pd(cod)-$(CH_2Si(CH_3)_3)_2$] (cod = 1,5-cyclooctadiene) as an alternative

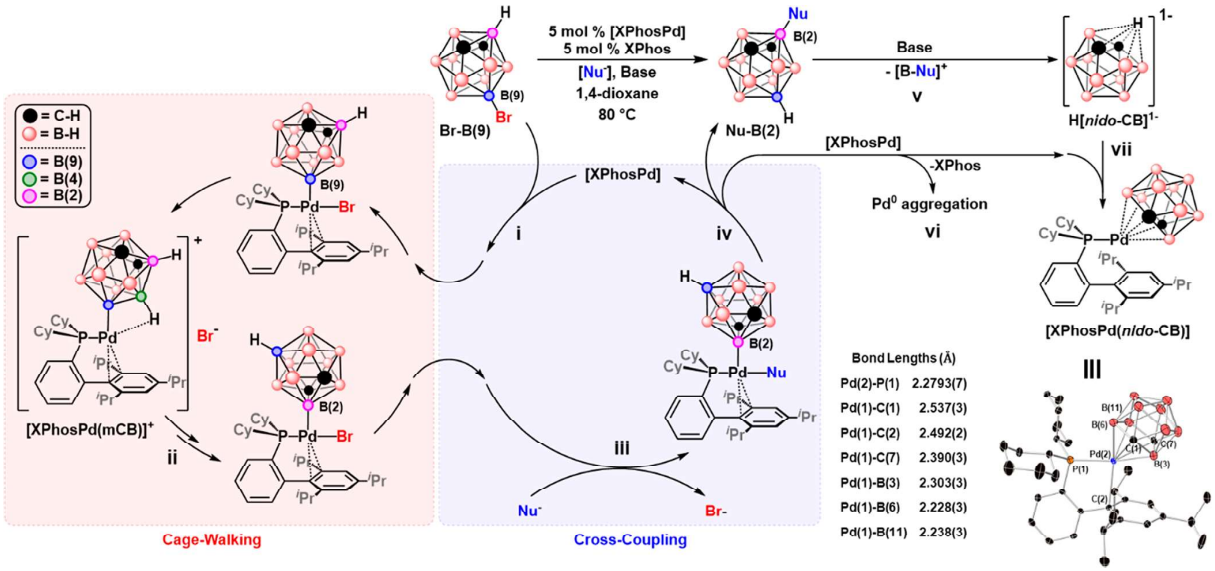

Figure 2. Proposed tandem cage-walking/cross-coupling cycle. The red box encapsulates the cage-walking process, and the blue box encapsulates the cross-coupling process. Deleterious off-cycle pathways are shown on the right side of the tandem cage-walking/cross-coupling, and the inset shows the single-crystal X-ray diffraction crystal structure of [XPhosPd(*nido*-**CB**)]. Steps: (i) oxidative addition; (ii) cage-walking; (iii) transmetalation; (iv) reductive elimination; (v) deboronation of **Nu-B(2)** by base; (vi) aggregation of palladium into palladium particles; (vii) ligation of [XPhosPd] by *nido*-**CB**.

Pd^0 source in the presence of dialkylbiarylphosphine ligands.[47] Similar to the [XPhos-Pd-G3] precatalyst system, we observed cage-walking when **Br-B(9)** was treated with a solution of [XPhosPd] at 80 °C (Figure 3), suggesting that the cage-

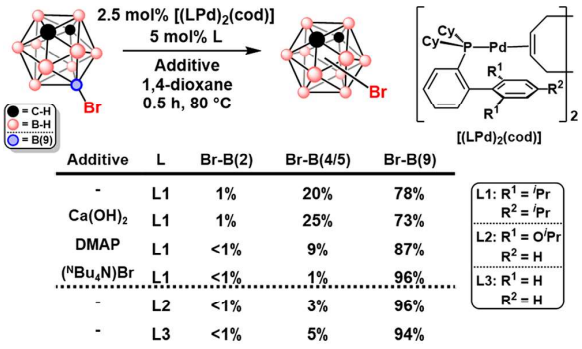

Additive	L	Br-B(2)	Br-B(4/5)	Br-B(9)
-	L1	1%	20%	78%
$Ca(OH)_2$	L1	1%	25%	73%
DMAP	L1	<1%	9%	87%
$(^nBu_4N)Br$	L1	<1%	1%	96%
-	L2	<1%	3%	96%
-	L3	<1%	5%	94%

L1: R^1 = ^{i}Pr, R^2 = ^{i}Pr
L2: R^1 = O^{i}Pr, R^2 = H
L3: R^1 = H, R^2 = H

Figure 3. GC–MS yields of **Br-mCB** regioisomers produced by Pd-catalyzed cage-walking starting with **Br-B(9)**.

walking process is independent of the presence of the base and likely proceeds via unimolecular isomerization. Since there is no oxidant in the reaction mixture strong enough to facilitate a Pd(II)/Pd(IV) cycle, we believe that the cage-walking process likely does not involve a Pd(IV) intermediate (see Figure S12 for proposed cage-walking mechanisms). Examination of other dialkylbiarylphosphine ligands (RuPhos, **L2**; CyJohnPhos, **L3**) revealed that the cage-walking process is not exclusive to the XPhos ligand. However, the total isomer yield is highest when XPhos (**L1**) is used. Notably, we did not observe cage-walking isomerization of 9-I-*m*-carborane in the presence of 5 mol % [XPhos-Pd-G3] precatalyst with K_3PO_4 in 1,4-dioxane at 80 °C.

Next, we examined whether certain additives could affect the amounts of **Br-mCB** isomers formed during cage-walking (Figure 3). We found that presence of Lewis bases or excess bromide reduces the relative ratios of cage-walked **Br-mCB** isomers. For example, addition of 4-dimethylaminopyridine (DMAP) or $(^nBu_4N)Br$ reduced the yield of B(2/4/5) **Br-mCB** isomers from 21% to 10% and 1%, respectively. These observations would be consistent with a catalytically relevant ($[XPhosPd(\mathbf{mCB})]^+$) intermediate for the cage-walking process in which the formally cationic Pd center bears a vacant coordination site (Figures 2 and S12). In order to probe this mechanistic hypothesis further, we focused on additives that might promote Pd–Br bond cleavage in [XPhosPd(**mCB**)Br] to yield an $[XPhosPd(\mathbf{mCB})]^+$ species with a vacant coordination site that we suspect is responsible for the activation of an adjacent B–H bond and subsequent cage-walking. Importantly, the total yield of B(2/4/5) **Br-mCB** isomers can be increased from 20% to 26% by addition of $Ca(OH)_2$ to the cage-walking reaction. This increase in the yield of **Br-mCB** isomers is attributed to the ability of layered hydroxides to intercalate anions and form OH···Br interactions that may promote the formation of $[XPhosPd(\mathbf{mCB})]^+$.[48] We also found that the identity of the base (including those soluble in organic media, e.g., triethylamine) had little effect on **Br-B(9)** isomerization, and only 1 equiv of base (relative to [XPhos-Pd-G3] precatalyst) was needed to form the [XPhosPd] complex. This set of experiments demonstrates how certain additives or reaction byproducts can affect the cage-walking process and the overall distribution of **mCB** regioisomers.

Tandem Cage-Walking/Suzuki–Miyaura Coupling. In our initial study of tandem cage-walking/cross-coupling with phenols, we observed that the combination of a sterically encumbered biarylphosphine ligand and a sterically encumbered substrate generate a higher percentage of B(2) regioisomers than their less hindered counterparts.[45] For example, under otherwise identical conditions, tandem cage-walking/cross-coupling of 3,5-dimethylphenol with **Br-B(9)** gave a 30% yield of B(2)-substituted **mCB**, whereas the bulkier but electronically comparable 2,6-trimethylphenol gave a 76% yield of B(2)-substituted **mCB**.[45] This pronounced selectivity for cage-walking was attributed to the substrate control engendered by the sterics of the phenol moiety that can modulate the rate of transmetalation. We hypothesized that such steric control may not be necessary in the case of other substrates such as arylboronic acids, where the electronic properties of the aryl substituent can dictate the rate of transmetalation. For example, the tandem cage-walking/Suzuki–Miyaura coupling of *p*-tolylboronic acid with **Br-B(9)** produced the *p*-tolyl-B(2) isomer as the major product.[45] This suggests that certain transmetalating agents can mitigate the nucleophilicity of the cross-coupling partner and allow the relative rates of cage-walking and transmetalation to be competitive with each other.

We surveyed the steric and electronic effects of –F and $-OCH_3$ substituents on the efficacy of tandem cage-walking/Suzuki–Miyaura cross-coupling. Generally, we found that electron-rich arylboronic acids (*p*/*m*/*o*-methoxyphenylboronic acid) produced more *B*-aryl-*m*-carborane (**Aryl-mCB**) than electron-poor arylboronic acids (*p*/*m*/*o*-fluorophenylboronic acid) (Figure 4). The presence of an ortho substituent appears

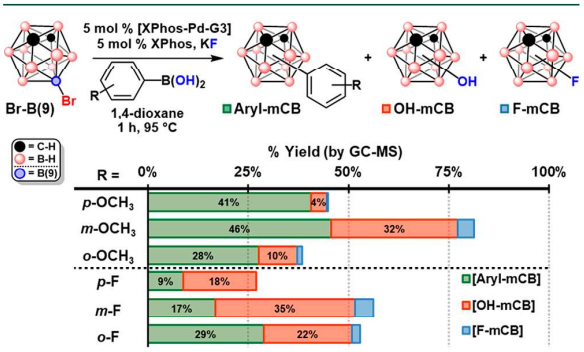

Figure 4. GC–MS yields of carborane-containing species produced during tandem cage-walking/Suzuki–Miyaura cross-coupling.

to have an inhibitory effect on the cross-coupling of *o*-methoxyphenylboronic acid but has a beneficial effect for *o*-fluorophenylboronic acid. Although both functional groups are ortho-directing, the increased steric bulk of the $-OCH_3$ group near the nucleophilic site may inhibit transmetalation and lead to less **Aryl-mCB** formation. Conversely, electron-poor arylboronic acids resulted in lower **Aryl-mCB** yields and more byproduct formation (vide infra). These differences in **Aryl-mCB** yield may be due to the reduced nucleophilicity of the arylboronic acid, which would make transmetalation of the aryl moiety more difficult. Additionally, arylboronic acids bearing Lewis basic groups such as 4-cyanophenylboronic acid

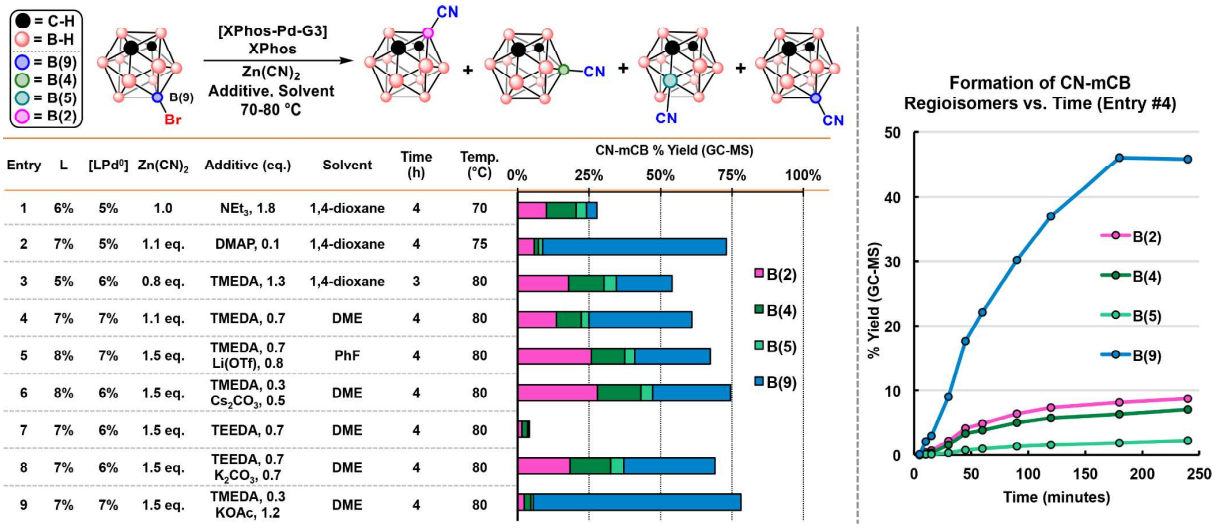

Figure 5. (left) Optimization of the tandem cage-walking/cross-coupling cyanation reaction. The bar graph indicates GC−MS yields of the cyano-*m*-carborane regioisomers for each reaction entry. (right) GC−MS reaction monitoring of cyano-*m*-carborane (**CN-mCB**) regioisomers produced during tandem cage-walking/cross-coupling.

and 3-pyridylboronic acid did not result in cross-coupling. The presence of Lewis basic groups in 4-cyanophenylboronic acid and 3-pyridylboronic acid can suppress the cage-walking process, which may prevent the formation of the more electrophilic B(2)-bound [XPhosPd(**mCB**)]$^+$ catalyst species.[49]

In addition to the formation of **Aryl-mCB**, we also observed the formation of *B*-hydroxy-*m*-carborane regioisomers (**OH-mCB**) and B-fluoro-*m*-carborane (**F-mCB**) as a byproduct of the tandem cage-walking/cross-coupling (Figure 4). While the formation of **OH-mCB** was observed previously by us and others[26,50] and is likely due to the presence of adventitious moisture in the system, the formation of **F-mCB** by cross-coupling of nucleophilic fluoride is rare.[27] Neither of these byproducts are surprising given the larger thermodynamic driving force for the formation of B−O and B−F bonds relative to C−O and C−F bonds.[51] This contrasts with Suzuki−Miyaura cross-coupling reactions, where off-cycle C−O and C−F bond formation is rarely observed even under aqueous reaction conditions. Notably, arylboronic acids with electron-withdrawing groups resulted in more **OH-mCB** than electron-rich arylboronic acids. The formation of **OH-mCB** may be due to transmetalation of the hydroxyl group from the boronic acid or from OH-containing byproducts resulting from its decomposition.

During the isolation of the **Aryl-mCB** compounds, we identified an air- and chromatographically stable ruby-colored compound that formed as a byproduct of the Suzuki−Miyaura cross-coupling reactions. Chromatographic isolation followed by spectroscopic analysis (^{11}B, ^{1}H, and ^{31}P NMR spectroscopy) suggested a species containing a metal-bound phosphine as well as a boron-cluster-containing fragment. Single-crystal X-ray crystallography of this material revealed a Pd-based complex containing an XPhos ligand bound in a κ^2-*P*,*C* fashion. The coordination sphere of the Pd center is completed by a dicarbollide ligand ([*nido*-7,9-$C_2B_9H_{11}]^{2-}$, *nido*-**CB**) bound in an η^5 fashion. On the basis of the nature of the phosphine and *nido*-**CB** ligands, the formal oxidation state of the Pd center in [XPhosPd(*nido*-**CB**)] is +2. Deboronation of carboranes is known to occur by nucleophilic attack at the electron-poor boron vertices of carboranes (Figure 2, step v).[52−54] Small nucleophiles such as F^- and OH^- can cause deboronation of **R-mCB** in situ to form the η^5-[*nido*-7,9-$C_2B_9H_{12}]^-$ ligand, which after deprotonation binds to the [XPhosPd] complex (vide infra).[52,53,55] To probe this pathway further, an independent synthesis of the [XPhosPd(*nido*-**CB**)] complex was accomplished by the reaction of (^{n}Bu$_4$N)[*nido*-7,9-$C_2B_9H_{12}$] with the [XPhos-Pd-G3] precatalyst. We found that [XPhosPd(*nido*-**CB**)] is not an active catalyst in carborane cross-coupling reactions, likely because of the greater coordinative saturation of the Pd center by the *nido*-**CB** ligand and the inability to regenerate Pd^0 from this species under the reaction conditions.[56−58]

A unique aspect of [XPhosPd(*nido*-**CB**)] is the lack of an exohedral functional group on the *nido*-**CB** ligand despite the use of functionalized carborane substrates. This suggests that cage-walking to the B(2) vertex may also activate the carborane toward deboronation and lead to deactivation of the [XPhosPd] catalyst by the formation of [XPhosPd(*nido*-**CB**)] (Figure 2, step vii). One possible decomposition route may be cage-walking/cross-coupling of OH^- or F^- at the B(2) vertex to generate a B(2)-X′-carborane (X′ = OH, F) that is more easily deboronated than B(2)-R-carborane (R = H, aryl).[52−55,59−61] Previous studies of carborane deboronation indicate that coordination of several nucleophiles to a B−H vertex is necessary to remove a boron vertex from the carborane cage.[54,59,60] Thus, off-cycle coupling of a small nucleophile such as OH^- or F^- at B(2) may activate the B(2)-X′-carborane (X′ = OH, F) toward deboronation and formation of *nido*-**CB**. This highlights the intricacies of using carborane substrates in cross-coupling, particularly in the presence of small nucleophiles, which can turn a substrate into a catalyst poison. Importantly, this mode of decomposition is distinctly different from the classical cross-coupling chemistry of aryl-based species and necessitates high Pd catalyst loadings.

Tandem Cage-Walking/Cyanation. Our studies of **Br-mCB** isomerization and tandem cage-walking/Suzuki−Miyaura coupling have so far revealed that tandem cage-

walking/cross-coupling is possible with sterically unencumbered nucleophiles. With these observations in mind, we set out to integrate the cage-walking cycle into Pd-catalyzed cross-coupling of a small nucleophile (CN^-). If successful, the resulting cyano-*m*-carborane (**CN-mCB**) regioisomers can be useful synthons in materials and medicinal chemistry.[30,62,63]

Cross-coupling of cyanide is a challenging transformation in general because of the strong affinity of the CN^- ligand to Pd(II), which leads to the formation of catalytically inactive species.[64] Efforts to prevent catalyst poisoning have previously focused on reducing and constantly maintaining a small amount of CN^- in the reaction mixture.[65] For our transformation, we chose $Zn(CN)_2$ as a cyanide source and transmetalation agent because of its strong CN^- binding affinity to Zn(II), which prevents the formation of free CN^- at high $Zn(CN)_2$ concentrations. Additionally, the redox nonactivity and weak binding of phosphine ligands to Zn(II) decreases the likelihood of [XPhosPd] oxidation or phosphine sequestration.[66]

Although $Zn(CN)_2$ is insoluble in most organic solvents because of the bridging μ^2 coordination of CN^- across zinc centers, forming Zn−CN−Zn-based coordination polymers in the solid state,[67] $Zn(CN)_2$ can be solubilized in alkaline and ammoniacal environments.[68−73] However, alkaline conditions may lead to undesirable **OH-mCB** formation or deboronation, as observed with the Suzuki−Miyaura cross-coupling reactions (vide supra). Alternatively, trialkylamines are suitable ligands for $Zn(CN)_2$ because they do not inhibit **Br-mCB** cage-walking, do not readily participate in the cross-coupling reaction, and can partially solubilize $Zn(CN)_2$.[68,71] Initially we used NEt_3 as a base to activate the [XPhos-Pd-G3] precatalyst and solubilize $Zn(CN)_2$, which led to a modest yield (<30% by GC−MS) of **CN-mCB** isomers (Figure 5, entry 1). Importantly, despite the low yield of **CN-mCB**, the **CN-B(2)** and **CN-B(4)** regioisomers were produced as the major **CN-mCB** products, validating our original hypothesis that under well-designed conditions small nucleophiles can be competent substrates in the discovered cage-walking process.

We then explored whether bidentate alkylamine ligands could increase the yield of **CN-mCB** by increasing the solubility of $Zn(CN)_2$ and promoting transmetalation of the CN^- anion from Zn to Pd. Use of *N*,*N*,*N*′,*N*′-tetramethylethylenediamine (TMEDA) as a ligand for $Zn(CN)_2$ increased the overall yield of **CN-mCB** regioisomers (65% by GC−MS), but the improvement in the **CN-mCB** yield also increased the amount of **CN-B(9)** relative to the B(2/4/5) **CN-mCB** regioisomers (Figure 5, entry 3). Switching to a larger bidentate alkylamine ligand, *N*,*N*,*N*′,*N*′-tetraethylethylenediamine (TEEDA), significantly decreased the amount of **CN-B(9)** relative to the B(2/4/5) **CN-mCB** regioisomers (Figure 5, entry 7), but it also decreased the overall **CN-mCB** yield (<5% by GC−MS). This shows that increasing the steric bulk of the transmetalating agent to promote tandem cage-walking/cross-coupling can have deleterious effects on the overall cross-coupling efficiency. In addition to using alkylamines, we also examined whether a N-donor heterocycle could increase the **CN-mCB** yield by increasing the solubility of $Zn(CN)_2$. The use of 4-(*N*,*N*-dimethylamino)pyridine (DMAP) as a ligand for $Zn(CN)_2$ significantly increased the yield of **CN-mCB** (74% by GC−MS), but the isomer distribution was mostly **CN-B(9)** (Figure 5, entry 2). We attribute this difference in regioisomer distribution to suppression of the cage-walking pathway through reversible coordination of DMAP to [XPhosPd(**mCB**)]$^+$ and the increased lability of CN^- when $Zn(CN)_2$ is ligated by the stronger N-donor DMAP ligand.

Despite improvements in the overall yield of **CN-mCB** regioisomers, we were unable to obtain complete conversion of **Br-B(9)** into **CN-mCB** regioisomers. As the tandem cage-walking/cross-coupling reaction proceeded, we observed darkening of the reaction mixture until a black/gray slurry formed within the first hour of the reaction. GC−MS analysis of a model cage-walking/cyanation reaction showed a gradual decay in the conversion of **Br-mCB** to **CN-mCB** until the reaction progress plateaued after ∼3 h (Figure 5). This suggests that the incomplete conversion of **Br-mCB** to **CN-mCB** is partially due to Pd^0 aggregation to form black Pd^0 particles, which are not effective catalysts for carborane cross-coupling (Figure 2, step vi).

Suspecting that accumulation of Br^- may inhibit further conversion of **Br-mCB** to **CN-mCB**, we examined whether addition of alkali metal salts could improve the **CN-mCB** yield by sequestering Br^-. Addition of Cs_2CO_3 or Li(OTf) increased the overall yield of **CN-mCB** regioisomers without inhibiting the cage-walking process, whereas KOAc had an opposite effect that predominantly produced **CN-B(9)** (Figure 5, entry 9). The differences in regioisomer yield with different alkali metal salts and N-donor ligands may be due to the speciation of $Zn(CN)_2$ into mono-, di-, tri-, and tetracyanozincate species.[71,74−76] The formation of various zinc cyanide species due to ligation by additives and reaction byproducts may alter the rate of CN^- transmetalation and account for the various **CN-mCB** regioisomer distributions observed throughout this study. Overall, through our optimization studies we developed several conditions to selectively control the incorporation of the cage-walking process into catalytic cross-coupling with small nucleophiles. In particular, if deactivation of the cage-walking process is desired, the addition of a Lewis base (e.g., DMAP; Figure 5, entry 2) effectively favors B(9) coupling. Alternatively, if the cage-walking process is desired, care should be taken to reduce the amount of Lewis basic species (e. g., Brønsted base or halide counterion) that can bind the proposed [XPhosPd(**mCB**)]$^+$ intermediate that leads to isomerization of **Br-mCB**.

CONCLUSIONS

Off-cycle processes in carborane cross-coupling were examined for their role in affecting tandem cage-walking/cross-coupling and in suppressing catalyst activity. The cage-walking process was studied in the absence and presence of a cross-coupling partner to identify conditions leading to tandem cage-walking/cross-coupling. We found that Pd-catalyzed cage-walking occurs with several dialkylbiarylphosphine ligands and that the cage-walking process can be enhanced or suppressed by the presence of additives such as $Ca(OH)_2$ or DMAP, respectively. These insights allowed us to identify substrate transmetalation strategies for tandem cage-walking/cross-coupling reactions with sterically unencumbered nucleophiles such as arylboronic acids and cyanide. The results reported here demonstrate the feasibility of using sterically unencumbered substrates in tandem cage-walking/cross-coupling to synthesize B-substituted carborane regioisomers. These studies further highlight the importance of the bulky biaryl-based phosphine ligands originally developed by Buchwald and co-workers in transition metal catalysis by extending their application to organomimetic clusters.

■ ASSOCIATED CONTENT

Supporting Information

The Supporting Information is available free of charge on the ACS Publications website at DOI: 10.1021/acs.oprd.9b00257.

Full procedures and crystallographic and other characterization data (PDF)

■ AUTHOR INFORMATION

Corresponding Author

*E-mail: spokoyny@chem.ucla.edu.

ORCID

Alexander M. Spokoyny: 0000-0002-5683-6240

Notes

The authors declare no competing financial interest.

■ ACKNOWLEDGMENTS

This article is dedicated to a mentor and friend, Professor Stephen L. Buchwald, whose seminal contributions to chemistry continue to inspire us all. We thank the NIGMS (R35GM124746) and the National Defense Science and Engineering Graduate Fellowship (NDSEG to R.M.D) for supporting this project.

■ REFERENCES

(1) *Metal-Catalyzed Cross-Coupling Reactions*; de Meijere, A., Diederich, F., Eds.; Wiley-VCH: Weinheim, Germany, 2004.

(2) Johansson Seechurn, C. C. C.; Kitching, M. O.; Colacot, T. J.; Snieckus, V. Palladium-Catalyzed Cross-Coupling: A Historical Contextual Perspective to the 2010 Nobel Prize. *Angew. Chem., Int. Ed.* **2012**, *51* (21), 5062−5085.

(3) Shultz, L. H.; Brookhart, M. Measurement of the Barrier to β-Hydride Elimination in a β-Agostic Palladium−Ethyl Complex: A Model for the Energetics of Chain-Walking in (α-Diimine)PdR$^+$ Olefin Polymerization Catalysts. *Organometallics* **2001**, *20* (19), 3975−3982.

(4) Crabtree, R. H. Deactivation in Homogeneous Transition Metal Catalysis: Causes, Avoidance, and Cure. *Chem. Rev.* **2015**, *115* (1), 127−150.

(5) Balcells, D.; Nova, A. Designing Pd and Ni Catalysts for Cross-Coupling Reactions by Minimizing Off-Cycle Species. *ACS Catal.* **2018**, *8* (4), 3499−3515.

(6) Hassam, M.; Taher, A.; Arnott, G. E.; Green, I. R.; van Otterlo, W. A. L. Isomerization of Allylbenzenes. *Chem. Rev.* **2015**, *115* (11), 5462−5569.

(7) Becica, J.; Glaze, O. D.; Wozniak, D. I.; Dobereiner, G. E. Selective Isomerization of Terminal Alkenes to (*Z*)-2-Alkenes Catalyzed by an Air-Stable Molybdenum(0) Complex. *Organometallics* **2018**, *37* (3), 482−490.

(8) Milner, P. J.; Kinzel, T.; Zhang, Y.; Buchwald, S. L. Studying Regioisomer Formation in the Pd-Catalyzed Fluorination of Aryl Triflates by Deuterium Labeling. *J. Am. Chem. Soc.* **2014**, *136* (44), 15757−15766.

(9) Li, J.; Sun, C.; Demerzhan, S.; Lee, D. Metal-Catalyzed Rearrangement of Cyclopropenes to Allenes. *J. Am. Chem. Soc.* **2011**, *133* (33), 12964−12967.

(10) Curran, K.; Risse, W.; Hamill, M.; Saunders, P.; Muldoon, J.; Asensio De La Rosa, R.; Tritto, I. Palladium(II)-Catalyzed Rearrangement and Oligomerization Reactions of *cis*-Bicyclo[4.2.0]oct-7-ene. *Organometallics* **2012**, *31* (3), 882−889.

(11) Wang, J. Y.; Strom, A. E.; Hartwig, J. F. Mechanistic Studies of Palladium-Catalyzed Aminocarbonylation of Aryl Chlorides with Carbon Monoxide and Ammonia. *J. Am. Chem. Soc.* **2018**, *140* (25), 7979−7993.

(12) Hartwig, J. F. Catalyst-Controlled Site-Selective Bond Activation. *Acc. Chem. Res.* **2017**, *50* (3), 549−555.

(13) Larsen, C. R.; Grotjahn, D. B. Stereoselective Alkene Isomerization over One Position. *J. Am. Chem. Soc.* **2012**, *134* (25), 10357−10360.

(14) Lee, C. W.; Zhuang, Z. P.; Kung, M. P.; Plössl, K.; Skovronsky, D.; Gur, T.; Hou, C.; Trojanowski, J. Q.; Lee, V. M. Y.; Kung, H. F. Isomerization of (*Z*,*Z*) to (*E*,*E*)1-Bromo-2,5-bis-(3-hydroxycarbonyl-4-hydroxy)-styrylbenzene in Strong Base: Probes for Amyloid Plaques in the Brain. *J. Med. Chem.* **2001**, *44* (14), 2270−2275.

(15) Li, J.; Logan, C. F.; Jones, M. Simple Syntheses and Alkylation Reactions of 3-Iodo-*o*-carborane and 9,12-Diiodo-*o*-carborane. *Inorg. Chem.* **1991**, *30* (25), 4866−4868.

(16) Eriksson, L.; Beletskaya, I.; Bregadze, V.; Sivaev, I.; Sjoberg, S. Palladium-Catalyzed Cross-Coupling Reactions of Arylboronic Acids and 2-I-*p*-Carborane. *J. Organomet. Chem.* **2002**, *657* (1−2), 267−272.

(17) Lin, F.; Yu, J.-L.; Shen, Y.; Zhang, S.-Q.; Spingler, B.; Liu, J.; Hong, X.; Duttwyler, S. Palladium-Catalyzed Selective Five-Fold Cascade Arylation of the 12-Vertex Monocarborane Anion by B−H Activation. *J. Am. Chem. Soc.* **2018**, *140* (42), 13798−13807.

(18) Cheng, R.; Li, B.; Wu, J.; Zhang, J.; Qiu, Z.; Tang, W.; You, S. L.; Tang, Y.; Xie, Z. Enantioselective Synthesis of Chiral-at-Cage o -Carboranes via Pd-Catalyzed Asymmetric B−H Substitution. *J. Am. Chem. Soc.* **2018**, *140* (13), 4508−4511.

(19) Anderson, K. P.; Mills, H. A.; Mao, C.; Kirlikovali, K. O.; Axtell, J. C.; Rheingold, A. L.; Spokoyny, A. M. Improved Synthesis of Icosahedral Carboranes Containing Exopolyhedral B−C and C−C Bonds. *Tetrahedron* **2019**, *75* (2), 187−191.

(20) Beletskaya, I. P.; Bregadze, V. I.; Ivushkin, V. A.; Zhigareva, G. G.; Petrovskii, P. V.; Sivaev, I. B. Palladium-Catalyzed Alkynylation of 2-Iodo-*p*-carboranes and 9-Iodo-*m*-carboranes. *Russ. J. Org. Chem.* **2005**, *41* (9), 1359−1366.

(21) Sevryugina, Y.; Julius, R. L.; Hawthorne, M. F. Novel Approach to Aminocarboranes by Mild Amidation of Selected Iodo-Carboranes. *Inorg. Chem.* **2010**, *49* (22), 10627−10634.

(22) Kabytaev, K. Z.; Everett, T. A.; Safronov, A. V.; Sevryugina, Y. V.; Jalisatgi, S. S.; Hawthorne, M. F. *B*-Mercaptocarboranes: A New Synthetic Route. *Eur. J. Inorg. Chem.* **2013**, *2013* (14), 2488−2491.

(23) Safronov, A. V.; Kabytaev, K. Z.; Jalisatgi, S. S.; Hawthorne, M. F. Novel Iodinated Carboranes: Synthesis of the 8-Iodo-7,9-dicarba-*nido*-undecaborate Anion and 2-Iodo-1,7-dicarba-*closo*-dodecaborane. *Dalton Trans.* **2014**, *43* (33), 12467.

(24) Wingen, L. M.; Scholz, M. S. *B*-Cyanodicarba-*closo*-dodecaboranes: Facile Synthesis and Spectroscopic Features. *Inorg. Chem.* **2016**, *55* (17), 8274−8276.

(25) Saleh, L. M. A.; Dziedzic, R. M.; Khan, S. I.; Spokoyny, A. M. Forging Unsupported Metal−Boryl Bonds with Icosahedral Carboranes. *Chem. - Eur. J.* **2016**, *22* (25), 8466−8470.

(26) Dziedzic, R. M.; Saleh, L. M. A.; Axtell, J. C.; Martin, J. L.; Stevens, S. L.; Royappa, A. T.; Rheingold, A. L.; Spokoyny, A. M. B−N, B−O, and B−CN Bond Formation via Palladium-Catalyzed Cross-Coupling of *B*-Bromo-Carboranes. *J. Am. Chem. Soc.* **2016**, *138* (29), 9081−9084.

(27) Ishita, K.; Khalil, A.; Tiwari, R.; Gallucci, J.; Tjarks, W. Bis(tri-*tert*-butylphosphine)palladium(0)-Catalyzed Iodine−Fluorine Exchange at *closo*-Carboranes. *Eur. J. Inorg. Chem.* **2018**, *2018* (24), 2821−2825.

(28) Leites, L. A.; Introductlon, I.; Boranes, I.; Boranes, I.; Modes, B.; Boranes, G. I.; Heteroatoms, C. Vibrational Spectroscopy of Carboranes and Parent Boranes and Its Capabilities in Carborane Chemistry. *Chem. Rev.* **1992**, *92* (2), 279−323.

(29) Bendel, P. Biomedical Applications of ^{10}B and ^{11}B NMR. *NMR Biomed.* **2005**, *18* (2), 74−82.

(30) Leśnikowski, Z. J. Challenges and Opportunities for the Application of Boron Clusters in Drug Design. *J. Med. Chem.* **2016**, *59* (17), 7738−7758.

(31) Messina, M. S.; Graefe, C. T.; Chong, P.; Ebrahim, O. M.; Pathuri, R. S.; Bernier, N. A.; Mills, H. A.; Rheingold, A. L.; Frontiera, R. R.; Maynard, H. D.; Spokoyny, A. M. Carborane RAFT Agents as

Tunable and Functional Molecular Probes for Polymer Materials. *Polym. Chem.* **2019**, *10* (13), 1660−1667.
(32) Serino, A. C.; Anderson, M. E.; Saleh, L. M. A.; Dziedzic, R. M.; Mills, H.; Heidenreich, L. K.; Spokoyny, A. M.; Weiss, P. S. Work Function Control of Germanium through Carborane-Carboxylic Acid Surface Passivation. *ACS Appl. Mater. Interfaces* **2017**, *9* (40), 34592−34596.
(33) Quan, Y.; Qiu, Z.; Xie, Z. Transition-Metal-Catalyzed Selective Cage B−H Functionalization of *o*-Carboranes. *Chem. - Eur. J.* **2018**, *24* (12), 2795−2805.
(34) Duttwyler, S. Recent Advances in B−H Functionalization of Icosahedral Carboranes and Boranes by Transition Metal Catalysis. *Pure Appl. Chem.* **2018**, *90* (4), 733−744.
(35) Quan, Y.; Xie, Z. Controlled Functionalization of *o*-Carborane via Transition Metal Catalyzed B−H Activation. *Chem. Soc. Rev.* **2019**, *48*, 3660−3673.
(36) Lyu, H.; Zhang, J.; Yang, J.; Quan, Y.; Xie, Z. Catalytic Regioselective Cage B(8)−H Arylation of *o*-Carboranes via "Cage-Walking" Strategy. *J. Am. Chem. Soc.* **2019**, *141* (10), 4219−4224.
(37) Eleazer, B. J.; Smith, M. D.; Popov, A. A.; Peryshkov, D. V. Expansion of the (BB)>Ru Metallacycle with Coinage Metal Cations: Formation of B−M−Ru−B (M = Cu, Ag, Au) Dimetalacyclodiboryls. *Chem. Sci.* **2018**, *9* (9), 2601−2608.
(38) Dziedzic, R. M.; Spokoyny, A. M. Metal-Catalyzed Cross-Coupling Chemistry with Polyhedral Boranes. *Chem. Commun.* **2019**, *55* (4), 430−442.
(39) Safronov, A. V; Sevryugina, Y. V; Jalisatgi, S. S.; Kennedy, R. D.; Barnes, C. L.; Hawthorne, M. F. Unfairly Forgotten Member of the Iodocarborane Family: Synthesis and Structural Characterization of 8-Iodo-1,2-dicarba-*closo*-dodecaborane, Its Precursors, and Derivatives. *Inorg. Chem.* **2012**, *51* (4), 2629−2637.
(40) Safronov, A. V.; Kabytaev, K. Z.; Jalisatgi, S. S.; Hawthorne, M. F. Novel Iodinated Carboranes: Synthesis of the 8-Iodo-7,9-dicarba-*nido*-undecaborate anion and 2-Iodo-1,7-dicarba-*closo*-dodecaborane. *Dalton Trans.* **2014**, *43* (33), 12467−12469.
(41) Lipscomb, W. N. Framework Rearrangement in Boranes and Carboranes. *Science* **1966**, *153* (3734), 373−378.
(42) Kalinin, V. N.; Kobel'kova, N. I.; Zakharkin, L. I. Synthesis of 2- and 4-Aryl-*m*-Carboranes and Electronic Effects of the 4-*m*-Carboranyl Group. *J. Organomet. Chem.* **1979**, *172* (4), 391−395.
(43) Baše, T.; Macháček, J.; Hájková, Z.; Langecker, J.; Kennedy, J. D.; Carr, M. J. Thermal Isomerizations of Monothiolated Carboranes $(HS)C_2B_{10}H_{11}$ and the Solid-State Investigation of 9-(HS)-1,2-$C_2B_{10}H_{11}$ and 9-(HS)-1,7-$C_2B_{10}H_{11}$. *J. Organomet. Chem.* **2015**, *798*, 132−140.
(44) Bakardjiev, M.; Štíbr, B.; Holub, J.; Padělková, Z.; Růžička, A. Simple Synthesis, Halogenation, and Rearrangement of *closo*-1,6-$C_2B_8H_{10}$. *Organometallics* **2015**, *34* (2), 450−454.
(45) Dziedzic, R. M.; Martin, J. L.; Axtell, J. C.; Saleh, L. M. A.; Ong, T. C.; Yang, Y. F.; Messina, M. S.; Rheingold, A. L.; Houk, K. N.; Spokoyny, A. M. Cage-Walking: Vertex Differentiation by Palladium-Catalyzed Isomerization of B(9)-Bromo-*meta*-Carborane. *J. Am. Chem. Soc.* **2017**, *139* (23), 7729−7732.
(46) Bruno, N. C.; Tudge, M. T.; Buchwald, S. L. Design and Preparation of New Palladium Precatalysts for C−C and C−N Cross-Coupling Reactions. *Chem. Sci.* **2013**, *4* (3), 916−920.
(47) Lee, H. G.; Milner, P. J.; Buchwald, S. L. An Improved Catalyst System for the Pd-Catalyzed Fluorination of (Hetero)aryl Triflates. *Org. Lett.* **2013**, *15* (21), 5602−5605.
(48) Rajamathi, M.; Vishnu Kamath, P.; Seshadri, R. Polymorphism in Nickel Hydroxide: Role of Interstratification. *J. Mater. Chem.* **2000**, *10* (2), 503−506.
(49) Düfert, M. A.; Billingsley, K. L.; Buchwald, S. L. Suzuki−Miyaura Cross-Coupling of Unprotected, Nitrogen-Rich Heterocycles: Substrate Scope and Mechanistic Investigation. *J. Am. Chem. Soc.* **2013**, *135* (34), 12877−12885.
(50) Beletskaya, I. P.; Bregadze, V. I.; Kabytaev, K. Z.; Zhigareva, G. G.; Petrovskii, P. V.; Glukhov, I. V.; Starikova, Z. A. Palladium-Catalyzed Amination of 2-Iodo-*para*-Carborane. *Organometallics* **2007**, *26* (9), 2340−2347.
(51) Darwent, B. deB. *Bond Dissociation Energies in Simple Molecules*; National Standard Reference Data Series, National Bureau of Standards, Vol. *31*; U.S. National Bureau of Standards: Gaithersburg, MD, 1970; p 48.
(52) Fox, M. A.; Gill, W. R.; Herbertson, P. L.; MacBride, J. A. H.; Wade, K.; Colquhoun, H. M. Deboronation of C-Substituted *ortho*- and *meta-closo*-Carboranes Using "Wet" Fluoride Ion Solutions. *Polyhedron* **1996**, *15* (4), 565−571.
(53) Fox, M. A.; Wade, K. Deboronation of 9-Substituted-*ortho*- and -*meta*-Carboranes. *J. Organomet. Chem.* **1999**, *573* (1−2), 279−291.
(54) Taoda, Y.; Sawabe, T.; Endo, Y.; Yamaguchi, K.; Fujii, S.; Kagechika, H. Identification of an Intermediate in the Deboronation of *ortho*-Carborane: An Adduct of *ortho*-Carborane with Two Nucleophiles on One Boron Atom. *Chem. Commun.* **2008**, No. 17, 2049−2051.
(55) Yoo, J.; Hwang, J. W.; Do, Y. Facile and Mild Deboronation of *o*-Carboranes Using Cesium Fluoride. *Inorg. Chem.* **2001**, *40* (3), 568−570.
(56) Warren Jr, L.; Hawthorne, M. Metallocene Analogs of Copper, Gold, and Palladium Derived from the (3)-1,2-Dicarbollide Ion. *J. Am. Chem. Soc.* **1968**, *90* (18), 4823−4828.
(57) Jasper, S. A.; Huffman, J. C.; Todd, L. J. Palladium-Assisted Cyano Substitution Reactions of $(PMe_2Ph)_2Pd(B_9H_9As_2)$ and $(PMe_2Ph)_2Pd(B_9C_2H_{11})$. X-ray Crystal and Molecular Structures of 5-CN-1,1-$(PMe_2Ph)_2$-*closo*-1,2,3-$PdAs_2B_9H_8$, 1-^{t}BuNC-5-CN-1-(PMe_2Ph)-*closo*-1,2,3-$PdAs_2B_9H_8$, and 4,5-$(CN)_2$-1,1-$(PMe_2Ph)_2$-*closo*-1,2,3-$PdC_2B_9H_8$. *Inorg. Chem.* **1995**, *34* (26), 6430−6439.
(58) Jasper, S. A.; Huffman, J. C.; Todd, L. J. Synthesis of a Metallaborane Complex Containing Pd(III) and the First Doubly Charge Compensated Ollide Ion. X-ray Crystal Structure of 1,4-Br_2-1,2,5-$(PMe_2Ph)_3$-*closo*-1-$PdB_{11}H_8$. *Inorg. Chem.* **1998**, *37* (23), 6060−6064.
(59) Willans, C. E.; Kilner, C. A.; Fox, M. A. Deboronation and Deprotonation of *ortho*-Carborane with N-Heterocyclic Carbenes. *Chem. - Eur. J.* **2010**, *16* (35), 10644−10648.
(60) Zheng, F.; Xie, Z. Reaction of *o*-Carboranes with Sterically Demanding N-Heterocyclic Carbene: Synthesis and Structural Characterization of 1:1 Adducts. *Dalton Trans.* **2012**, *41* (41), 12907−12914.
(61) Zhang, C. Y.; Cao, K.; Xu, T. T.; Wu, J.; Jiang, L.; Yang, J. A Facile Approach for the Synthesis of *Nido*-Carborane Fused Oxazoles via One Pot Deboronation/Cyclization of 9-Amide-*o*-Carboranes. *Chem. Commun.* **2019**, *55* (6), 830−833.
(62) Issa, F.; Kassiou, M.; Rendina, L. M. Boron in Drug Discovery: Carboranes as Unique Pharmacophores in Biologically Active Compounds. *Chem. Rev.* **2011**, *111* (9), 5701−5722.
(63) Scholz, M.; Hey-Hawkins, E. Carbaboranes as Pharmacophores: Properties, Synthesis, and Application Strategies. *Chem. Rev.* **2011**, *111* (11), 7035−7062.
(64) Erhardt, S.; Grushin, V. V.; Kilpatrick, A. H.; Macgregor, S. A.; Marshall, W. J.; Roe, D. C. Mechanisms of Catalyst Poisoning in Palladium-Catalyzed Cyanation of Haloarenes. Remarkably Facile C−N Bond Activation in the $[(Ph^3P)^4Pd]/[Bu^4N]^+$ CN-System. *J. Am. Chem. Soc.* **2008**, *130* (14), 4828−4845.
(65) Anbarasan, P.; Schareina, T.; Beller, M. Recent Developments and Perspectives in Palladium-Catalyzed Cyanation of Aryl Halides: Synthesis of Benzonitriles. *Chem. Soc. Rev.* **2011**, *40* (10), 5049−5067.
(66) Heaney, H. Zinc Cyanide. In *Encyclopedia of Reagents for Organic Synthesis*; John Wiley & Sons: Chichester, U.K., 2001; Vol. 3, p 533.
(67) Hoskins, B. F.; Robson, R. Design and Construction of a New Class of Scaffolding-like Materials Comprising Infinite Polymeric Frameworks of 3D-Linked Molecular Rods. A Reappraisal of the $Zn(CN)^2$ and $Cd(CN)^2$ Structures and the Synthesis and Structure of the Diamond-Related Framework. *J. Am. Chem. Soc.* **1990**, *112* (4), 1546−1554.

(68) Ahuja, I. S.; Singh, R. Bidentate Bridged Morpholine Complexes with Zinc(II) and Cadmium(II) Cyanides. *J. Coord. Chem.* **1976**, *5* (3), 167–170.
(69) Monge, A.; Martínez-Ripoll, M.; García-Blanco, S. The Adduct Zinc Dicyanide–Bis(2,9-Dimethyl-1,10-Phenanthroline) Trihydrate. *Acta Crystallogr., Sect. B: Struct. Crystallogr. Cryst. Chem.* **1978**, *34* (9), 2847–2850.
(70) Ho, K.; Yu, W.; Cheung, K.; Che, C. A Blue Photoluminescent $[Zn(L)(CN)_2]$ (L = 2,2′-Dipyridylamine) Material with a Supramolecular One-Dimensional Chain Structure. *Chem. Commun.* **1998**, *3* (19), 2101–2102.
(71) Jasiewicz, B.; Boczoń, W.; Mumot, A.; Warzajtis, B.; Rychlewska, U. Synthesis, Spectroscopy and Crystal Structure of α-Isosparteine Complexes with ZnX^2 (X = Br, CN, Cl). *J. Mol. Struct.* **2005**, *737* (2–3), 239–244.
(72) Das, S.; Nag, A.; Goswami, D.; Bharadwaj, P. K. Zinc(II)- and Copper(I)-Mediated Large Two-Photon Absorption Cross Sections in a Bis-Cinnamaldiminato Schiff Base. *J. Am. Chem. Soc.* **2006**, *128* (2), 402–403.
(73) Sayin, E.; Kürkçüoğlu, G. S.; Yeşilel, O. Z.; Hökelek, T. Synthesis, Crystal Structure and Spectroscopic Properties of One-Dimensional Zinc(II)–Cyanide Complex with 1-Methylimidazole, $[Zn(\mu\text{-}CN)(CN)(1\text{-meim})]_n$. *Z. Kristallogr. - Cryst. Mater.* **2015**, *230* (6), 421–426.
(74) Pickardt, J.; Staub, B. Kristallstruktur Des Cyanoverbrückten Polymeren Zinkcyanid-Pyridin-Komplexes $[Zn(Py)^2][Zn(CN)^4]$/ Crystal Structure of the Cyano Linked Polymeric Zinc Cyanide Pyridine Complex $[Zn(Py)^2][Zn(CN)^4]$. *Z. Naturforsch., B: J. Chem. Sci.* **1995**, *50* (10), 1517–1520.
(75) Guo, Y.; Weiss, R.; Boese, R.; Epple, M. Synthesis, Structural Characterization and Thermochemical Reactivity of Tris-(Ethylenediamine)Zinc Tetracyanozincate, a Precursor for Nanoscale ZnO. *Thermochim. Acta* **2006**, *446* (1–2), 101–105.
(76) Kürkçüoğlu, G. S.; Yeşilel, O. Z.; Şahin, O.; Sayin, E.; Büyükgüngör, O. Dinuclear Zinc(II) Complex with Tris(2-Aminoethyl) Amine Ligand: Synthesis, Structure and Properties. *Z. Kristallogr. - Cryst. Mater.* **2015**, *230* (6), 407–412.

Chapter 5. Reversible Silver Electrodeposition from Boron Cluster Ionic Liquid Electrolytes

This chapter describes our work on creating a boron cluster based ionic liquid electrolyte for electrodeposition of silver films for controlling the properties (e.g. infrared transmissivity) of electrochemical cells.

Chapter 5 is a reprint of Dziedzic, R. M.; Waddington, M. A.; Lee, S. E.; Kleinsasser, J.; Plumley, J. B.; Ewing, W. C.; Bosley, B. D.; Lavallo, V.; Peng, T. L.; Spokoyny, A. M. Reversible Silver Electrodeposition from Boron Cluster Ionic Liquid (BCIL) Electrolytes. *ACS Appl. Mater. Interfaces* **2018**, *10*, 6825-6830. DOI: 10.1021/acsami.7b19302 with permission from the American Chemical Society.

Additional supporting information is available free of charge from https://pubs.acs.org/doi/abs/10.1021/acsami.7b19302.

Reversible Silver Electrodeposition from Boron Cluster Ionic Liquid (BCIL) Electrolytes

Rafal M. Dziedzic,[†,‡] Mary A. Waddington,[†,‡] Sarah E. Lee,[§] Jack Kleinsasser,[§] John B. Plumley,[⊥,∥] William C. Ewing, Beth D. Bosley,[*,#] Vincent Lavallo,[*,§] Thomas L. Peng,[*,⊥] and Alexander M. Spokoyny[*,‡,▽]

[‡]Department of Chemistry and Biochemistry, University of California, Los Angeles, 607 Charles E. Young Drive East, Los Angeles, California 90095, United States

[§]Department of Chemistry, University of California, Riverside, 501 Big Springs Road, Riverside, California 92521, United States

[⊥]Air Force Research Laboratory, Kirtland AFB, Albuquerque, New Mexico 87117, United States

[∥]Department of Chemistry and Chemical Biology, University of New Mexico, 300 Terrace Street Northeast, Albuquerque, New Mexico 87131, United States

[#]Boron Specialties LLC, 2301 Duss Avenue, Building 9, Ambridge, Pennsylvania 15003, United States

[▽]California NanoSystems Institute (CNSI), University of California, Los Angeles, 570 Westwood Plaza, Los Angeles, California 90095, United States

Supporting Information

ABSTRACT: Electrochemical systems offer a versatile means for creating adaptive devices. However, the utility of electrochemical deposition is inherently limited by the properties of the electrolyte. The development of ionic liquids enables electrodeposition in high-vacuum environments and presents opportunities for creating electrochemically adaptive and regenerative spacecraft components. In this work, we developed a silver-rich, boron cluster ionic liquid (BCIL) for reversible electrodeposition of silver films. This air and moisture stable electrolyte was used to deposit metallic films in an electrochemical cell to tune the emissivity of the cell in situ, demonstrating a proof-of-concept design for spacecraft thermal control.

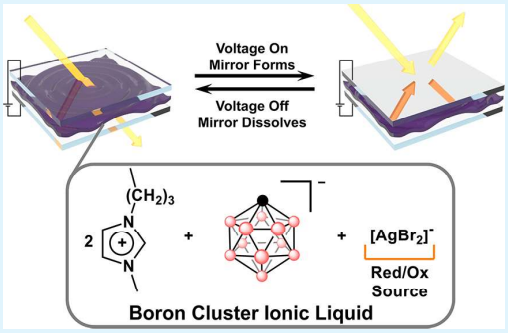

KEYWORDS: *electrodeposition, ionic liquids, infrared transparent electrochemical cell, carboranes, boron clusters*

Electrodeposited metallic structures are ubiquitous in modern technologies (e.g., batteries, protective coatings, displays, and microchips) and emerging technologies such as resistive memory and reconfigurable electronics.[1,2] The broad utility of electrochemically deposited structures grows as new electrolytes enable electrodeposition in increasingly challenging environments. Controlled reversible electrodeposition of metallic structures offers tunable optical properties and electrical conductivity along with the ability to adapt the electrochemical system to changing application needs. This adaptability is appealling in the context of reconfigurable electronic components which could extend a device's lifetime through in situ restructuring.

Early electrodeposition methods used aqueous electrolytes because of the solubility of common metal ions.[1] The development of nonaqueous electrolytes has enabled safe electrodeposition of water sensitive metals for new electrochemical applications such as high density energy storage.[3] Additionally, electrodepostion from ionic liquids has emerged as a potential alternative to organic solvent electrolytes, presenting new opportunities for electrodeposition in high vacuum and hostile environments such as electron microscopes and plasma chambers.[4]

Ionic liquids (ILs), salts with low melting points (typically <100 °C), combine the high ion solubility of aqueous media, the chemical flexibility of organic solvents, and low volatility and wide electrochemical windows achievable with molten salts.[7] The versatility of ILs is increased by tailoring the cation−anion pairs for individual applications.[5] Yet, despite the numerous cation−anion pairs that can form ionic liquids, much of ionic liquid tunability is achieved by modifying the cationic component.[5,6] This disparity is largely due to the synthetic availability of cationic molecular scaffolds such as ammonium, phosphonium, and heterocyclic motifs. Conversely, ionic liquids in which the anionic component

Received: December 22, 2017
Accepted: February 6, 2018
Published: February 6, 2018

engenders the IL properties are scarce and the anions are seldom amenable to additional functionalization.[7−10] Furthermore, the relative instability of commonly used IL anions limits the longevity of IL-based electrochemical devices. This becomes especially problematic when designing systems which require prolonged operation time. Therefore, we sought to develop an ionic liquid that contains a highly stable and easily tunable anionic component. Such "anion-based" ILs could use the metal of interest as the cation and enable high metal loadings suitable for rapid electrodeposition. Anionic polyhedral boranes represent a class of modular molecular building blocks suitable for designing "anion-based" boron cluster ionic liquids (BCILs).[11,12] Their robust boron-cluster framework provides an anionic scaffold amenable to tuning of melting point, solubility, and redox potential.[13,14] In this work, we set out to develop an all-ionic electrolyte suitable for reversible deposition of silver films. Specifically, we describe an all-ionic electrolyte to reversibly deposit silver films for the purpose of controlling infrared (IR) emission from an electrochemical cell as a means of actively regulating thermal emission. This technology complements existing approaches to controlling thermal emission from spacecraft surfaces.[15−18] Importantly, BCILs represent a critical component allowing these devices to perform reliably without having to exclude air and moisture, common contaminants that are introduced during electrochemical device assembly that are difficult to remove.

Silver films play an important technological role as electrical conductors and optical coatings. Silver offers unique advantages over other transition metals because of its high spectral reflectivity, high electrical conductivity, and corrosion resistance.[19] These qualities make silver an attractive metal for tuning the properties of spacecraft surfaces. Additionally, the low volatility of IL electrolytes offers a means of performing electrodeposition in high vacuum environments. Because of its positive reduction potential, only small voltages are required to electrodeposit silver from ionic salt precursors.[1] Electrodeposition of silver was historically performed using cyanide-based electrolytes due to the formation of stable $Ag(CN)_x^{1-x}$ complexes.[1] However, the toxicity of aqueous cyanide baths lead to the development of silver electrodeposition from ILs and organic solvents.[5,20] These nonaqueous electrolytes were suitable for reversible silver electrodeposition and served as proof-of-concept works for electrochemically modulated optical films.[21−23] The reversibility in these systems is attained from the halide-trihalide redox couples (X^-/X_3^-, X = Cl, Br, or I)[24,25] and stable $[AgX_2]^-$ complexes.[26] Despite these advances, reversibility in all-ionic electrolytes was limited only to a handful of ILs. The majority of these, however, still generate unstable, volatile, or corrosive decomposition products (Figure 1A).[27,28] In this report, we detail our work on creating an electrolyte for silver deposition containing a stable anion amenable to additional functionalization.

We developed a salt metathesis reaction between 1-butyl-3-methyl-imidazolium bromide, [BMIM]Br, and silver monocarborane, $Ag[HCB_{11}H_{11}]$, to generate a boron cluster ionic liquid, **BCIL-1,** with high silver content (Figure 2A). The parent carborane salt can be easily synthesized via a salt metathesis reaction between $Cs[HCB_{11}H_{11}]$ and $AgNO_3$ with an 82% yield (see the Supporting Information) This ionic liquid features an inert ionic matrix of $[BMIM]^+$ and $[HCB_{11}H_{11}]^-$ ions with $[AgBr_2]^-$ ions acting as the primary redox species (Figure 2A). Dialkylimidazolium cations and

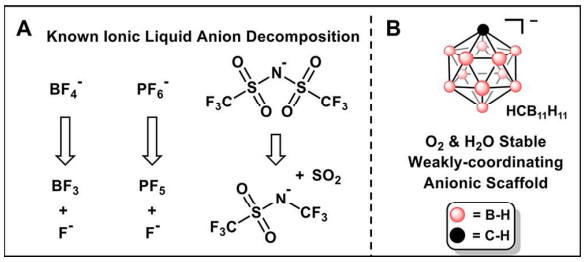

Figure 1. (A) some decomposition products of commonly used ionic liquid anions. (B) a representative monocarborane anion used in this work.

monocarborane anions were selected due to their electrochemical stability and weakly coordinating characteristics suitable for designing an inert ionic matrix.[29] The BCILs were enclosed between two FTO electrodes to form a transparent, two-electrode electrodeposition cell (Figure 2A). One FTO electrode was set as the working electrode while the other was set as both the counter and reference electrode. Cyclic voltammograms (CVs) show a reduction peak corresponding to reduction of silver complexes to form silver deposits at the working electrode (Figures 2 and 3). Electrodeposition begins at −1.5 V vs FTO with a distinct current loop occurring in the cathodic region which indicates a nucleation-limited deposition.[20] Reversing the polarity of the electrochemical cell toward +0.3 V vs FTO leads to dissolution of the silver deposits at the working electrode back into the electrolyte. It was also observed that halide and metal ion addives can affect the rate of the silver deposition and etching (Figure 2B and Figure 3). A general feature of these IL based electrolytes is an excess of halide, X^- (X = Br or Cl), to Ag^+. Typically, X^-:Ag^+ ion ratios of 2.5:1 were sufficient to fully dissolve the silver salts at room temperature. The excess halide promotes the formation of $AgBr_x^{1-x}$ species and provides additional halide ions to access the halide-trihalide (X^-/X_3^-) redox couple.

As the composition of the electrolyte, with a fixed halide concentration, is varied from chloride-rich to bromide-rich the potential for silver electrodeposition shifts to less cathodic potentials (Figure 3). This dependence on halide identity in the BCIL provides a simple method for tuning the onset of silver reduction and the current density of silver electrodeposition. Similar irreversible behavior in previously reported optical modulation devices were resolved by adding Cu(II) salts.[20,22] Related studies on the effects of $CuBr_2$ in [BMIM]Br ionic liquids found that $CuBr_2$ complexes were effective at etching copper films.[30] Likewise, addition of 10 mol % $CuBr_2$ (relative to Ag^+) to **BCIL-1** dramatically improved the reversibility of the ionic liquid formulation, generating **BCIL-2** (Figure 2B). Noteworthy was the change in film dissolution dynamics, wherein silver films deposited in the presence of Cu(II) were readily removed and exhibited larger oxidative currents (Figures 2B and 3).

Previously, it has been shown that water content present in ILs during their ambient handling can alter the reversibility of silver deposition.[31] Importantly, **BCIL-2** containing devices placed into a 98% humidity chamber did not experience alterations in device performance (Figure S2). CV experiments showed identical operating currents even after 4 days at these conditions. Such water tolerance enabled an easy benchtop assembly. Despite the electrochemical and moisture stability of

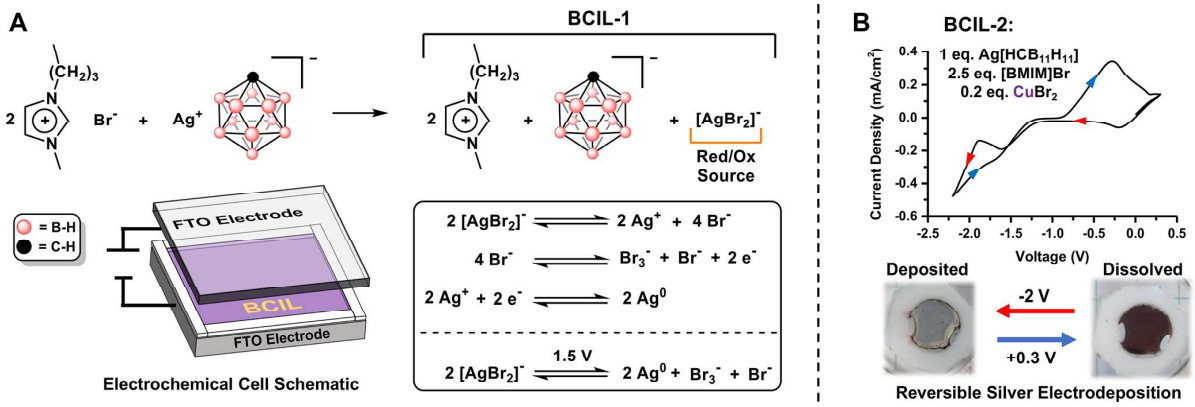

Figure 2. (A) Formation of **BCIL-1** by mixing [BMIM]Br with $Ag[HCB_{11}H_{11}]$. Inset shows the elementary steps associated with silver electrodeposition in **BCIL-1**. (B) Representative cyclic voltammogram (100 mV/s) of **BCIL-2**, Red and blue arrows indicate forward (deposition) and reverse (dissolution) potential sweep direction, respectively.

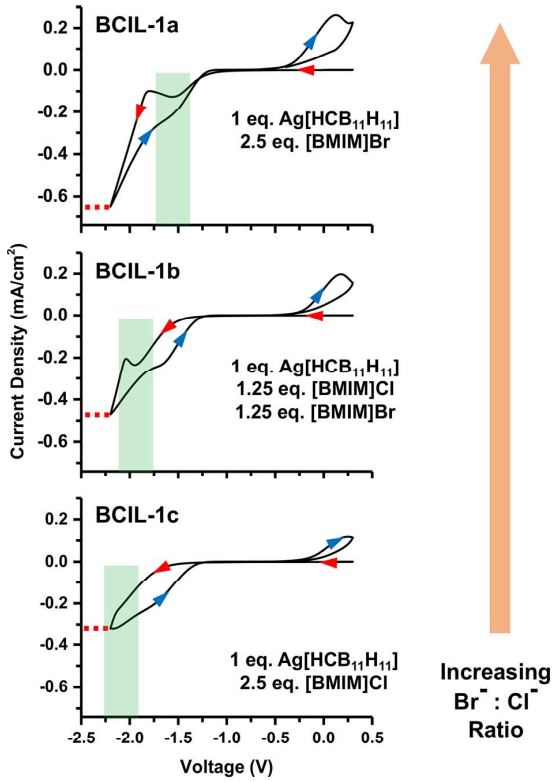

Figure 3. Two-electrode cyclic voltammograms (100 mV/s) of **BCIL-1** without $CuBr_2$ additive. Increasing the Br^-:Cl^- ratio increases the electrodeposition current. Red and blue arrows indicate cathodic and anodic sweep direction, respectively. Green areas indicate the composition dependent FTO | $[AgX_2]^-$, X_3^- | Ag^0 | FTO process, red dashed lines indicate the maximum electrodeposition current density at −2.3 V vs FTO counter electrode.

BCIL-2, a gradual decrease in electrodeposition current was observed during electrochemical cycling of **BCIL-2** cells (Figure S4). After leaving the electrochemical cell overnight at room temperature, the electrodeposition current through the cell decayed and redox features became indistinguishable (Figure 4A). Visual inspection of the electrolyte showed partial crystallization of the BCIL. Heating the cell to 60 °C for 1 hour dissolved the visble crystallites thereby restoring the cell to the original performance. This ultimately suggests that formation of small crystallites leads to reduced ion mobility and electrodeposition current.

Contrary to prevailing approaches of changing the physical properties of ILs by altering the cation, we sought to inhibit crystallite formation by functionalizing the monocarborane anion. A third electrolytic mixture, **BCIL-3**, was prepared using a monocarborane functionalized with a *sec*-butyl group appended on the carbon vertex of the boron-rich cluster (Figure 4B). After the electrochemical cell containing **BCIL-3** was kept at room temperature for 24 hours, the deposition currrents were comparable to those obtained from freshly prepared **BCIL-3** suggesting that, at this time scale, no obeservable crystallization occurs and hence the device performance remains unaffected. Heating of the **BCIL-3** cell to 60 °C for 1 hour further increased the electrodeposition current and eliminated the hysteresis current loop completely (Figure 4B).

The quality of the electrodeposited films was monitored using a 633 nm laser to correlate the film growth to the electrochemical behavior of the cells. Extended electrochemical cycling of a **BCIL-3** cell revealed a decay in reflectance change (Figure 4C), likely due to partial crystallization of **BCIL-3**. These effects were mitigated by heating the cell every 40 cycles (Figure 4C) to restore reflectance changes of up to 80%.

The silver film electrodeposition from **BCIL-3** can reach maximum reflectance within ~3 s when applying a −2.5 V cathodic potential, and it can be quickly removed by reversing the polarity of the electrochemical cell to +2.5 V (Figure 4C). Oxidative etching of the electrodeposited silver film is likely accelerated by electromigration of halides toward the working electrode and subsequent removal of electrodeposited silver as solvated silver halide anions.[20−23] Applying a voltage (−1.8 V) for 450 s produced a thick film which could be analyzed by scanning electron microscopy (SEM).[32] Consistent with nucleation-limited deposition, the silver deposits grow as a film of silver crystallites approximately 500 nm in diameter (Figure 5). EDX elemental mapping shows two types of silver-containing deposits, an underlying Ag film with AgBr crystals on top of the film. The AgBr deposits likely formed during the washing of the working electrode, as described previously.[21]

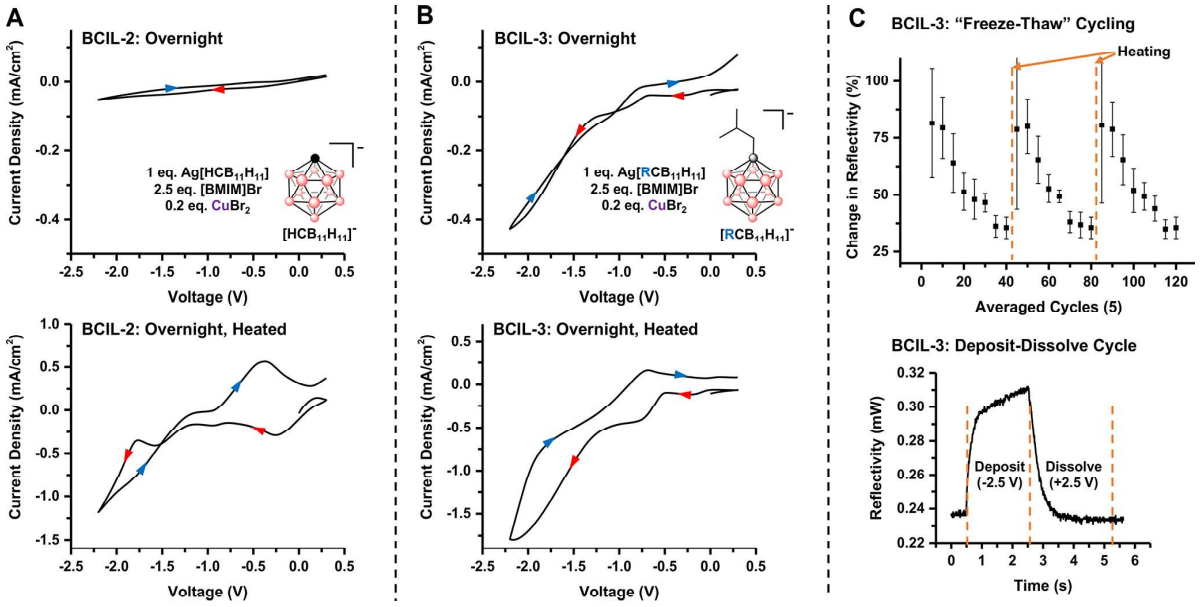

Figure 4. (A) Two-electrode cyclic voltammograms (100 mV/s) of **BCIL-2** after equilibrating at ambient conditions overnight and after heating the equilibrated cell to 60 °C, top and bottom, respectively. (B) Two-electrode cyclic voltammograms (100 mV/s) of **BCIL-3** after equilibrating at ambient conditions overnight and after heating the equilibrated cell to 60 °C, top and bottom, respectively. Red and blue arrows indicate cathodic and anodic sweep direction, respectively. (C) Change in reflectivity ($\Delta\rho$) at 633 nm of **BCIL-3** electrochemical cell during extended "freeze−thaw" cycling and during a single deposition-dissolution cycle, top and bottom, respectively. The electrochemical cell was regenerated every 40 cycles by heating to 60 °C.

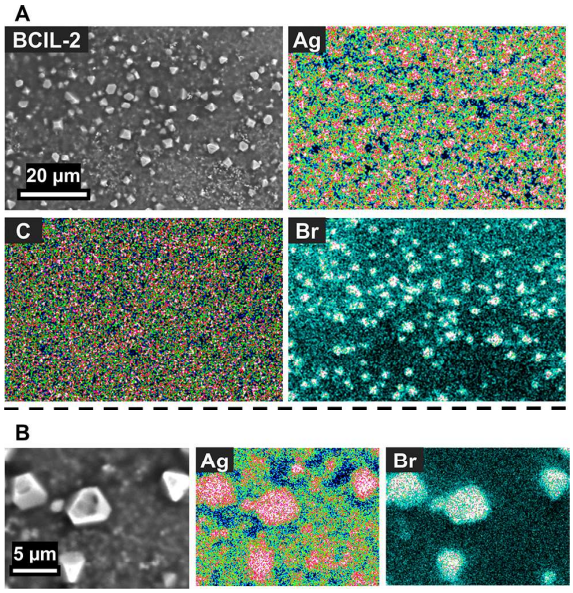

Figure 5. (A) Scanning electron micrographs and EDX elemental mapping of **BCIL-3** working electrode after deposition of a silver film. (B) Magnified scanning electron micrographs and EDX elemental mapping showing a silver film beneath AgBr deposits.

Having identified a suitably resilient electrolyte capable of depositing silver films, we set out to control the IR transmission of the electrochemical cell by depositing a metallic film. From the law of conservation of energy, the sum of the absorption/emission (α/ε), transmission (τ), and reflection (ρ) interactions of an incident electromagnetic wave must sum to unity (eq 1).[33]

$$\alpha + \rho + \tau = 1 = \varepsilon + \rho + \tau \quad (1)$$

$$\alpha = \varepsilon$$

As such, a perfect blackbody radiator ($\alpha = \varepsilon = 1$) is not reflective ($\rho = 0$) because the absorption term dominates eq 1. Conversely, a perfectly reflective surface ($\rho = 1$) would not absorb/emit energy ($\alpha = \varepsilon = 0$). Thus, the emissivity (ε) of a fixed transparency object can be altered by changing the surface reflectivity (ρ) (eq 2).

$$\Delta\varepsilon = -\Delta\rho \quad (2)$$

Similarly, electrodeposition of a reflective film onto an IR emitter would block the IR emission of the underlying IR sources (e.g., electrolyte and counter electrode), see the Supporting Information for demonstration.[15−18,34] Such variable emissivity materials serve as the basis for adaptive surfaces for spacecraft thermal control. However, environmental instability and slow switching times limit their widespread application.

Metal-rich, all-ionic electrolytes can offer the vacuum stability of solid-state materials and rapid deposition rates of liquid electrolytes. A proof-of-concept IR transparent electrochemical cell was fabricated by enclosing **BCIL-3** between two IR transparent conductors composed of a 200 nm ITO film deposited onto a sapphire (Al_2O_3) window which is IR transparent up to ~6 μm (1667 cm^{-1}). The electrochemical cell was mounted in an FTIR spectrometer with the working electrode facing the detector and IR transmission spectra were collected for the electrochemical cell in the unplated and plated states (Figure 6). Electrodeposition of a metallic film reduced the IR energy transmission (1500−4000 cm^{-1}) from 16% in the

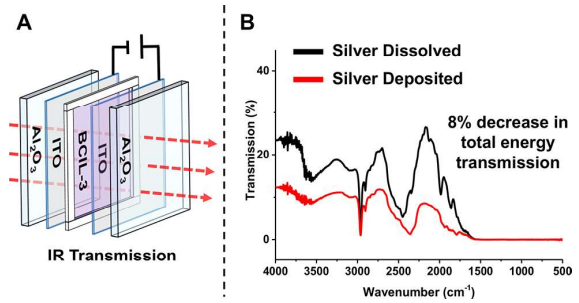

Figure 6. (A) schematic of IR transparent electrochemical cell. (B) FTIR transmission spectrum of **BCIL-3** IR transparent cell before and after silver film electrodeposition.

dissolved state to 8% in the deposited state, indicating that the deposition of a reflective film blocked the emission of the underlying IR sources (see the Supporting Information for energy transmission calculation). Strong absorption at ~3000 and ~2400 cm^{-1} is attributed to the imidazolium and carborane ions, respectively. Although the longevity of the IR transparent cell was limited by the ITO electrode instability (Figure S3), it showcases the potential liquid-based technologies achieveable with ionic liquids.

In summary, we prepared a stable, all-ionic electrolyte designed around the weakly coordinating carborane framework for reversible electrodeposition of silver films. The metal-rich electrolyte enables rapid, reversible silver electrodeposition. Meanwhile, the ionic composition presents opportunities for electrodeposition in extreme environments (such as high temperature and low pressure). We demonstrate the utility of this electrolyte in electrochemically modulated optical devices.

■ ASSOCIATED CONTENT

Supporting Information

The Supporting Information is available free of charge on the ACS Publications website at DOI: 10.1021/acsami.7b19302.

Full procedures and crystallographic and other characterizing data (PDF)
Video S1 (MPG)
Video S2 (MPG)

■ AUTHOR INFORMATION

Corresponding Authors

*E-mail: beth@boron.com (B.D.B.).
*E-mail: vincent.lavallo@ucr.edu (V.L.).
*E-mail: AFRL.VSSVOrgMailbox@us.af.mil (T.L.P.).
*E-mail: spokoyny@chem.ucla.edu (A.M.S.).

ORCID

Alexander M. Spokoyny: 0000-0002-5683-6240

Author Contributions

†R.M.D. and M.A.W. contributed equally to the work.

Notes

The authors declare no competing financial interest.

■ ACKNOWLEDGMENTS

The authors thank the Air Force Research Laboratory for funding through STTR program (Topic AF16-AT20). A.M.S. acknowledges the Department of Chemistry and Biochemistry at UCLA for start-up funds and the NSF for partial support (CHE-1048804). A.M.S. also thanks 3M for a Non-Tenured Faculty Award and Alfred P Sloan Foundation for the Sloan Research Fellowship support. R.M.D. thanks the National Defense Science and Engineering Graduate Fellowship Program for support. V.L. acknowledges the NSF for partial support of this project (DMR-1508537).

■ REFERENCES

(1) *Modern Electroplating*; Schlesinger, M., Paunovic, M., Eds.; John Wiley & Sons: Hoboken, NJ, 2014.
(2) Harada, A.; Yamaoka, H.; Watanabe, K.; Kinoshita, K.; Kishida, S.; Fukaya, Y.; Nokami, T.; Itoh, T. Copper Ion-containing Ionic Liquids Provide Improved Endurance and Switching Voltage Distributions of Conducting-bridge Random Access Memory. *Chem. Lett.* **2015**, *44*, 1578−1580.
(3) Watanabe, M.; Thomas, M. L.; Zhang, S.; Ueno, K.; Yasuda, T.; Dokko, K. Application of Ionic Liquids to Energy Storage and Conversion Devices. *Chem. Rev.* **2017**, *117*, 7190−7239.
(4) Kuwabata, S.; Tsuda, T.; Torimoto, T. Room-temperature Ionic Liquid. A New Medium for Material Production and Analyses under Vacuum Conditions. *J. Phys. Chem. Lett.* **2010**, *1*, 3177−3188.
(5) Simka, W.; Puszczyk, D.; Nawrat, G. Electrodeposition of Metals from Non-aqueous Solutions. *Electrochim. Acta* **2009**, *54*, 5307−5319.
(6) Baker, G. A.; Baker, S. N.; Pandey, S.; Bright, F. V. An Analytical View of Ionic Liquids. *Analyst* **2005**, *130*, 800−808.
(7) Zeng, Z.; Twamley, B.; Shreeve, J. Structure and Properties of Substituted Imidazolium, Triazolium, and Tetrazolium Poly(1,2,4-triazolyl)borate Salts. *Organometallics* **2007**, *26*, 1782−1787.
(8) Türp, D.; Wagner, M.; Enkelmann, V.; Müllen, K. Synthesis of Nanometer-sized, Rigid, and Hydrophobic Anions. *Angew. Chem., Int. Ed.* **2011**, *50*, 4962−4965.
(9) Shkrob, I. A.; Marin, T. W.; Wishart, J. F. Ionic Liquids Based on Polynitrile Anions: Hydrophobicity, Low Proton Affinity, and High Radiolytic Resistance Combined. *J. Phys. Chem. B* **2013**, *117*, 7084−7094.
(10) Gelinas, B.; Das, D.; Rochefort, D. Air-stable, Self-bleaching Electrochromic Devices Based on Viologen- and Ferrocene-containing Triflimide Redox Ionic Liquids. *ACS Appl. Mater. Interfaces* **2017**, *9*, 28726−28736.
(11) Vöge, A.; Gabel, D. Boron in Weakly Coordinating Anions and Ionic Liquids. In *Boron Science: New Technologies and Applications*; Hosmane, N. S., Ed.; CRC Press, Boca Raton, FL, 2012; pp 807−826.
(12) Reed, C. A. Carborane Acids. New "Strong Yet Gentle" Acids for Organic and Inorganic Chemistry. *Chem. Commun.* **2005**, *0*, 1669−1677.
(13) Zhu, Y.; Hosmane, N. S. Ionic Liquids: Recent Advances and Applications in Boron Chemistry. *Eur. J. Inorg. Chem.* **2017**, *2017*, 4369−4377.
(14) Sivaev, I. B. Nitrogen Heterocyclic Salts of Polyhedral Borane Anions: from Ionic Liquids to Energetic Materials. *Chem. Heterocycl. Compd.* **2017**, *53*, 638−658.
(15) Shannon, K. C., III; Sheets, J.; Groger, H.; Williams, A. Thermal Management Integration using Plug-and-play Variable Emissivity Devices. *Proc. SPIE* **2009**, *7330*, 73300F.
(16) Chandrasekhar, P.; Zay, B. J.; Lawrence, D.; Caldwell, E.; Sheth, R.; Stephan, R.; Cornwell, J. Variable-emittance Infrared Electrochromic Skins Combining Unique Conducting Polymers, Ionic Liquid Electrolytes, Microporous Polymer Membranes, and Semiconductor/Polymer Coatings, for Spacecraft Thermal Control. *J. Appl. Polym. Sci.* **2014**, *131*, 40850.
(17) Farrar, D.; Douglas, D. M.; Swanson, T.; Collins, C.; Darrin, A.; Osiander, R. MEMS Shutters for Thermal Control − Flight Validation and Lessons Learned. *AIP Conf. Proc.* **2007**, *880*, 73.
(18) Bergeron, B. V.; White, K. C.; Boehme, J. L.; Gelb, A. H.; Joshi, P. B. Variable Absorptance and Emittance Devices for Thermal Control. *J. Phys. Chem. C* **2008**, *112*, 832−838.
(19) *CRC Handbook of Chemistry and Physics*, 98th ed.; Rumble, J. R., Ed.; CRC Press/Taylor & Francis: Boca Raton, FL, 2018.

(20) Reyna-González, J. M.; Reyes-López, J. C.; Aguilar-Martínez, M. Silver and Silver-copper Electrodeposition from a Pyridinium-based Ionic Liquid. *Electrochim. Acta* **2013**, *94*, 344−352.
(21) Stocker, H. J.; Van Uitert, L. G.; Loomis, T. C.; Koch, F. B. An SEM Study of the Nature of the Electrochemical Deposit in Reversible Electrodeposition Displays. *J. Electrochem. Soc.* **1981**, *128*, 746−748.
(22) Mascaro, L. H.; Kaibara, E. K.; Bulhões, L. O. An Electrochemical System Based on the Reversible Electrodeposition of Lead. *J. Electrochem. Soc.* **1997**, *144*, L273−L274.
(23) Lu, W.; Fadeev, A. G.; Qi, B.; Mattes, B. R. Fabricating Conducting Polymer Electrochromic Devices Using Ionic Liquids. *J. Electrochem. Soc.* **2004**, *151*, H33−H39.
(24) Popov, A. I.; Geske, D. H. Studies on the Chemistry of Halogen and of Polyhalides. XVI. Voltammetry of Bromine and Interhalogen Species in Acetonitrile. *J. Am. Chem. Soc.* **1958**, *80*, 5346−5349.
(25) Allen, G. D.; Buzzeo, M. C.; Villagrán, C.; Hardacre, C.; Compton, R. G. A Mechanistic Study of the Electro-oxidation of Bromide in Acetonitrile and the Room Temperature Ionic Liquid, 1-butyl-3-methylimidazolium bis(trifluoromethylsulfonyl)imide at Platinum Electrodes. *J. Electroanal. Chem.* **2005**, *575*, 311−320.
(26) Luehrs, D. C.; Iwamoto, R. T.; Kleinberg, J. Solubility of Silver Halides and Stability of Silver Halide Complexes in Selected Nonaqueous Media. *Inorg. Chem.* **1966**, *5*, 201−204.
(27) Freire, M. G.; Neves, C. M. S. S.; Marrucho, I. M.; Coutinho, J. A. P.; Fernandes, A. M. Hydrolysis of Tetrafluoroborate and Hexafluorophosphate Counter Ions in Imidazolium-based Ionic Liquids. *J. Phys. Chem. A* **2010**, *114*, 3744−3749.
(28) Wang, B.; Qin, L.; Mu, T.; Xue, Z.; Gao, G. Are Ionic Liquids Chemically Stable? *Chem. Rev.* **2017**, *117*, 7113−7131.
(29) Douvris, C.; Michl, J. Update 1 of: Chemistry of the Carba-*closo*-dodecaborate(−) Anion, $CB_{11}H_{12}^-$. *Chem. Rev.* **2013**, *113*, PR179−PR233.
(30) Grishina, E. P.; Kudryakova, N. O.; Pimenova, A. M. Corrosion and Anodic Oxidation of Copper in 1-butyl-3-methylimidazolium Bromide-Copper(II) Bromide Ionic Liquid. *Prot. Met. Phys. Chem. Surf.* **2017**, *53*, 663−669.
(31) Basile, A.; Bhatt, A. I.; O'Mullane, A. P.; Bhargava, S. K. An Investigation of Silver Electrodeposition from Ionic Liquids: Influence of Atmospheric Water Uptake on the Silver Electrodeposition Mechanism and Film Morphology. *Electrochim. Acta* **2011**, *56*, 2895−2905.
(32) SEM studies required thicker Ag films because of etching of the films by solvent used to remove excess BCIL and expose the underlying Ag deposits.
(33) Rybicki, G. B.; Lightman, A. P., Fundamentals of Radiative Transfer, *Radiative Processes in Astrophysics*; Wiley−VCH: Weinheim, Germany, 2004.
(34) Clawson, J. F.; Tsuyuki, G. T.; Anderson, B. J.; Justus, C. G.; Batts, W.; Ferguson, D.; Gilmore, D. G. Spacecraft Thermal Environments. In *Spacecraft Thermal Control Handbook*, 2nd ed.; The Aerospace Press: Reston, VA, 2002; *Vol. 1: Fundamental Technologies*, pp 21−69.

Chapter 6. Synthesis of Weakly Coordinating Dodecaborate-based Anions for Ionic Liquids and Electrolytes

6.1 Introduction

Anionic polyhedral borates are renowned for their ability to serve as robust, weakly coordinating anions.[1–3] These properties make polyhedral borates interesting components in ionic materials such as ionic liquids and solid electrolytes.[4–6] In particular, persubstituted icosahedral borates, $[B_{12}R_{12}]^{2-}$, are known for their electrochemical stability, stability to acids and bases, and weakly coordinating nature due to the delocalized 3-dimensional aromaticity.[2] Despite their weakly coordinating nature, ionic liquids based on polyhedral boranes do not exhibit the low melting points such as those observed for bis(trifluorosulfonyl)imide or cyanimide containing ionic liquids.[4,5,7–9]

The higher melting points of dodecaborate-based ionic liquids may be due to their dianionic (2−) charge and icosahedral symmetry. The dianionic charge of dodecaborate can lead to higher lattice energies when compared to the lattice energies of salts composed of singly-charged anions. One approach to reducing the coulombic attraction between the cations and the dodecaborate anions is to appending a formally cationic functional group such as ammonium, sulfonium, or phophonium group to the dodecaborate which results in a charge-compensated monoanionic dodecaborates.[10–12] Another strategy for lowering the melting point of dodecaborate-based salts is to install alkyl chains which are believed to disrupt crystal packing by increasing the structural anisotropy of the anion.[12–14] Alternatively, dodecaborate-containing ionic liquids can be formed by using long-chain alkyl imidazolium cations to further disrupt crystal packing.

In previous studies of dodecaborate-based ionic liquids, halogenation of the exohedral B−H bonds to B−X bonds (X = F, Cl, Br, or I) is used to increase the chemical stability of the dodecaborate anions against oxidative degradation.[1,15] Despite the body of work on chlorinated dodecaborates, only a handful of chlorination techniques are reported.[11,16–18] Although chlorination of PBs using chlorine gas is simple, the corrosive nature of Cl_2 gas requires specialized gas fittings and safety protocols that can discourage synthesis of unique chlorinated dodecaborates for new applications. Alternative chlorination methods use highly corrosive $SbCl_5$ as a chlorinating agent or use SO_2Cl_2 in refluxing acetonitrile to produce Cl_2 gas *in situ*.[18,19] Furthermore, the products of acid catalyzed hydroxylation and amination of dodecaborate in aqueous media require extensive drying prior to using SO_2Cl_2 as a chlorinating agent.[20,21] This chapter describes the large scale, one-pot synthesis of $[B_{12}Cl_9(OH)_3]^{2-}$ which can serve a versatile precursor in dodecaborate-based ionic liquids, electrolytes, flow-batteries, and weakly coordinating anions.

6.2 One-pot Hydroxylation and Chlorination of $[B_{12}H_{12}]^{2-}$

In order to create a weakly coordinating anionic matrix for ionic liquid applications we sought to increase the anisotropy of the dodecaborate anion by appending alkyl groups to the boron cluster through B−O−C linkages. Furthermore, halogenation of the unfunctionalized B−H vertices would further delocalize the negative charge of the dodecaborate anion and increase the oxidative stability of the dodecaborate anions. We chose to investigate the $[B_{12}Cl_9(OH)_3]^{2-}$ anion for ionic liquids and weakly coordinating anions because it has three hydroxyl groups that can be further functionalized. Notably, previous studies observed that addition of alkyl groups to the monohydroxyl $[B_{12}Cl_{11}(OH)]^{2-}$ anion decreased the melting point of its imidazolium salts relative to their perchlorinated $[B_{12}Cl_{12}]^{2-}$ analogs.[14]

Upon synthesis of the $[B_{12}H_9(OH)_3]^{2-}$ anions we encountered great difficulty in isolating the dry salts for chlorination with SO_2Cl_2. In fact, the original report of the acid-catalyzed hydroxylation of $[B_{12}H_{12}]^{2-}$ required large hydrophobic cations such as $MePPh_3^+$ and bis(triphenylphosphino)iminium (PPN^+) to precipitate the product.[20] Likewise, our attempts to precipitate the $[B_{12}H_9(OH)_3]^{2-}$ with various organic cations ($HNEt_3^+$, NBu_4^+ and $MePPh_3^+$) were unsuccessful. The presence of hydroxyl groups on the $[B_{12}H_9(OH)_3]^{2-}$ anion enables hydrogen bonding interactions that prevent precipitation of $[B_{12}H_9(OH)_3]^{2-}$ salts. The high solubility of $[B_{12}H_9(OH)_3]^{2-}$ in water makes the chlorination with SO_2Cl_2 tedious because residual water can cause degradation of $SO_2Cl_{2(l)}$. Despite the hazardous nature of Cl_2 gas, Cl_2 sources are often found in household items such as bleach and pool cleaners. In particular, hypochlorous acid (HOCl), the main active ingredient in bleach, decomposes to Cl_2 gas and water in the presence of acid. Thus, addition of $NaOCl_{(aq)}$ to an acidic solution of $[B_{12}H_9(OH)_3]^{2-}$ creates Cl_2 gas that reacts leads to chlorination of the $[B_{12}H_9(OH)_3]^{2-}$anion, Figure 6.1. After chlorination, the $[B_{12}Cl_9(OH)_3]^{2-}$ anion readily precipitates as $HNBu_3^+$, NBu_4^+ and $MePPh_3^+$ salts from the aqueous reaction medium.

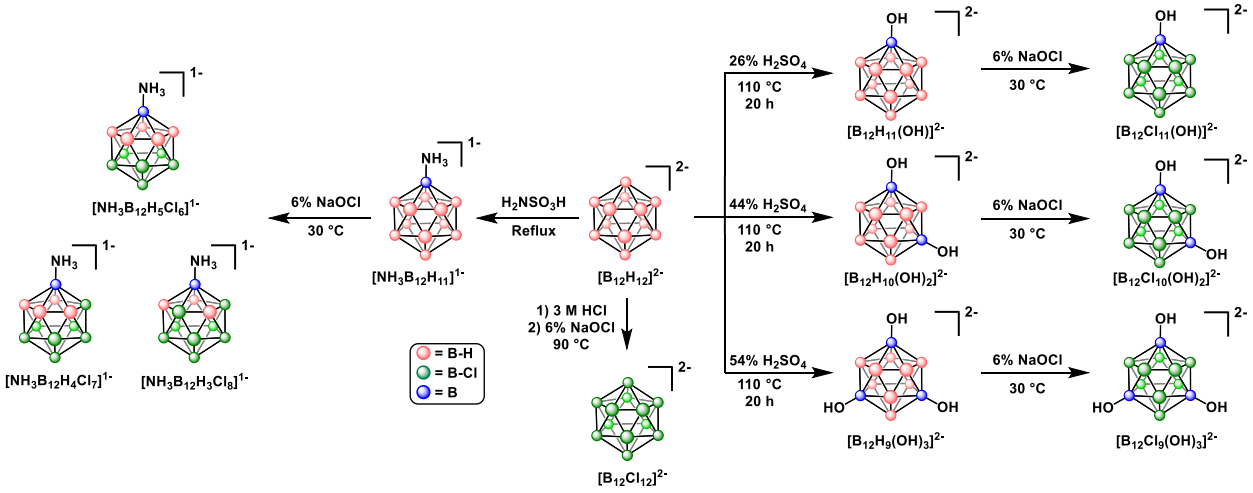

Figure 6.1: Schematic of the one-pot hydroxylation/chlorination procedure for synthesizing amino- and hydroxy-dodecaborate anions and their subsequent chlorinated derivatives.

6.3 Functionalization of $[B_{12}Cl_9(OH)_3]^{2-}$

With the $[B_{12}Cl_9(OH)_3]^{2-}$ salts in hand, we proceeded to alkylate the clusters using a previously reported method that uses a superbasic KOH/DMSO mixture to deprotonate the hydroxyl groups.[14,22] However, we found that the alkylation reactions proceeded slowly and often did not produce fully alkylated products. This may be due to two factors: 1) the steric bulk of the chlorine atoms near the B−OH vertices inhibits Sn2 reactivity and 2) the high pKa of the B−OH group requires a superbasic reaction medium to produce a small amount of reactive $[B_{12}Cl_9(OH)_2O]^{3-}$. The long reaction times and partial conversion prompted us to search for a better reaction system.

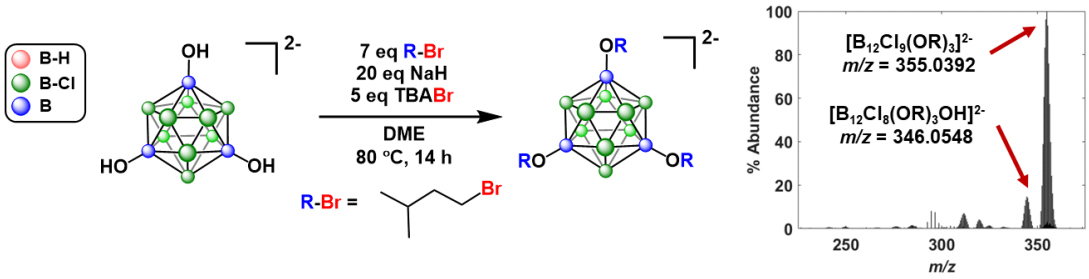

Figure 6.2: Schematic for the alkylation of $(NBu_4)_2[B_{12}Cl_9(OH)_3]$ in dimethoxyethane which requires a phase transfer agent $(NBu_4)Br$ to improve the solubility of the $(NBu_4)_2[B_{12}Cl_9(OH)_3]$ salt. The inset shows the electrospray ionization – mass spectrum of the alkylated products $[B_{12}Cl_9(OC_5H_{11})_3]^{2-}$ and $[B_{12}Cl_8(OC_5H_{11})_3(OH)]^{2-}$ which forms due to a $[B_{12}Cl_8(OH)_4]^{2-}$ impurity.

Our attempts to use a stronger base such as K^{t}BuO in refluxing DME yielded trace amounts of alkylated $[B_{12}Cl_9(OH)_3]^{2-}$. We resorted to using NaH as a strong, non-nucleophilic base in dimethoxyethane (DME) to deprotonate the $[B_{12}Cl_9(OH)_3]^{2-}$, however the poor solubility of the $[B_{12}Cl_9(OH)_3]^{2-}$ in organic solvents, along with the steric blocking, only afforded partially alkylated $[B_{12}Cl_9(OH)_3]^{2-}$. Analysis of the unsuccessful reactions revealed the presence of 1-hexene by GC−MS suggesting that that steric bulk surrounding the active B−O vertex causes competition between S_n2 and E2 when reacting with 1-bromohexane. To remedy these issues, we

used $(NBu_4)Br$ to overcome the poor solubility of $[B_{12}Cl_9(OH)_3]^{2-}$ in organic solvents, Figure 6.2. This combination of additives allowed us to achieve complete alkylation within 14 hours, as opposed to the 7+ day alkylation in superbasic KOH/DMSO mixtures. Having developed a versatile method for synthesizing $(NBu_4)_2[B_{12}Cl_9(O^nHex)_3]$, the melting point of the salt was measured with differential scanning calorimetry and an optical melting point apparatus which showed melting occurring at ~83 °C, Figure 6.3. In contrast, the monoalkoxylated $(NBu_4)_2[B_{12}Cl_{11}(OR)]$ (R = propyl, octyl, or dodecyl) do not melt below 300 °C, which highlights the effect of appending multiple alkoxy groups to lower the melting point.[14]

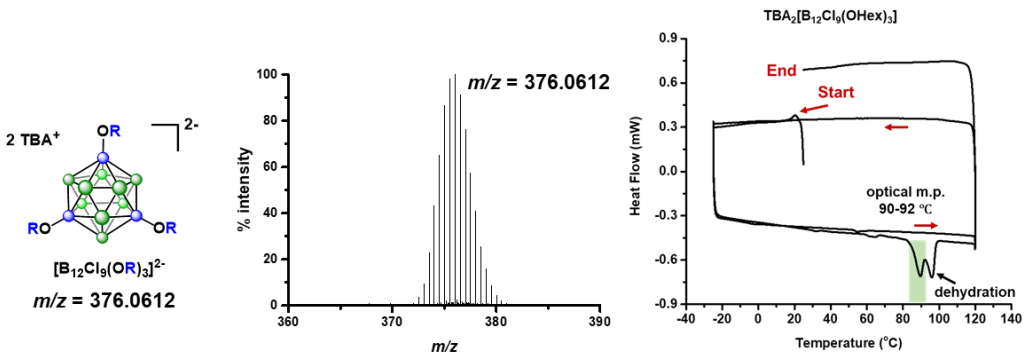

Figure 6.3: The electrospray ionization – mass spectrum of $[B_{12}Cl_9(O^nHex)_3]^{2-}$ and the differential scanning calorimetry of $(NBu_4)_2[B_{12}Cl_9(O^nHex)_3]$ which shows melting at ~83 °C.

While developing the alkylation procedure for $[B_{12}Cl_9(OH)_3]^{2-}$ we sought to resolve the poor solubility of the $[B_{12}Cl_9(OH)_3]^{2-}$ in organic solvents by using acetonitrile as a polar, aprotic solvent. Although acetonitrile readily dissolves $[B_{12}Cl_9(OH)_3]^{2-}$ salts, it is not compatible with NaH due to reduction of the nitrile group its subsequent reaction with alkyl halides. Thus, we employed potassium bis(trimethylsilyl)amide (KHMDS) as a strong, non-nucleophilic base that is capable of deprotonating the BOH group without generating by-products of acetonitrile reduction. Reaction of $(NBu_4)_2[B_{12}Cl_9(OH)_3]$ with 1-bromohexane and KHMDS in acetonitrile resulted in

quantitative conversion of B−OH to B−OSi$(CH_3)_3$ groups, Figure 6.4. In contrast, reaction of $(NBu_4)_2[B_{12}Cl_9(OH)_3]$ with KHMDS in acetonitrile without alkyl bromide lead to partial silylation of the hydroxyl groups. This difference in reaction outcome suggested that formation of neutral $HN(Si(CH_3)_3)_2$ and $(C_5H_{11})N(Si(CH_3)_3)_2$, formed via deprotonation of B−OH groups and S_n2 alkylation with 1-bromohexane respectively, act as the active silylation reagent. Indeed, reaction of $(NBu_4)_2[B_{12}Cl_9(OH)_3]$ with $HN(Si(CH_3)_3)_2$ in acetonitrile resulted in quantitative conversion of B−OH to B−OSi$(CH_3)_3$ groups.

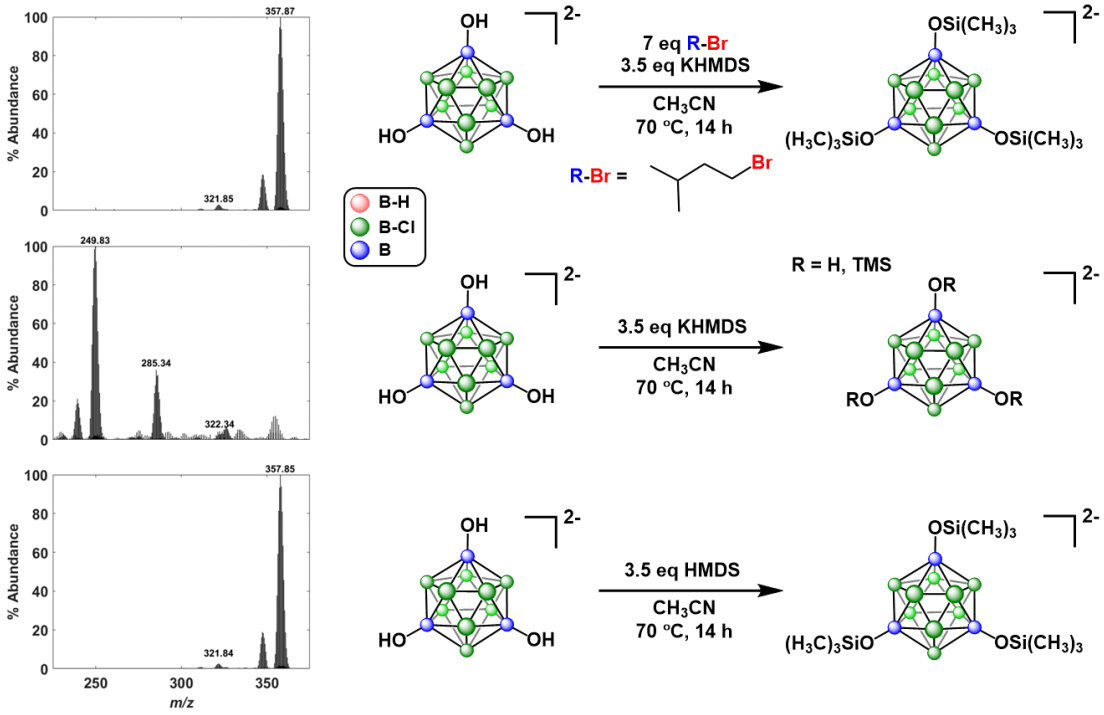

Figure 6.4: Electrospray ionization – mass spectra of $(NBu_4)_2[B_{12}Cl_9(OH)_3]$ silylation reactions. Top, reaction of $(NBu_4)_2[B_{12}Cl_9(OH)_3]$ with $KN(Si(CH_3)_3)_2$ (KHMDS) and 1-isopentylbromide. Middle, reaction of $(NBu_4)_2[B_{12}Cl_9(OH)_3]$ with (KHMDS). Bottom, reaction of $(NBu_4)_2[B_{12}Cl_9(OH)_3]$ with $HN(Si(CH_3)_3)_2$ (HMDS).

6.4 Electrochemical Analysis

Perfunctionalized dodecaborates can exhibit reversible oxidation events corresponding to the 2−/1− and 1−/0 oxidation states. For perhalogenated $[B_{12}X_{12}]^{2-}$ clusters, the oxidation potential

for the 2−/1− redox couple shifts to less positive potentials as X = I > Br > Cl > F. This shift in redox potential is attributed to a combination of σ-withdrawing effect and π-backbonding of the p-orbitals of the X substituent to the boron cluster cage.[23] Similarly, $[B_{12}(OR)_{12}]^{2-}$ (R = alkyl or benzyl) species have much lower oxidation potentials due to increased π-backbonding of the oxygen lone pairs and diminished σ-withdrawing effects due to the presence of the R group.

Electrochemical analysis of $(NBu_4)_2[B_{12}Cl_9(OH)_3]$ and $(NBu_4)_2[B_{12}Cl_9(O^nHex)_3]$ did not display any reduction waves corresponding to a 2−/3− reduction event, however an oxidation peak was observed at voltages greater than +1.1 V vs Fc/Fc^+, Figure 6.5. The oxidation of the $[B_{12}Cl_9(OH)_3]^{2-}$ anion (+1.2 V vs Fc/Fc^+) is not reversible, as evidenced by the lack of a reduction wave on the reverse voltage scan. In contrast, the oxidation of the $[B_{12}Cl_9(O^nHex)_3]^{2-}$ anion (+1.1 V vs Fc/Fc^+) is cathodically shifted by ~0.1 V and it is reversible, as evidence by the presence of a reduction wave on the reverse voltage scan. A second oxidation event corresponding to the 1−/0 oxidation is not observable due to decomposition of the electrolyte above +1.8 V. The cathodic shift in the oxidation potential of $(NBu_4)_2[B_{12}Cl_9(O^nHex)_3]$, relative to $(NBu_4)_2[B_{12}Cl_9(OH)_3]$, is due to reduced σ-withdrawing effects of the alkoxy group compared to a hydroxyl group. The high cathodic stability of the $[B_{12}Cl_9(OH)_3]^{2-}$ and $[B_{12}Cl_9(O^nHex)_3]^{2-}$ anions, along with the reversible oxidation of the $[B_{12}Cl_9(O^nHex)_3]^{2-}$ anion, presents new opportunities for boron cluster based electrolytes and flow-batteries.

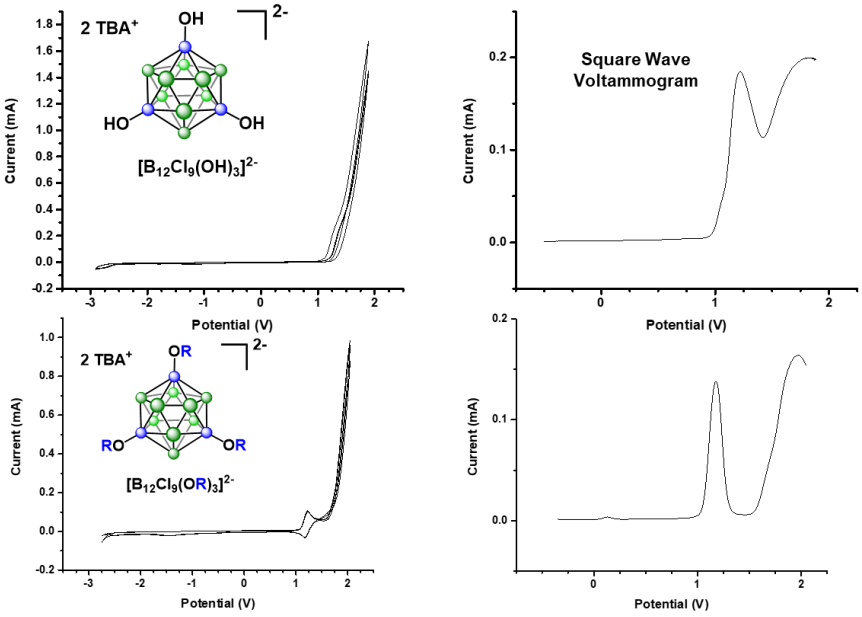

Figure 6.5: Cyclic voltammograms (left) and square wave voltammograms (right) of $(NBu_4)_2[B_{12}Cl_9(OH)_3]$ (top) and $(NBu_4)_2[B_{12}Cl_9(O^nHex)_3]$ (bottom) in acetonitrile. 0.1 M $(NBu_4)[PF_6]$ supporting electrolyte 0.01 M analyte in acetonitrile, 0.1 V/s sweep rate. Glassy carbon working-electrode, Pt counter-electrode, Ag wire reference electrodes. All potentials are referenced to Fc/Fc^+.

6.5 Experimental Details

Synthesis of $(NBu_4)_2[B_{12}Cl_9(OH)_3]$

6 g $Cs_2B_{12}H_{12}$ was mixed with 54 mL H_2O in a 200 mL Schlenk flask and cooled 0 °C in an ice bath. 66 mL of H_2SO_4 was slowly added using an addition funnel to the rapidly stirring, cooled reaction mixture (this is to limit heating of the reaction and prevent formation of $[B_{12}H_8(OH)_4]^{2-}$). Then the reaction mixture was fitted with an air-cooled reflux condenser and gradually heated to 110 °C over the course of ~15 minutes and left stirring at 110 °C for 20 hours. ^{11}B NMR of aliquots of the reaction mixture diluted in H_2O were collected to measure production of $[B_{12}H_9(OH)_3]^{2-}$. The reaction mixture was cooled to room temperature and 240 mL of 5.5-6% NaOCl(aq) was added dropwise by using an addition funnel. After addition of the NaOCl solution,

the reaction mixture was stirred for 1 hour at room temperature and then heated to 100 °C for 2 hours to fully chlorinate the $[B_{12}H_9(OH)_3]^{2-}$. The reaction progress was determined by electrospray ionization – mass spectrometry (ESI-MS) and was consistent with our previous reports of $[B_{12}Cl_9(OH)_3]^{2-}$ synthesis.

Upon completion of the chlorination reaction, the reaction was cooled to room temperature and 2 g of $Na_2S_2O_3 \cdot 5H_2O$ was added to the rapidly stirred reaction mixture to reduce the residual chlorine gas to chloride ions. Next, 12 g of $(NBu_4)Br$ was added slowly to the rapidly stirring reaction mixture to precipitate $(NBu_4)_2[B_{12}Cl_9(OH)_3]$. The $(NBu_4)_2[B_{12}Cl_9(OH)_3]$ was collected on a fritted glass filter frit and washed with excess water. Next, the $(NBu_4)_2[B_{12}Cl_9(OH)_3]$ was dissolved in a minimal amount of CH_2Cl_2, dried with $MgSO_4$, filtered through 2 cm of Celite, and dried by rotary evaporation to yield an off-white waxy solid. The waxy solid was transferred onto a fritted glass filter frit, washed with hexanes, and dried to yield 10 g (78%) of a powdery white solid. **^{1}H NMR (500 MHz, MeCN-D$_3$):** δ 3.09 (t, 16H), 1.61 (q, 16H) 1.37 (q, 16H), 0.98 (q, 24H); **^{11}B NMR (160 MHz):** δ -9.6 (s, 3B), -16.0 (s, 6B), -17.7 (s, 3B).

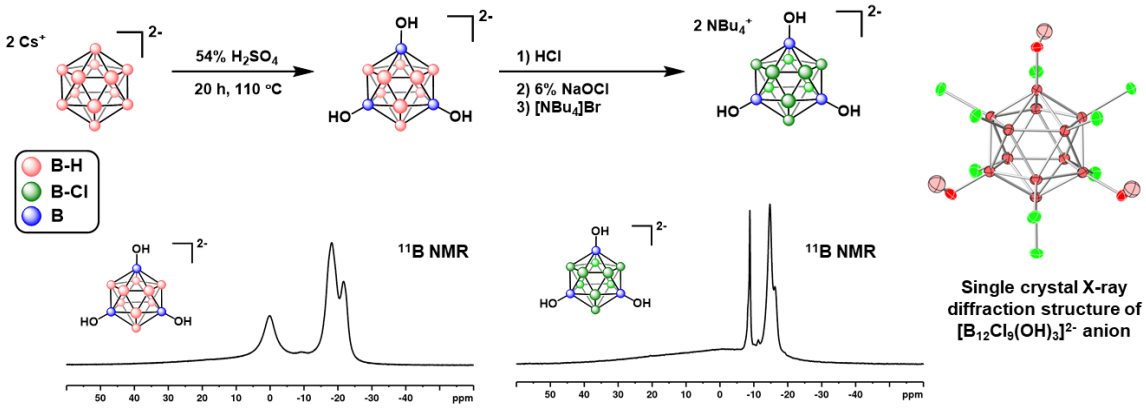

Figure 6.6: Reaction scheme for one-pot synthesis of $[B_{12}Cl_9(OH)_3]^{2-}$ anion. ^{11}B NMR spectra for $[B_{12}H_9(OH)_3]^{2-}$ (left) and $[B_{12}Cl_9(OH)_3]^{2-}$ (right) anions. Inset shows single crystal X-ray diffraction structure of $(MePPh_3)_2[B_{12}Cl_9(OH)_3]$ prepared by precipitating the $[B_{12}Cl_9(OH)_3]^{2-}$ anion with $(MePPh_3)Br$ and recrystallized by evaporation of acetone from a solution of $(MePPh_3)_2[B_{12}Cl_9(OH)_3]$ in a water:acetone mixture (pink = B, green = Cl, red = O, light pink = H atoms)

Synthesis of $(NBu_4)_2[B_{12}Cl_9(O^nHex)_3]$

250 mg of $(NBu_4)_2[B_{12}Cl_9(OH)_3]$ and 185 mg $(NBu_4)I$ was added to an oven dried reaction tube and transferred into an N_2 filed glovebox. 120 mg of NaH and 5 mL of anhydrous dimethoxyethane (DME) was added into the reaction tube and sealed with a PTFE lined septum cap. The reaction tube was brought outside of the glovebox, 400 μL of 1-bromohexane was injected through the septum cap and the reaction was heated at 80 °C for 14 hours. Upon completion, the NaH was quenched with a few drops of water and the DME was removed by vacuum evaporation to yield a white waxy solid which was washed with three 5 mL portions of water followed by washing with three 5 mL portions of hexanes. The remaining solid was dissolved in dichloromethane (DCM), load onto a 3 cm tall plug of silica gel, washed with 5 mL of DCM, and the remaining product was eluted with a 50%:50% (v/v) mixture of acetone:DCM, which upon drying yielded 300 mg of a clear oil that turned waxy upon drying under vacuum. **^{1}H NMR (500 MHz, MeCN-D_3):** δ 3.91 (t, 6H), 3.09 (t, 16H), 1.61 (q, 16H), 1.43 (m, 6H), 1.37 (q, 16H), 1.33-1.24 (m, 18H), 0.98 (q, 24H), 0.89 (t, 9H); **^{11}B NMR (160 MHz):** δ -8.5 (s, 3B), -13.7 (s, 6B), -15.7 (s, 3B).

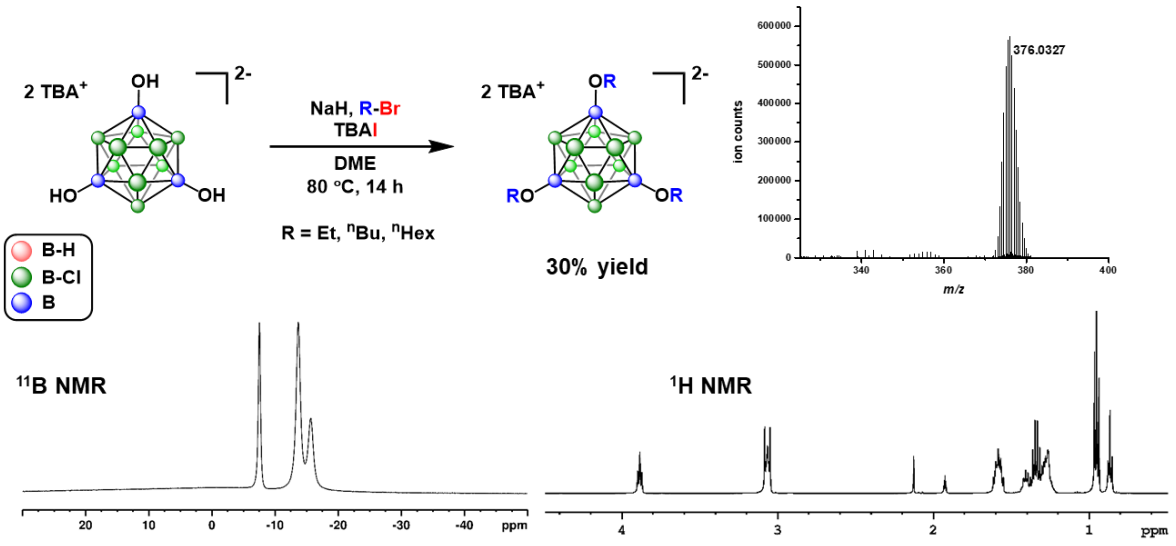

Figure 6.7: Reaction scheme for alkylation of the $[B_{12}Cl_9(OH)_3]^{2-}$ anion. ^{11}B NMR (bottom left) and ^{1}H NMR (bottom right) spectra of $(NBu_4)_2[B_{12}Cl_9(OH)_3]$. Inset shows electrospray ionization – mass spectra (negative mode) of the $[B_{12}Cl_9(O^nHex)_3]^{2-}$ anion.

Synthesis of $(NBu_4)_2[B_{12}Cl_9(O(Si(CH_3)_3)_3)_3]$

983 mg of $(NBu_4)_2[B_{12}Cl_9(OH)_3]$ was added to an oven dried reaction tube and transferred into an N_2 filed glovebox. 800 mg of $K[N(Si(CH_3)_3)_2]$ (KHMDS) and 5 mL of anhydrous acetonitrile (MeCN) was added into the reaction tube and sealed with a PTFE lined septum cap. The reaction tube was brought outside of the glovebox, 3.6 mL of 1-bromo-3-methylbutane was injected through the septum cap and the reaction was heated at 70 °C for 14 hours. ESI-MS showed 97% conversion of the $[B_{12}Cl_9(OH)_3]^{2-}$ anion into the $[B_{12}Cl_9(O(Si(CH_3)_3)_3]^{2-}$ anion. Similar reactions without any alkyl bromide (1-bromo-3-methylbutane) showed <5% conversion of the $[B_{12}Cl_9(OH)_3]^{2-}$ anion into the $[B_{12}Cl_9(O(Si(CH_3)_3)_3]^{2-}$ anion.

983 mg of $(NBu_4)_2[B_{12}Cl_9(OH)_3]$ was added to an oven dried reaction tube and transferred into an N_2 filed glovebox, 5 mL of anhydrous acetonitrile (MeCN) was added into the reaction tube and sealed with a PTFE lined septum cap. The reaction tube was brought outside of the

glovebox, 75 µL of $HN(Si(CH_3)_3)_2$ (HMDS) was injected through the septum cap and the reaction was heated at 70 °C for 14 hours. ESI-MS showed 97% conversion of the $[B_{12}Cl_9(OH)_3]^{2-}$ anion into the $[B_{12}Cl_9(O(Si(CH_3)_3)_3]^{2-}$ anion.

The reaction mixture was evaporated to dryness to yield a white waxy solid. The solid was washed with three 5 mL portions of water. The resulting solid was dissolved in ethyl acetate and washed with a saturated NH_4Cl solution. The ethyl acetate layer was collected, dried with MgSO4, filtered and evaporated to dryness to yield 950 mg of white solid. **^{1}H NMR (500 MHz, MeCN-D_3):** δ 3.09 (t, 16H), 1.61 (q, 16H) 1.37 (q, 16H), 0.98 (q, 24H), 0.07 (s, 27H); **^{11}B NMR (160 MHz):** δ -9.9 (s, 3B), -16.0 (s, 6B), -18.1 (s, 3B).

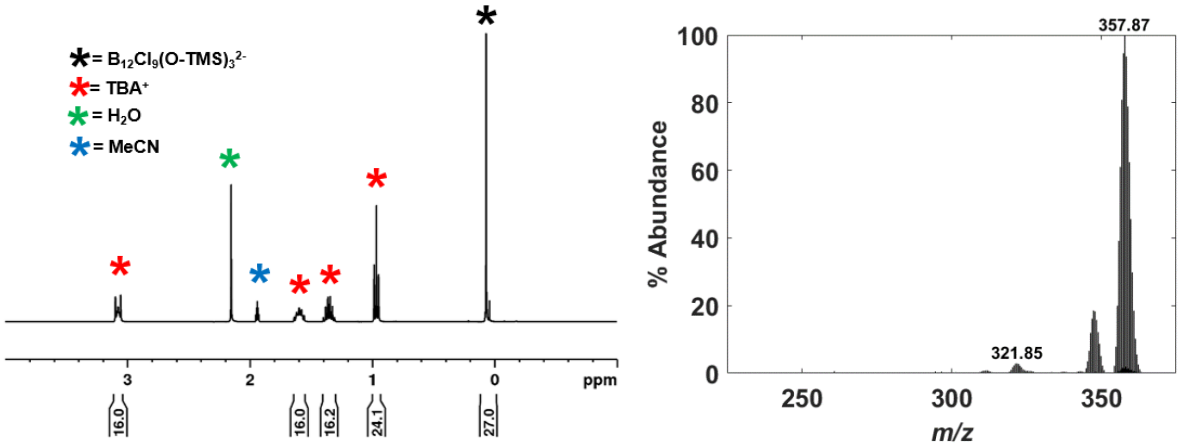

Figure 6.8: ^{1}H NMR (left) spectra of $(NBu_4)_2[B_{12}Cl_9(OSi(CH_3)_3)_3]$ and electrospray ionization – mass spectra (right, negative mode) of the $[B_{12}Cl_9(OSi(CH_3)_3)_3]^{2-}$ anion. Additional peaks at 321 and 345 m/z correspond to $[B_{12}Cl_9(OSi(CH_3)_3)_3]^{2-}$ and $[B_{12}Cl_8(OSi(CH_3)_3)_3(OH)]^{2-}$ anion

Cyclic Voltammetry

All cyclic voltammetry data was collected utilizing a glassy carbon working electrode, platinum counter-electrode and Ag wire reference. Both pure $(NBu_4)_2[B_{12}Cl_9(OH)_3]$ and $(NBu_4)_2[B_{12}Cl_9(O^nHex)_3]$ were dissolved in N_2 purged acetonitrile to 0.01 M in a supporting 0.1

M electrolyte of tetrabutylammonium hexafluorophosphate. All potentials are referenced to Fc/Fc^+. All solutions were stirred prior to collection of CV and left unperturbed during collection of the measurement.

6.6 Bibliography

(1) Knapp, C. Weakly Coordinating Anions: Halogenated Borates and Dodecaborates. In *Comprehensive Inorganic Chemistry II*; Elsevier, 2013; pp 651–679.

(2) Axtell, J. C.; Saleh, L. M. A.; Qian, E. A.; Wixtrom, A. I.; Spokoyny, A. M. Synthesis and Applications of Perfunctionalized Boron Clusters. *Inorg. Chem.* **2018**, *57* (5), 2333–2350.

(3) Grimes, R. N. Carboranes in the Chemist's Toolbox. *Dalt. Trans.* **2015**, *44* (13), 5939–5956.

(4) Nieuwenhuyzen, M.; Seddon, K. R.; Teixidor, F.; Puga, A. V.; Viñas, C. Ionic Liquids Containing Boron Cluster Anions. *Inorg. Chem.* **2009**, *48* (3), 889–901.

(5) Zhu, Y.; Hosmane, N. S. Ionic Liquids: Recent Advances and Applications in Boron Chemistry. *Eur. J. Inorg. Chem.* **2017**, *2017* (38), 4369–4377.

(6) Dziedzic, R. M.; Waddington, M. A.; Lee, S. E.; Kleinsasser, J.; Plumley, J. B.; Ewing, W. C.; Bosley, B. D.; Lavallo, V.; Peng, T. L.; Spokoyny, A. M. Reversible Silver Electrodeposition from Boron Cluster Ionic Liquid (BCIL) Electrolytes. *ACS Appl. Mater. Interfaces* **2018**, *10* (8), 6825–6830.

(7) Galiński, M.; Lewandowski, A.; Stepniak, I. Ionic Liquids as Electrolytes. *Electrochim. Acta* **2006**, *51* (26), 5567–5580.

(8) Shkrob, I. A.; Marin, T. W.; Wishart, J. F. Ionic Liquids Based on Polynitrile Anions: Hydrophobicity, Low Proton Affinity, and High Radiolytic Resistance Combined. *J. Phys. Chem. B* **2013**, *117* (23), 7084–7094.

(9) Kubota, K.; Nohira, T.; Hagiwara, R. New Inorganic Ionic Liquids Possessing Low Melting Temperatures and Wide Electrochemical Windows: Ternary Mixtures of Alkali Bis(Fluorosulfonyl)Amides. *Electrochim. Acta* **2012**, *66*, 320–324.

(10) Justus, E.; Rischka, K.; Wishart, J. F.; Werner, K.; Gabel, D. Trialkylammoniododecaborates: Anions for Ionic Liquids with Potassium, Lithium and Protons as Cations. *Chem. - A Eur. J.* **2008**, *14* (6), 1918–1923.

(11) Bolli, C.; Derendorf, J.; Jenne, C.; Scherer, H.; Sindlinger, C. P.; Wegener, B. Synthesis and Properties of the Weakly Coordinating Anion $[Me_3NB_{12}Cl_{11}]^-$. *Chem. – A Eur. J.* **2014**, *20* (42), 13783–13792.

(12) Bertocco, P.; Derendorf, J.; Jenne, C.; Kirsch, C. Improving the Solubility of Halogenated 1-Ammonio-Closo-Dodecaborate Anions. *Inorg. Chem.* **2017**, *56* (6), 3459–3466.

(13) Larsen, A. S.; Holbrey, J. D.; Tham, F. S.; Reed, C. A. Designing Ionic Liquids:

Imidazolium Melts with Inert Carborane Anions. *J. Am. Chem. Soc.* **2000**, *122* (30), 7264–7272.

(14) Jenne, C.; Kirsch, C. Alkoxy Substituted Halogenated Closo-Dodecaborates as Anions for Ionic Liquids. *Dalt. Trans.* **2015**, *44* (29), 13119–13124.

(15) Warneke, J.; Hou, G. L.; Aprà, E.; Jenne, C.; Yang, Z.; Qin, Z.; Kowalski, K.; Wang, X. Bin; Xantheas, S. S. Electronic Structure and Stability of $[B_{12}X_{12}]^{2-}$ (X = F-At): A Combined Photoelectron Spectroscopic and Theoretical Study. *J. Am. Chem. Soc.* **2017**, *139* (41), 14749–14756.

(16) Knoth, W. H.; Miller, H. C.; Sauer, J. C.; Balthis, J. H.; Chia, Y. T.; Muetterties, E. L. Chemistry of Boranes. IX. Halogenation of $B_{10}H_{10}^{-2}$ and $B_{12}H_{12}^{-2}$. *Inorg. Chem.* **1964**, *3* (2), 159–167.

(17) Geis, V.; Guttsche, K.; Knapp, C.; Scherer, H.; Uzun, R. Synthesis and Characterization of Synthetically Useful Salts of the Weakly-Coordinating Dianion $[B_{12}Cl_{12}]^{2-}$. *J. Chem. Soc. Dalt. Trans.* **2009**, No. 15, 2687–2694.

(18) Gu, W.; Ozerov, O. V. Exhaustive Chlorination of $[B_{12}H_{12}]^{2-}$ without Chlorine Gas and the Use of $[B_{12}Cl_{12}]^{2-}$ as a Supporting Anion in Catalytic Hydrodefluorination of Aliphatic C−F Bonds. *Inorg. Chem.* **2011**, *50* (7), 2726–2728.

(19) Gu, W.; McCulloch, B. J.; Reibenspies, J. H.; Ozerov, O. V. Improved Methods for the Halogenation of the $[HCB_{11}H_{11}]^{-}$ Anion. *Chemical Communications*. 2010, p 2820.

(20) Peymann, T.; Knobler, C. B.; Hawthorne, M. F. A Study of the Sequential Acid-Catalyzed Hydroxylation of Dodecahydro-Closo-Dodecaborate(2-). *Inorg. Chem.* **2000**, *39* (6), 1163–1170.

(21) Hertler, W. R.; Raasch, M. S. Chemistry of Boranes. XIV. Amination of $B_{10}H_{10}^{-2}$ and $B_{12}H_{12}^{-2}$ with Hydroxylamine-O-Sulfonic Acid. *J. Am. Chem. Soc.* **1964**, *86* (18), 3661–3668.

(22) Peymann, T.; Lurk, E.; Gabel, D. Hydroxoundecahydro-Closo-Dodecaborate(2-) as a Nucleophile. Preparation and Structural Characterization of O-Alkyl and O-Acyl Derivatives of Hydroxoundecahydro-Closo-Dodecaborate(2-). *Inorg. Chem.* **1996**, *35* (5), 1355–1360.

(23) Boeré, R. T.; Derendorf, J.; Jenne, C.; Kacprzak, S.; Keßler, M.; Riebau, R.; Riedel, S.; Roemmele, T. L.; Rühle, M.; Scherer, H.; et al. On the Oxidation of the Three-Dimensional Aromatics $[B_{12}X_{12}]^{2-}$ (X=F, Cl, Br, I). *Chem. - A Eur. J.* **2014**, *20* (15), 4447–4459.